Ab Initio Nonadiabatic Quantum Molecular Dynamics

Basile F. E. Curchod[1] and Todd J. Martínez*[3,4]
[1]*Department of Chemistry, Durham University, South Road, Durham DH1 3LE, UK*
[3]*Department of Chemistry and the PULSE Institute, Stanford University, Stanford, CA 94305, USA*
[4]*SLAC National Accelerator Laboratory, Menlo Park, CA 94025, USA*
**Corresponding author: todd.martinez@stanford.edu*

Abstract: The Born-Oppenheimer approximation underlies much of chemical simulation and provides the framework defining the potential energy surfaces that are used for much of our pictorial understanding of chemical phenomena. However, this approximation breaks down when considering the dynamics of molecules in excited electronic states. Describing dynamics when the Born-Oppenheimer approximation breaks down requires a quantum mechanical description of the nuclei. Chemical reaction dynamics on excited electronic states is critical for many applications in renewable energy, chemical synthesis, and bioimaging. Furthermore, it is necessary in order to connect with many ultrafast pump-probe spectroscopic experiments. In this review, we provide an overview of methods that can describe nonadiabatic dynamics with emphasis on those that are able to simultaneously address the quantum mechanics of both electrons and nuclei. Such *ab initio* quantum molecular dynamics methods solve the electronic Schrödinger equation alongside the nuclear dynamics and thereby avoid the need for precalculation of potential energy surfaces and nonadiabatic coupling matrix elements. Two main families of methods are commonly employed to simulate nonadiabatic dynamics in molecules: full quantum dynamics such as the multiconfigurational time-dependent Hartree method and classical trajectory-based approaches such as trajectory surface hopping. In this review, we describe a third class of methods that is intermediate between the two – Gaussian basis set expansions built around trajectories.

Table of contents

1. Introduction

In many chemical problems, the electrons respond nearly instantaneously to nuclear motion and the details of electronic dynamics can be ignored. In these cases, the Born-Oppenheimer approximation (BOA) allows us to decouple the electronic and nuclear problems, defining the very concept of the potential energy surface. However, when the dynamics starts on an excited electronic state, there are almost invariably nonadiabatic transitions between electronic states corresponding to a breakdown of the BOA and demanding a quantum mechanical treatment of both the nuclei and the electrons. There are numerous examples of chemical problems that involve excited electronic states from photochemistry to electron transfer with applications in renewable energy, chemical synthesis, and bioimaging. It is thus a major theoretical challenge to describe the quantum mechanical behavior of both electrons and nuclei in the context of nonadiabatic effects and excited state chemistry.

A number of computational methods have been proposed in the past decades in order to meet the challenge of simulating dynamics beyond the BOA. A schematic representation of some of the most commonly employed nonadiabatic dynamics methods is provided in Figure 1, and numerous reviews of the subject have been published.[1-4] Methods such as Multi-configuration Time-Dependent Hartree (MCTDH) can provide numerically exact results for molecules with a few tens of nuclear degrees of freedom.[5-6] MCTDH is often considered as a reference method for excited-state dynamics, when high accuracy potential energy surfaces and nonadiabatic coupling matrix elements are available. Unfortunately, the method requires a precalculated potential energy surface (implying the necessity for a computationally challenging global fit) and the limitation to relatively few degrees of freedom requires a reduced dimensionality treatment for most molecules, i.e. freezing some of the internal coordinates. Multilayer MCTDH[7-8] (ML-

MCTDH) offers a way to circumvent reduced dimensionality in some cases, but further approximations are needed if one is interested in the dynamics of molecules in their full configuration space. In mixed quantum/classical methods[9] such as Ehrenfest and trajectory surface hopping dynamics, the nuclei are treated classically. In the former, the nuclear forces are directly derived from the time-dependent propagation of an electronic wavefunction or density matrix and trajectories evolve on a time-dependent average of the electronic states.[3,10-11] In surface hopping dynamics,[12-13] a set of electronic amplitudes are integrated together with the classical trajectories and dictate the probability that the trajectory will "hop" from one electronic state to the other (additional details on the surface hopping method can be found below).

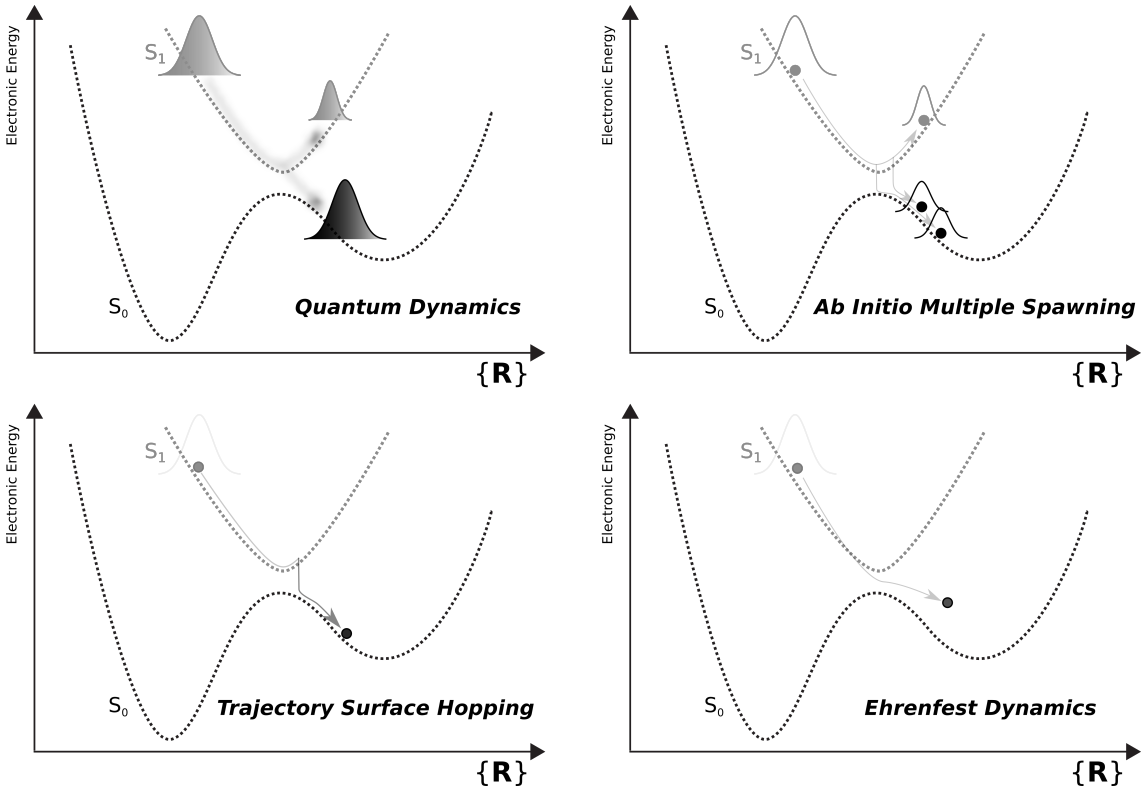

Figure 1. Schematic representation of different methods for excited-state molecular dynamics.

The aforementioned techniques are far from the only way of modeling nonadiabatic molecular dynamics, and we briefly mention semiclassical approaches,[14-15] quantum-classical Liouville approaches,[16-19] symmetrical quasi-classical windowing,[20-24] linearized nonadiabatic dynamics,[25] Bohmian dynamics,[26-31] and exact-factorization based mixed quantum/classical algorithms.[32-36]

This review focuses on nonadiabatic dynamics methods that expand the nuclear wavefunction in terms of a linear combination of traveling Gaussian basis functions.[37-39] This idea is rooted in the seminal work of Heller.[37] Before Heller's work, the most common approach to chemical dynamics was based on a scattering formalism in the energy domain. Heller proposed to use *classically-driven Gaussian functions* to describe the semiclassical dynamics of nuclear wavepackets. Heller further introduced a time-dependent perspective on photoabsorption, where the direct propagation of nuclear wavefunctions replaces the expensive calculation of Franck-Condon factors.[38,40] In 1981, Heller introduced the use of *frozen Gaussians*, i.e., Gaussians with a fixed width, as a basis for the nuclear wavefunction.[39] This proposal seeded the development of the methods presented in this review.

One particularly compelling feature of Gaussian-based quantum dynamics methods is that they are easily amenable to an *ab initio* molecular dynamics formulation, where the required electronic structure quantities (such as electronic state energies and gradients) are calculated "on the fly," i.e. simultaneously with the nuclear dynamics. Additionally, they can be derived from first principles and made exact in well-defined limits. In principle, the "traveling" nature of the Gaussian basis functions allows a compact set of basis functions to describe the dynamics and therefore can be much more computationally efficient than methods based on a fixed set of basis functions. We focus on the Full Multiple Spawning (FMS) and Ab Initio Multiple Spawning

(AIMS) methods, but we also discuss other methods based on traveling Gaussian wavepackets such as variational multi-configurational Gaussians[41-42] (vMCG) and multiconfigurational Ehrenfest[43-44] (MCE). The AIMS method avoids precalculated potential energy surfaces and instead solves the electronic Schrödinger equation as needed during the dynamics to obtain these quantities. AIMS constitutes the earliest reported incarnation[45-47] of *ab initio* nonadiabatic quantum molecular dynamics. Subsequently, other nonadiabatic dynamics methods have also been used in the context of ab initio molecular dynamics.[42,48-54]

2. The time-dependent molecular Schrödinger equation

Ab initio quantum molecular dynamics aims to solve the time-dependent Schrödinger equation (TDSE) for a molecular system (usually in the non-relativistic limit, as shown here):

$$i\frac{\partial\Psi(\mathbf{r},\mathbf{R},t)}{\partial t}=\hat{H}(\mathbf{r},\mathbf{R})\Psi(\mathbf{r},\mathbf{R},t) \tag{1}$$

In this equation, $\mathbf{r}$ and $\mathbf{R}$ are the collection of $3N_{el}$ electronic and $3N$ nuclear coordinates, respectively. We make use of atomic units here and throughout this review, i.e. $\hbar=m_e=1$. The molecular Hamiltonian is given as

$$\begin{aligned}\hat{H}(\mathbf{r},\mathbf{R})&=\hat{T}_{nuc}+\hat{T}_e+\hat{V}_{e-e}(\mathbf{r})+\hat{V}_{e-n}(\mathbf{r},\mathbf{R})+\hat{V}_{n-n}(\mathbf{R})\\&=\hat{T}_{nuc}+\hat{H}_{el}(\mathbf{r},\mathbf{R})\end{aligned} \tag{2}$$

where $\hat{T}_{nuc}=-\sum_{\gamma}^{N}\frac{1}{2M_\gamma}\nabla^2_{\mathbf{R}_\gamma}$ is the nuclear kinetic energy operator and the γth nucleus has bare mass M_γ. The electronic Hamiltonian $\hat{H}_{el}(\mathbf{r},\mathbf{R})$ contains the electronic kinetic energy operator as well as all the Coulomb operators involving electrons and nuclei.

2.1 Representations of the molecular wavefunction

The Born-Huang representation[55-56] is a formally exact separation of the molecular wavefunction into electronic and nuclear contributions:

$$\Psi(\mathbf{r},\mathbf{R},t) = \sum_{J}^{\infty} \Omega_J(\mathbf{R},t)\Phi_J(\mathbf{r};\mathbf{R}) \tag{3}$$

where the subscript J denotes the electronic state and $\Omega_J(\mathbf{R},t)$ is the time-dependent nuclear wave function associated with the Jth electronic state. The electronic part in Eq. (3) is expanded in an orthonormal electronic basis, $\{\Phi(\mathbf{r};\mathbf{R})\}$. Often one chooses the adiabatic representation, meaning that the electronic basis consists of eigenfunctions of the time-independent electronic Schrödinger equation for a given nuclear configuration **R**:

$$\hat{H}_{el}(\mathbf{r},\mathbf{R})\Phi_J(\mathbf{r};\mathbf{R}) = E_J(\mathbf{R})\Phi_J(\mathbf{r};\mathbf{R}) \tag{4}$$

where $E_J(\mathbf{R})$ is the Jth eigenvalue at a given nuclear position **R**. These eigenvalues correspond to the adiabatic potential energy surface for the Jth electronic state. Diabatic representations, where the electronic states are not eigenfunctions of the electronic Hamiltonian, are also possible (and in some cases advantageous).[57-59] For simplicity, we focus on the adiabatic representation throughout most of this article.

In principle, the Born-Huang expansion is formally exact only when an infinite number of electronic states are included. In practice, an excellent approximation is often obtained with a few electronic states. Several alternative formulations exist which simplify the Born-Huang representation by restricting it to a single product. The most common is the Born-Oppenheimer approximation (BOA). In the BOA, the Born-Huang summation in Eq. (3) is limited to a single time-independent electronic term: $\Psi(\mathbf{r},\mathbf{R},t) \approx \Omega_J(\mathbf{R},t)\Phi_J(\mathbf{r};\mathbf{R})$, where J is often taken as the

ground electronic state. (Note that this approximation is also known as the "Born-Huang approximation", and that the Born-Oppenheimer *adiabatic* approximation further implies the neglect of diagonal Born-Oppenheimer corrections.[60]) Effectively, the BOA assumes that the electrons relax instantaneously as the nuclei move, i.e. that the electrons and nuclei are perfectly correlated.[61-62] However, this correlation is restricted to a single electronic state, and therefore breaks down when two electronic states become nearly or exactly degenerate. Although this breakdown of the BOA is rarely a major concern on the ground electronic state, it is practically the rule for molecules undergoing dynamics on excited electronic states, for example in many ultrafast pump-probe type experiments.

An alternative single product formulation leads to the time-dependent self-consistent field (TDSCF) equations. In this approximation, the molecular wavefunction is given by $\Psi(\mathbf{r},\mathbf{R},t) \approx \Omega(\mathbf{R},t)\Phi(\mathbf{r},t)$, i.e. a product of time-dependent molecular and electronic wavefunctions.[9,63-64] At first glance, this might seem similar to the BOA, but it is actually very different. Because the electronic wavefunction does not depend on the nuclear coordinates, the electronic and nuclear degrees of freedom are completely uncorrelated in this wavefunction ansatz. Indeed, when the TDSCF ansatz is inserted in the TDSE, Eq. (1), it leads to a set of coupled mean-field equations for both the electronic and the nuclear wavefunctions. Taking a classical limit for the nuclear degrees of freedom then leads to Ehrenfest dynamics. For more details on the classical limit leading to Ehrenfest dynamics and its implication for mixed quantum/classical dynamics, the reader is referred to previous work.[9-11,65-66]

A final single product formulation that bears mention is the "exact factorization approach." As its name suggests, this formulation is formally exact, in spite of its restriction to a single product. This feat is accomplished[67-70] by allowing *both* the nuclear and electronic wavefunctions

to be explicitly time-dependent: $\Psi(\mathbf{r},\mathbf{R},t)=\Omega(\mathbf{R},t)\Phi(\mathbf{r},t;\mathbf{R})$. The explicit time-dependence of the electronic wavefunction results in a potential energy surface that depends on *both* nuclear coordinates and time, as well as a time-dependent vector potential.[32,71-76] Unlike the BOA ansatz, the electronic wavefunction is time-dependent. Unlike the TDSCF ansatz, the electronic wavefunction depends parameterically on the nuclear degrees of freedom. Even though this single product formulation is formally exact, it is unclear how to formulate an efficient and accurate implementation and this is currently a topic of considerable research effort.[36]

2.2 The coupled time-dependent nuclear equations

Upon insertion of the Born-Huang representation of Eq. (3) into the time-dependent Schrödinger equation, Eq.(1); left multiplication by $\Phi_I^*(\mathbf{r};\mathbf{R})$; and integration over the electronic coordinates, we obtain a set of coupled equations of motion for the nuclear wavefunctions $\Omega_I(\mathbf{R},t)$:

$$\begin{aligned} i\frac{\partial\Omega_I(\mathbf{R},t)}{\partial t} &= \left(\hat{T}_N + E_I(\mathbf{R})\right)\Omega_I(\mathbf{R},t) \\ &\quad -\sum_J^{\infty}\left[\sum_{\rho=1}^{3N}\left(\frac{1}{M_\rho}\left\langle\Phi_I\middle|\frac{\partial}{\partial R_\rho}\middle|\Phi_J\right\rangle_{\mathbf{r}}\frac{\partial}{\partial R_\rho}+\frac{1}{2M_\rho}\left\langle\Phi_I\middle|\frac{\partial^2}{\partial R_\rho^2}\middle|\Phi_J\right\rangle_{\mathbf{r}}\right)\right]\Omega_J(\mathbf{R},t) \end{aligned} \tag{5}$$

where ρ indexes the *3N* nuclear coordinates. The first term of Eq. (5) describes adiabatic evolution of the nuclear component $\Omega_I(\mathbf{R},t)$ on the *I*th electronic state corresponding to the potential energy surface $E_I(\mathbf{R})$. The second term, i.e. the second line of Eq. (5), describes coupling with other electronic states through the first- and second-order nonadiabatic derivative couplings: $\mathbf{d}_{IJ}(\mathbf{R})=\left\langle\Phi_I\middle|\nabla_{\mathbf{R}}\middle|\Phi_J\right\rangle_{\mathbf{r}}$ and $D_{IJ}(\mathbf{R})=\left\langle\Phi_I\middle|\nabla_{\mathbf{R}}^2\middle|\Phi_J\right\rangle_{\mathbf{r}}$. These quantities couple the electronic states through nuclear motion, and are critical in nonadiabatic dynamics. When the

nonadiabatic coupling terms are neglected in Eq. (5), we obtain the so-called Born-Oppenheimer adiabatic approximation,[56,60] which leads to Born-Oppenheimer molecular dynamics after taking a classical limit for the nuclear degrees of freedom.[10] When only the diagonal second-order couplings are retained, we obtain an adiabatic equation of motion for the nuclei that corresponds to inserting the BOA ansatz (discussed above) in the TDSE (with a mass-dependent PES).

Diabatic electronic representations rotate the electronic states such that the nonadiabatic couplings are small (ideally they would vanish, but this is not possible for polyatomic molecules).[57-59,77-78] This rotation necessarily leads to finite off-diagonal elements in the electronic Hamiltonian, i.e. any rotation that diagonalizes the kinetic part of the Hamiltonian will "undiagonalize" the potential part.[79] In a diabatic representation, electronic transitions are primarily promoted by the off-diagonal elements in the electronic Hamiltonian (as opposed to the nonadiabatic derivative couplings that promote transitions in the adiabatic representation).

In conventional quantum dynamics simulations, the (nuclear) wavefunctions and Hamiltonian elements are represented on a fixed grid (see below). Numerically exact solution of the TDSE can be obtained, given that electronic energies and coupling terms are known along the selected coordinates of the molecular configuration space.[80-82]

A very different philosophy is to approximate the dynamics of the nuclear wavepackets by a swarm of classical trajectories, which can for example *hop* from one electronic state to the other based on a stochastic algorithm. This technique, referred to as *surface hopping*, was first proposed in 1971 by Tully and Preston[12] and further refined by Tully in 1990 as the Fewest-Switches algorithm.[13] As trajectory surface hopping (TSH) is based on independent classical trajectories, it is well suited to *on-the-fly* dynamics, where the required electronic structure quantities are computed at each time step of a trajectory. The reliance on classical trajectories

also enables dynamical simulations of molecules in their full dimensionality (since the effort in classical propagation scales weakly with the number of degrees of freedom). Unfortunately, TSH cannot be fully derived from first principles. Numerous "quasi-derivations" have been proposed,[31,83-86] based on different starting formalisms. However, in each of these at least one step is uncertain and this makes it difficult to clearly delineate situations where TSH will or will not succeed. Some limitations are well-known and widely discussed. For example, the predicted dynamics from TSH depend (often quite strongly) on the electronic representation that is used (with the adiabatic representation being preferred).[9] In contrast, the exact solution of the TDSE is independent of the electronic representation used. Decoherence of nuclear wavepackets is also a problem[1,13,87-92] in TSH, although a number of different fixes have been proposed to overcome this limitation.[93-100] A number of recent reviews on the TSH are available.[11,91,101-103]

In the remaining part of this review, we focus on basis set expansions of Eq. (5), resulting in expressions for molecular quantum dynamics simulation that lead to well-controlled approximations.

3. Ab initio quantum dynamics with a basis set

The nuclear wavefunction for electronic state *J* can be written as a linear combination of N_J basis functions, denoted as $\left\{\chi_i^{(J)}\right\}_{i=1}^{N_J}$, whose elements are defined as $\chi_i^{(J)} \equiv \chi_i^{(J)}\left(\mathbf{R};a_{i,1}^{(J)}(t),\ldots,a_{i,N_p}^{(J)}(t)\right)$, i.e., the basis set only has explicit time-dependence through its N_p parameters denoted by $a_{i,1}^{(J)}(t),\ldots,a_{i,N_p}^{(J)}(t)$. The superscript "(*J*)" is to be understood as an electronic-state label for the basis functions. Expanded in this basis, the Born-Huang representation of Eq. (3) reads:

$$\Psi(\mathbf{r},\mathbf{R},t)=\sum_{J}^{\infty}\sum_{i}^{N_J}C_i^{(J)}(t)\chi_i^{(J)}\left(\mathbf{R};a_{i,1}^{(J)}(t),\ldots,a_{i,N_p}^{(J)}(t)\right)\Phi_J(\mathbf{r};\mathbf{R}) \tag{6}$$

with complex time-dependent expansion coefficients $\left\{C_i^{(J)}\right\}_{i=1}^{N_J}$ for each basis function on each electronic state. Combination of Eq. (6) with the TDSE, Eq. (1), will be the common starting point for the description of different nonadiabatic quantum dynamics methods.

We mentioned previously that the coupled time-dependent nuclear equations can be solved on a grid (quantum dynamics). The grid can be formulated in such a way that it appears as a choice of basis set for the expression of the nuclear wavefunction, e.g. as a series of δ-functions (or sinc functions) centered on each of the grid points. When this grid has a direct product structure, the basis is greatly simplified and a given nuclear wavefunction on state J with f nuclear degrees of freedom becomes:[5]

$$\Omega_J(R_1,\ldots,R_f,t)=\sum_{j_1\cdots j_f=1}^{N_1\cdots N_f}C_{j_1\cdots j_f}^{(J)}(t)\prod_{\kappa=1}^{f}\chi_{j_\kappa}^{(\kappa)}(R_\kappa) \tag{7}$$

where $\chi_{j_f}^{(f)}(R_f)$ represents one of the N_f functions used to describe the fth nuclear degree of freedom. These functions can be considered a dual space representation connecting physical space and function space, and this is the perspective taken explicitly in discrete variable (DVR)[80,104] and finite basis (FBR)[80] representations. (Note that we keep $\mathbf{R}$ as a generic label for the Cartesian nuclear coordinates. Internal coordinates can also be used, but we do not discuss the implications of such representations in this article.)

The curse of dimensionality in quantum dynamics clearly appears in Eq. (7), as the size of the problem grows as N^f if each of the f degrees of freedom is described by N functions. The Multiconfiguration Time-Dependent Hartree (MCTDH) method[5-6,105] proposes a clever way to

alleviate the problem: the grid functions – now called single-particle functions (SPFs) – acquire a time-dependence that allows for a considerable reduction in the number of time-independent grid points:

$$\Omega_J\left(R_1,\ldots,R_f,t\right)=\sum_{j_1\cdots j_f=1}^{n_1\cdots n_f} C^{(J)}_{j_1\cdots j_f}(t)\prod_{\kappa=1}^{f}\varphi^{(\kappa)}_{j_\kappa}\left(R_\kappa,t\right) \tag{8}$$

where a SPF is constructed from the primitive functions as $\varphi^{(\kappa)}_{j_\kappa}\left(R_\kappa,t\right)=\sum_{i_\kappa=1}^{N_\kappa} c^{(\kappa)}_{i_\kappa j_\kappa}(t)\chi^{(\kappa)}_{i_\kappa}\left(R_\kappa\right)$.

MCTDH becomes equivalent to a numerically exact (within the primitive basis set) solution of the time-dependent Schrödinger equation when $n_1,\cdots,n_f=N_1,\cdots,N_f$.

Another commonly employed basis set – that will be described in great detail in the following – is composed of multidimensional Gaussian functions with explicit time-dependent parameters given by:

$$\left(a^{(J)}_{i,1}(t),\ldots,a^{(J)}_{i,N_p}(t)\right)\equiv\left(\bar{\mathbf{R}}^{(J)}_i(t),\bar{\mathbf{P}}^{(J)}_i(t),\boldsymbol{\alpha}^{(J)}_i(t),\bar{\gamma}^{(J)}_i(t)\right) \tag{9}$$

Inserting Eq. (6) with this definition in the TDSE, multiplying on the left by $\left(\chi^{(I)}_j\left(\mathbf{R},a^{(I)}_{j,1}(t),\ldots,a^{(I)}_{j,N_p}(t)\right)\Phi_I\left(\mathbf{r};\mathbf{R}\right)\right)^*$, and integrating over both electronic and nuclear coordinates leads to general equations of motion for the expansion coefficients:

$$\dot{\mathbf{C}}=-i\mathbf{S}^{-1}\left[\left(\mathbf{H}-i\dot{\mathbf{S}}\right)\mathbf{C}\right] \tag{10}$$

Eq. (10) is simply the time-dependent Schrödinger equation expressed in a time-dependent nonorthogonal basis set, where $\left(\mathbf{S}\right)^{JI}_{ji}=\left\langle\chi^{(J)}_j\middle|\chi^{(I)}_i\right\rangle_{\mathbf{R}}$, $\left(\mathbf{H}\right)^{JI}_{ji}=\left\langle\chi^{(J)}_j\middle|\hat{H}\middle|\chi^{(I)}_i\right\rangle_{\mathbf{r},\mathbf{R}}$, and $\dot{\mathbf{S}}$ is an overlap matrix including the time-derivatives of the basis functions, which will be defined more

precisely in the following. The finite basis represents the only approximation made so far and Eq. (10) fully accounts for the coupling between nuclear motion and electronic states.

From the form of Eq. (10), it becomes immediately clear that the basis functions are mutually *coupled*, both in an intra- and interstate fashion. However, several questions about solutions and approximations to this equation arise at this stage: *How should we define equations of motion for the time-dependent parameters of the basis, and how do they influence the dynamics? How can we compute or approximate the matrix elements in Eq.* (10)*?* Answering these questions is the goal of the following sections, and we will see that it defines a hierarchy for nonadiabatic quantum dynamics methods.[4,106-108]

4. Full Multiple Spawning

Full Multiple Spawning (FMS) constitutes a framework for nonadiabatic dynamics, where nuclear wavefunctions are represented by an adaptive linear combination of frozen Gaussian functions that follow classical trajectories. In a complete basis, FMS would be exact. Applying a series of well-controlled approximations leads to the Ab Initio Multiple Spawning (AIMS) method which is well-suited to on-the fly excited state dynamics of molecules. We first discuss the FMS method and AIMS will be treated subsequently.

4.1 Equations of motion

In FMS,[109-113] the time-dependent nuclear wavefunction for each electronic state I is represented as a linear combination of multidimensional, frozen Gaussian basis functions with complex time-dependent coefficients:

$$\chi_i^{(J)}\left(\mathbf{R}, a_{i,1}^{(J)}(t), \ldots, a_{i,N_p}^{(J)}(t)\right) \equiv \chi_i^{(J)}\left(\mathbf{R}; \bar{\mathbf{R}}_i^{(J)}(t), \bar{\mathbf{P}}_i^{(J)}(t), \bar{\gamma}_i^{(J)}(t), \boldsymbol{\alpha}\right) \tag{11}$$

In the language of FMS, the $\chi_i^{(J)}$ are called trajectory basis functions (TBFs); each one is labeled with a compound index denoting the corresponding electronic state *J* and because there can be many TBFs on each electronic state, also by a second index *i*. As previously described, the frozen Gaussian is centered at position $\bar{\mathbf{R}}_i^{(J)}(t)$ and momenta $\bar{\mathbf{P}}_i^{(J)}(t)$, both of which evolve in time. The time-independent width of the Gaussian is denoted as $\boldsymbol{\alpha}$ and $\bar{\gamma}_i^{(J)}(t)$ is a phase.

Each multidimensional Gaussian basis function $\chi_i^{(J)}\left(\mathbf{R};\bar{\mathbf{R}}_i^{(J)}(t),\bar{\mathbf{P}}_i^{(J)}(t),\bar{\gamma}_i^{(J)}(t),\boldsymbol{\alpha}\right)$ is a product of one-dimensional Gaussian basis functions – one for each nuclear degree of freedom ρ:

$$\chi_i^{(J)}\left(\mathbf{R};\bar{\mathbf{R}}_i^{(J)}(t),\bar{\mathbf{P}}_i^{(J)}(t),\bar{\gamma}_i^{(J)}(t),\boldsymbol{\alpha}\right)=e^{i\bar{\gamma}_i^{(J)}(t)}\prod_{\rho=1}^{3N}\chi_{i\rho}^{(J)}\left(R_\rho;\bar{R}_{i\rho}^{(J)}(t),\bar{P}_{i\rho}^{(J)}(t),\alpha_\rho\right) \tag{12}$$

$$\chi_{i\rho}^{(J)}\left(R_\rho;\bar{R}_{i\rho}^{(J)}(t),\bar{P}_{i\rho}^{(J)}(t),\alpha_\rho\right)=\left(\frac{2\alpha_\rho}{\pi}\right)^{1/4}\exp\left[-\alpha_\rho\left(R_\rho-\bar{R}_{i\rho}^{(J)}(t)\right)^2+i\bar{P}_{i\rho}^{(J)}(t)\left(R_\rho-\bar{R}_{i\rho}^{(J)}(t)\right)\right] \tag{13}$$

In its usual form, FMS prescribes that a TBF on electronic state *J* follows a *classical trajectory*, evolving adiabatically on the potential energy surfaces given by $E_J(\mathbf{R})$ – the eigenvalue of the time-independent electronic Schrödinger equation in Eq. (4). Hence, the time-dependent positions and momenta associated with each Gaussian basis function are propagated using Hamilton's equations of motion:

$$\frac{\partial\bar{R}_{i\rho}^{(J)}(t)}{\partial t}=\frac{\bar{P}_{i\rho}^{(J)}(t)}{M_\rho} \tag{14}$$

$$\frac{\partial\bar{P}_{i\rho}^{(J)}(t)}{\partial t}=-\left.\frac{\partial E_J(\mathbf{R})}{\partial R_{i\rho}}\right|_{R_{i\rho}=\bar{R}_{i\rho}^{(J)}(t)} \tag{15}$$

The time-dependent phase $\bar{\gamma}_i^{(J)}(t)$ is obtained from semiclassical arguments, namely by integrating the classical Lagrangian

$$\frac{\partial \overline{\gamma}_i^{(J)}(t)}{\partial t} = \sum_{\rho}^{3N} \frac{\left(\overline{P}_{i\rho}^{(J)}(t)\right)^2}{2M_\rho} - E_J\left(\overline{\mathbf{R}}_i^{(J)}(t)\right) \tag{16}$$

The Born-Huang expansion obtained by inserting the FMS representation is:

$$\Psi(\mathbf{r},\mathbf{R},t) = \sum_{J}^{\infty} \sum_{i}^{N_J(t)} C_i^{(J)}(t) \chi_i^{(J)}\left(\mathbf{R};\overline{\mathbf{R}}_i^{(J)}(t),\overline{\mathbf{P}}_i^{(J)}(t),\overline{\gamma}_i^{(J)}(t),\boldsymbol{\alpha}\right) \Phi_J(\mathbf{r};\mathbf{R}) \tag{17}$$

Comparing to Eq. (6), the major differences are the specific use of a Gaussian basis set, and the time-dependence of the number of terms used to describe the nuclear wavefunction in state J, $N_J(t)$. The central idea of FMS is to use an *adaptive* basis set to better describe the nonadiabatic dynamics, and to prevent limitations arising from a fixed number of basis functions. The number of TBFs will indeed increase during the dynamics due to *spawning processes* (see Sec. 4.2 for a complete description). Interesting alterations of Eq. (17) have recently been proposed, where the global adiabatic electronic wavefunctions are replaced by electronic wavefunctions evaluated at the center of the corresponding Gaussian function[114] or by time-dependent quasi-diabatic electronic wavefunctions.[115] As we will see below, in AIMS, a similar interpretation arises naturally.

Inserting Eq. (17) into the time-dependent Schrödinger equation – multiplying on the left by $\left(\chi_k^{(I)}\left(\mathbf{R};\overline{\mathbf{R}}_k^{(I)}(t),\overline{\mathbf{P}}_k^{(I)}(t),\overline{\gamma}_k^{(I)}(t),\boldsymbol{\alpha}\right)\Phi_I(\mathbf{r};\mathbf{R})\right)^*$ and integrating over both nuclear and electronic coordinates – leads to equations of motion for the complex coefficients (or amplitudes) $\left\{C_i^{(I)}(t)\right\}_{i=1}^{N_I(t)}$. This projection defines a spectral method (defined entirely in the space of basis functions), but pseudospectral Gaussian methods (defined in a dual space of basis functions and physical space gridpoints) have also been proposed.[116] These equations of motion are similar to

the general one given in Eq. (10). Focusing on the amplitudes for TBFs associated with the *I*th electronic state, one obtains

$$\frac{d\mathbf{C}^I}{dt} = -i\left(\mathbf{S}_{II}^{-1}\right)\left[\left[\mathbf{H}_{II} - i\dot{\mathbf{S}}_{II}\right]\mathbf{C}^I + \sum_{J\neq I}\mathbf{H}_{IJ}\mathbf{C}^J\right] \tag{18}$$

where bold symbols indicate matrices or vectors in the space of Gaussian basis functions.[117] The nuclear overlap matrices in Eq. (18) are a direct consequence of the time-dependent and nonorthonormal Gaussian basis and the elements are defined as:

$$\left(\mathbf{S}_{II}\right)_{ki} = \left\langle \chi_k^{(I)} \middle| \chi_i^{(I)} \right\rangle_{\mathbf{R}} \tag{19}$$

$$\left(\dot{\mathbf{S}}_{II}\right)_{ki} = \left\langle \chi_k^{(I)} \middle| \frac{\partial}{\partial t}\chi_i^{(I)} \right\rangle_{\mathbf{R}} \tag{20}$$

The Hamiltonian matrix $\mathbf{H}$ contains both inter- and intrastate couplings between TBFs. As an example, the Hamiltonian matrix element between TBF *k* evolving on state *J* and TBF *i* evolving on state *I* is given as:

$$\begin{aligned} H_{ki}^{JI} &= \left\langle \chi_k^{(J)}\Phi_J \middle| \hat{H} \middle| \chi_i^{(I)}\Phi_I \right\rangle_{\mathbf{R},\mathbf{r}} \\ &= \left\langle \chi_k^{(J)} \middle| \hat{T}_{nuc} \middle| \chi_i^{(I)} \right\rangle_{\mathbf{R}} \delta_{JI} + \left\langle \chi_k^{(J)} \middle| E_I \middle| \chi_i^{(I)} \right\rangle_{\mathbf{R}} \delta_{JI} - 2D_{ki}^{JI} - G_{ki}^{JI} \end{aligned} \tag{21}$$

where we used the molecular Hamiltonian given in Eq. (2) and the definition of adiabatic electronic states $E_I(\mathbf{R}) = \left\langle \Phi_J \middle| \hat{H}_{el}(\mathbf{R}) \middle| \Phi_I \right\rangle_{\mathbf{r}} \delta_{JI}$. The last two terms of Eq. (21) are linked to the nuclear kinetic energy operator and read

$$D_{ki}^{JI} = \left\langle \chi_k^{(J)} \middle| \sum_{\rho=1}^{3N} \left\langle \Phi_J \middle| \frac{\partial}{\partial R_\rho} \middle| \Phi_I \right\rangle_{\mathbf{r}} \frac{1}{2M_\rho} \frac{\partial}{\partial R_\rho} \middle| \chi_i^{(I)} \right\rangle_{\mathbf{R}} \tag{22}$$

$$G_{ki}^{JI} = \left\langle \chi_k^{(J)} \middle| \sum_{\rho=1}^{3N} \frac{1}{2M_\rho} \left\langle \Phi_J \middle| \frac{\partial^2}{\partial R_\rho^2} \middle| \Phi_I \right\rangle_{\mathbf{r}} \middle| \chi_i^{(I)} \right\rangle_{\mathbf{R}} \tag{23}$$

where we recognize the first- and second-order nonadiabatic coupling terms described in Sec. 2.2, sandwiched between TBFs.

We note that the time-dependent phase $\bar{\gamma}_i^{(J)}(t)$ could easily be absorbed into the FMS complex amplitudes. However, the definition of this phase and its semiclassical evolution leads to an interaction picture for the propagation of the complex coefficients. By using the equation of motion for the phase given in Eq. (16), oscillations in the complex amplitudes are reduced (increasing the time step that can be used in the integration of the equations of motion) and changes in the complex amplitudes are largely confined to times when TBFs are coupled (simplifying the interpretation of simulation results).

Couplings between TBFs described by the Hamiltonian matrix can be summarized as follows. Diagonal elements of **H** correspond to the energy of each TBF, while off-diagonal elements give rise to the coupling between TBFs (Figure 2). For instance, two TBFs – *k* and *m* – evolving on the same electronic state (S_0) will be coupled through the nuclear kinetic energy operator and the electronic energy, as well as through diagonal Born-Oppenheimer terms (blue area in Figure 2):

$$H_{km}^{S_0S_0} = \left\langle \chi_k^{(S_0)} \middle| \hat{T}_{nuc} \middle| \chi_m^{(S_0)} \right\rangle_{\mathbf{R}} + \left\langle \chi_k^{(S_0)} \middle| E_{S_0} \middle| \chi_m^{(S_0)} \right\rangle_{\mathbf{R}} - \left\langle \chi_k^{(S_0)} \middle| \sum_{\rho=1}^{3N} \frac{1}{2M_\rho} \left\langle \Phi_{S_0} \middle| \frac{\partial^2}{\partial R_\rho^2} \middle| \Phi_{S_0} \right\rangle_{\mathbf{r}} \middle| \chi_m^{(S_0)} \right\rangle_{\mathbf{R}} \quad (24)$$

The coupling between TBFs *k* and *i* evolving on different electronic states (S_0 and S_1) is mediated by nonadiabatic coupling terms (red area in Figure 2):

$$H_{ki}^{S_0S_1} = -\left\langle \chi_k^{(S_0)} \middle| \sum_{\rho=1}^{3N} \left\langle \Phi_{S_0} \middle| \frac{\partial}{\partial R_\rho} \middle| \Phi_{S_1} \right\rangle_{\mathbf{r}} \frac{1}{M_\rho} \frac{\partial}{\partial R_\rho} \middle| \chi_i^{(S_1)} \right\rangle_{\mathbf{R}} - \left\langle \chi_k^{(S_0)} \middle| \sum_{\rho=1}^{3N} \frac{1}{2M_\rho} \left\langle \Phi_{S_0} \middle| \frac{\partial^2}{\partial R_\rho^2} \middle| \Phi_{S_1} \right\rangle_{\mathbf{r}} \middle| \chi_i^{(S_1)} \right\rangle_{\mathbf{R}} \quad (25)$$

The second-derivative coupling terms given in Eq. (23) are often neglected.[46,118] It is important to note, however, that the molecular Hamiltonian is no longer Hermitian without these terms,[56]

and hermiticity has to be enforced by construction.[119] Furthermore, the potential influence of second-order nonadiabatic couplings and diagonal Born-Oppenheimer corrections on nonadiabatic dynamics has recently been highlighted.[62,115,120-123]

The physical interpretation of the first-order term, D_{kl}^{IJ}, is that changes in the nuclear coordinates induce coupling between electronic states (because the electronic states change character as the nuclei move). In the diabatic representation, these terms vanish and the coupling is instead described by the off-diagonal elements of the electronic Hamiltonian. However, both descriptions are interchangeable. An advantage of the adiabatic representation is its uniqueness, being determined by the solution of the electronic Schrödinger equation alone. In contrast, diabatic representations are normally not unique and usually require global information about the potential energy surfaces that can be difficult to reconcile with "on-the-fly" treatments. In the context of surface hopping, a "locally diabatic" compromise between the two representations has been proposed.[124-125] This locally diabatic representation might also prove useful in other nonadiabatic dynamics methods, but this has not yet been explored.

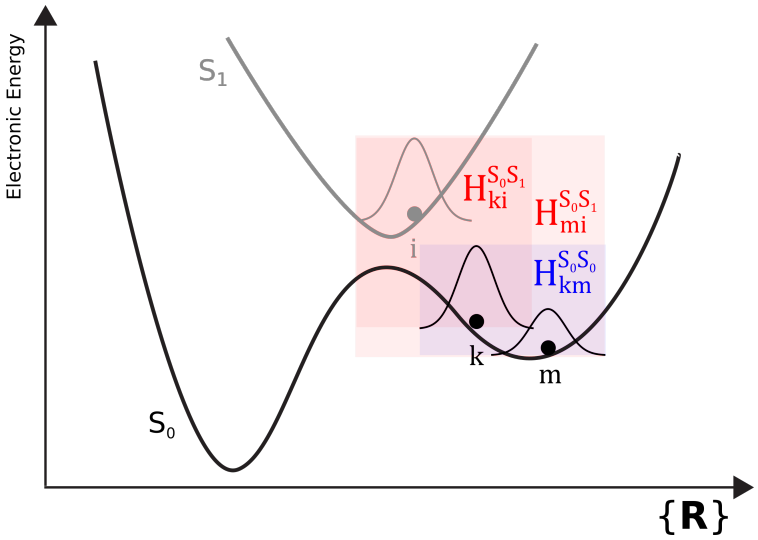

Figure 2. Schematic representation of matrix elements coupling between TBFs in FMS. The blue colored area indicates TBFs coupled by intrastate coupling, while the red area indicates TBFs coupled by interstate coupling.

If the basis set is large enough and all matrix elements are computed exactly, FMS provides an exact solution to the molecular time-dependent Schrödinger equation. The exactness of the dynamics in the limit of a complete basis set does not depend on the equations of motion used for the basis functions (and even a fixed set of basis functions would lead to the exact answer). However, the choice of equations of motion for the basis functions is expected to influence convergence substantially.

4.2 Adapting the size of the basis using the spawning algorithm

In FMS, the initial wavefunction at time $t=0$ is prepared as a linear combination of N_{ini} coupled TBFs, called initial parent TBFs (see Figure 3). To better understand how FMS adapts the basis set, it is useful to rewrite the FMS Born-Huang representation of Eq.(17) to make the initial number of parent TBFs explicit:[126]

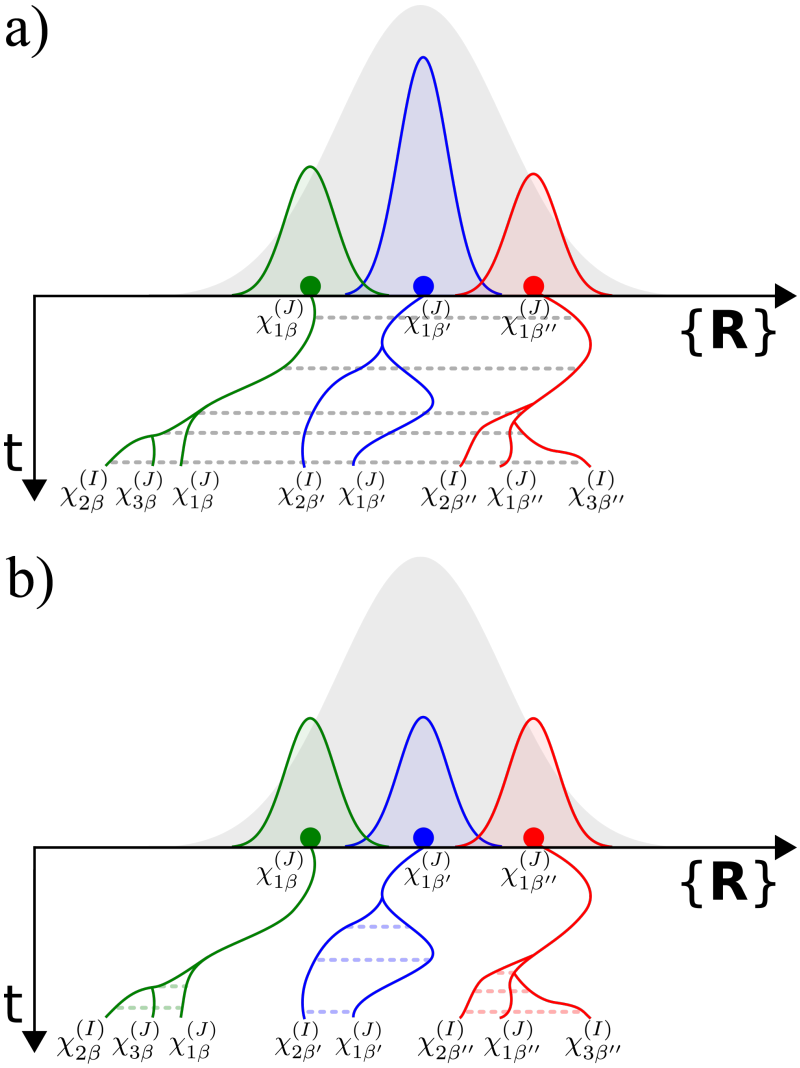

Figure 3. Coupling pattern between parent TBFs and their respective children without (a) and within (b) the independent first generation approximation. The grey dashed horizontal lines represent the couplings between different TBFs that are included in the calculation.

$$\begin{aligned}\Psi(\mathbf{r},\mathbf{R},t) &= \sum_{\beta}^{N_{ini}} \tilde{\Psi}_{\beta}(\mathbf{r},\mathbf{R},t) \\ &= \sum_{\beta}^{N_{ini}} \sum_{J}^{\infty} \sum_{i}^{N_J^{\beta}(t)} C_{i\beta}^{(J)}(t) \chi_{i\beta}^{(J)}\left(\mathbf{R};\bar{\mathbf{R}}_{i\beta}^{(J)}(t),\bar{\mathbf{P}}_{i\beta}^{(J)}(t),\bar{\gamma}_{i\beta}^{(J)}(t),\boldsymbol{\alpha}\right)\Phi_J^{\beta}(\mathbf{r};\mathbf{R})\end{aligned} \tag{26}$$

This equation highlights the fact that all initial parent TBFs are coupled to each other from the very beginning of the FMS dynamics, and they are also all coupled to any additional TBFs

created during the simulation (see Figure 3a). For example, if a simulation starts at time *t=0* in the S_1 electronic state with ten parent TBFs, Eq. (26) will read

$$\Psi(\mathbf{r},\mathbf{R},t_0)=\sum_{\beta=1}^{10}C_{1\beta}^{(S_1)}(t_0)\chi_{1\beta}^{(S_1)}\left(\mathbf{R};\bar{\mathbf{R}}_{1\beta}^{(S_1)}(t_0),\bar{\mathbf{P}}_{1\beta}^{(S_1)}(t_0),\bar{\gamma}_{1\beta}^{(S_1)}(t_0),\boldsymbol{\alpha}\right)\Phi_{S_1}^{\beta}(\mathbf{r};\mathbf{R}) \tag{27}$$

While this notation may appear cumbersome, it helps distinguish between the original N_{ini} parent TBF and their respective child TBFs, labeled as $i=\left\{1,\ldots,N_J^{\beta}(t)\right\}$. The value of each complex amplitude is obtained by projection on the desired (exact) initial wavefunction (or the best available approximation) at time $t=0$:

$$C_{1\beta'}^{(J)}(t=0)=\sum_{\beta}^{N_{ini}}\left(\mathbf{S}_{JJ}^{-1}\right)_{1\beta'1\beta}\left\langle\chi_{1\beta}^{(J)}(t=0)\middle|\Omega_J^{exact}(t=0)\right\rangle_{\mathbf{R}} \tag{28}$$

The natural question at this stage is *when* and *how* should the basis set be adaptively expanded? From the initial conditions provided by Eq. (27), it is clear that the description of nonadiabatic events requires the creation of TBFs in different electronic states. Hence, the spawning algorithm should generate new TBFs whenever an existing TBF approaches a nonadiabatic coupling region.

The spawning algorithm – in its most common implementation[127] (see Sec. 4.2 for additional details) – works as follows (Figure 4): at every time step, each TBF of a FMS run monitors the strength of the nonadiabatic coupling between its assigned electronic state (the "running state") and any other electronic state considered in the dynamics (an energy threshold can be set to prevent the calculations of nonadiabatic coupling vectors for states that are energetically distant from the running state). In the adiabatic representation, the most common metric for the coupling strength between a TBF on state *I* at position $\bar{\mathbf{R}}_i$ and the electronic state *J* is simply

$$\Lambda_{IJ}^{eff}\left(\bar{\mathbf{R}}_i\right)=\left|\mathbf{d}_{IJ}\left(\bar{\mathbf{R}}_i\right)\right| \tag{29}$$

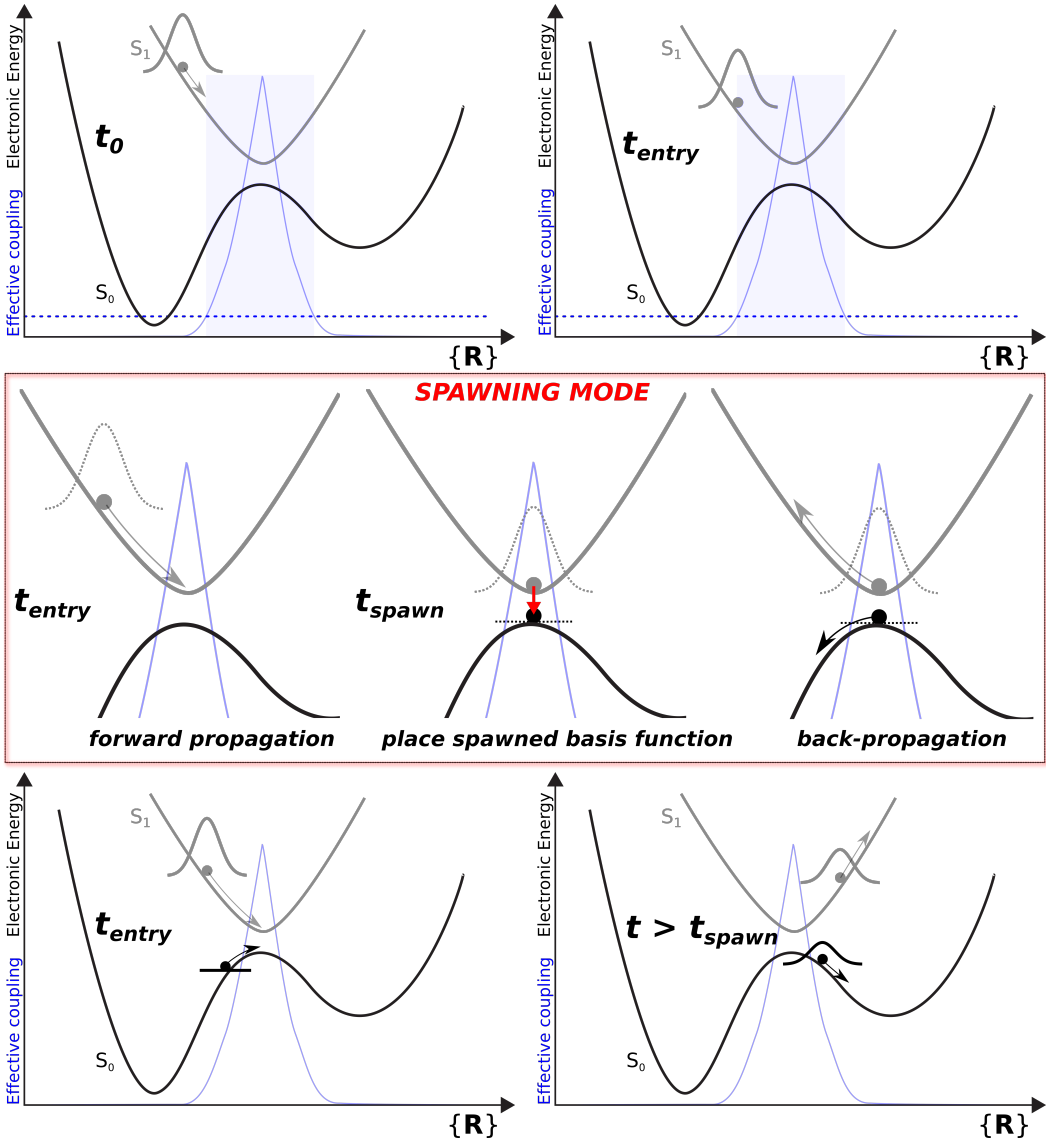

Figure 4. Schematic representation of the simplest spawning algorithm in FMS.

i.e., the norm of the nonadiabatic coupling vector. Another commonly employed criterion accounts for the projection of the nonadiabatic coupling vectors on the TBF classical velocities

$$\Lambda_{IJ}^{eff}\left(\bar{\mathbf{R}}_i\right)=\left|\mathbf{d}_{IJ}\left(\bar{\mathbf{R}}_i\right)\cdot\dot{\bar{\mathbf{R}}}_i\right| \tag{30}$$

The latter choice is a closer approximant of the off-diagonal matrix element that governs the propensity for nonadiabatic transitions, *à la* Landau-Zener,[128-130] and thus one might expect it to be preferred. However, it is also more oscillatory than the choice in Eq. (29), which can be numerically cumbersome. Both choices have been used successfully and we do not distinguish between them in what follows. If a TBF reaches a region where Λ^{eff} exceeds a predefined threshold, the entire FMS propagation is frozen and the TBF enters a "Spawning mode" (middle panel in Figure 4); this time in the dynamics is called the "entry time" (t_{entry}). When the dynamics is in spawning mode, the propagation of the complex amplitudes is suspended (dotted lines for the TBF in Figure 4), and only the spawning parent TBF continues its classical propagation, which is being used at this stage as a probe for nonadiabaticity. The TBF monitors the strength of Λ^{eff} as it propagates from t_{entry} and stops when Λ^{eff} reaches a maximum.[131] At this time, called the spawning time t_{spawn}, a new TBF is spawned on the coupled state if and only if: (1) energy conservation can be ensured – the kinetic energy should be sufficient to balance a gain of potential energy[113,132-134] – and (2) the newly created TBF (child TBF) has sufficient overlap with the parent TBF.[135] If the spawn is successful, the child TBF inherits all the properties of its parent TBF, except for a rescaled momentum (p-jump) and a complex coefficient set to zero. At this point, the child TBF needs to be back-propagated in time from t_{spawn} to t_{entry}, as it evolves on a different electronic state. Once the back-propagation is complete, the dynamics leaves the "spawning mode" and the integration of the complex amplitudes can resume. The equations of motion now include the additional complex amplitude for the child TBF, having a value of zero at t_{entry}, and the corresponding coupling and overlap terms.

We note that "frustrated spawns" can take place when a child TBF should be created in a classically forbidden region with respect to the parent TBF, i.e., a region where the classical kinetic energy of the parent TBF is not enough to compensate for the change of potential energy associated with the creation of a child TBF on an upper electronic state. Normally, these are handled by steepest descent minimization until the potential energy decreases sufficiently to allow TBF placement.[127,132] In this sense, spawning can involve both position and momentum jumps of the child TBF relative to its parent TBF. In any case, it is important to realize that frustrated spawns do *not* affect detailed balance in FMS – as frustrated hops do in TSH[88,136-138] – because the evolution of the complex amplitudes in FMS follows the time-dependent Schrödinger equation.[132]

4.3. Ab Initio Multiple Spawning

FMS is well suited to "on the fly" evaluation of the potential energy surfaces and nonadiabatic couplings since it is based on trajectories. However, there are two central approximations that are employed to transform FMS into Ab Initio Multiple Spawning (AIMS).

The critical bottleneck that hampers the use of FMS for molecules without pretabulated potential energy surfaces is the evaluation of the integrals that form the Hamiltonian matrix in Eq. (21). Calculating the terms containing the electronic energy and the nonadiabatic coupling vectors implies integration over the entire nuclear configuration space. Hence, numerically exact matrix elements can only be obtained if the potential energy surfaces and nonadiabatic couplings are known over all the space covered by the nuclear coordinates of interest.

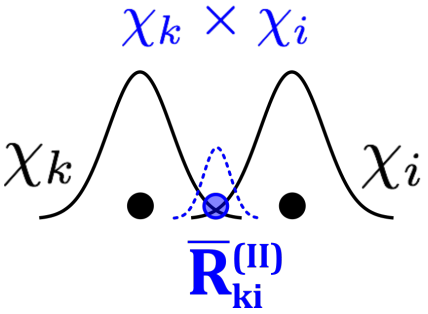

Figure 5. Definition of the centroid between two TBFs, used to calculate integrals in the saddle point approximation.

However, the TBFs are spatially localized, and this localization can be exploited to approximate the required integrals. The product of any two TBFs will itself be another Gaussian basis function, located at a centroid position between the two TBFs. This is shown schematically in Figure 5. One can then Taylor expand the electronic energy and/or nonadiabatic coupling about this centroid and evaluate the resulting integral analytically.[113,127,139-140] As an example, we consider the expansion of the intrastate coupling term – containing the electronic energy – between two TBFs k and i with centroid position $\bar{\mathbf{R}}_{ki}^{(II)} = \frac{\bar{\mathbf{R}}_k^{(I)} + \bar{\mathbf{R}}_i^{(I)}}{2}$, i.e., at the maximum of the product $\left|\left(\chi_k^{(I)}\right)^* \chi_i^{(I)}\right|$:

$$E_I(\mathbf{R}) = E_I\left(\bar{\mathbf{R}}_{ki}^{(II)}\right) + \sum_{\rho}^{3N}\left(R_\rho - \bar{R}_{\rho,ki}^{(II)}\right)\left.\frac{\partial E_I(\mathbf{R})}{\partial R_\rho}\right|_{R_\rho = \bar{R}_{\rho,ki}^{(II)}} + \frac{1}{2}\sum_{\rho,\rho'}^{3N}\left(R_\rho - \bar{R}_{\rho,ki}^{(II)}\right)\left.\frac{\partial^2 E_I(\mathbf{R})}{\partial R_\rho \partial R_{\rho'}}\right|_{R_\rho = \bar{R}_{\rho,ki}^{(II)}, R_{\rho'} = \bar{R}_{\rho',ki}^{(II)}}\left(R_{\rho'} - \bar{R}_{\rho',ki}^{(II)}\right) + \ldots \tag{31}$$

Upon inserting this expansion into the corresponding Hamiltonian integral, we obtain

$$\left\langle \chi_k^{(I)} \middle| E_I \middle| \chi_i^{(I)} \right\rangle_{\mathbf{R}} = E_I\left(\bar{\mathbf{R}}_{ki}^{(II)}\right)\left\langle \chi_k^{(I)} \middle| \chi_i^{(I)} \right\rangle_{\mathbf{R}} + \sum_{\rho}^{3N} \left.\frac{\partial E_I(\mathbf{R})}{\partial R_\rho}\right|_{R_\rho=\bar{R}_{\rho,ki}^{(II)}} \left\langle \chi_k^{(I)} \middle| \left(R_\rho - \bar{R}_{\rho,ki}^{(II)}\right) \middle| \chi_i^{(I)} \right\rangle_{\mathbf{R}}$$
$$+\frac{1}{2}\sum_{\rho,\rho'}^{3N} \left.\frac{\partial^2 E_I(\mathbf{R})}{\partial R_\rho\, \partial R_{\rho'}}\right|_{R_\rho=\bar{R}_{\rho,ki}^{(II)}, R_{\rho'}=\bar{R}_{\rho',ki}^{(II)}} \left\langle \chi_k^{(I)} \middle| \left(R_\rho - \bar{R}_{\rho,ki}^{(II)}\right)\left(R_{\rho'} - \bar{R}_{\rho',ki}^{(II)}\right) \middle| \chi_i^{(I)} \right\rangle_{\mathbf{R}} + \ldots \tag{32}$$

Hence, the Hamiltonian matrix element has been expressed as a product of analytically soluble integrals (moments of Gaussian functions) multiplied by electronic structure contributions evaluated at the centroid.[141] This type of expansion has been commonly used in combination with Gaussian basis sets. In AIMS, the Taylor series is often truncated after zeroth order, all second-order nonadiabatic coupling terms are neglected, and Eq. (21) is therefore approximated as:

$$H_{ki}^{JI} \approx \left\langle \chi_k^{(J)} \middle| \hat{T}_{nuc} \middle| \chi_i^{(I)} \right\rangle_{\mathbf{R}} \delta_{JI} + E_I\left(\bar{\mathbf{R}}_{ki}^{(JI)}\right)\left\langle \chi_k^{(J)} \middle| \chi_i^{(I)} \right\rangle_{\mathbf{R}} \delta_{JI}$$
$$-\sum_{\rho=1}^{3N} \frac{1}{M_\rho} \left\langle \chi_k^{(J)} \middle| \frac{\partial}{\partial R_\rho} \middle| \chi_i^{(I)} \right\rangle_{\mathbf{R}} \left\langle \Phi_J \middle| \frac{\partial}{\partial R_\rho} \middle| \Phi_I \right\rangle_{\mathbf{r}} \Bigg|_{R_\rho=\left(\bar{\mathbf{R}}_{ki}^{(JI)}\right)_\rho} \tag{33}$$

This appears to require $N_{TBF} \times \left(N_{TBF}+1\right)/2$ electronic structure calculations, i.e., at the position of each TBF and the centroids for each pair of TBFs.[127] However, this is a gross overestimate because the overlap (and higher moment) integrals decay quickly with distance between TBFs. Thus, one only needs to calculate electronic energies and/or nonadiabatic couplings for pairs of TBFs that are close to each other and the effective computational effort is normally nearly linear in N_{TBF}. This "zeroth-order saddle point" approximation facilitates an "on-the-fly" solution of the FMS equations of motion, where any electronic structure information is computed as needed at each integration time step. Higher order saddle point approximations are also possible, by also calculating first and/or second derivatives of the electronic energies and/or nonadiabatic coupling matrix elements.[142] However, this has rarely been pursued because of the considerable expense

associated with derivatives of the nonadiabatic coupling matrix elements or second derivatives of the electronic energy. A promising alternative that has been recently suggested uses Gaussian process regression to calculate these matrix elements.[140]

If one is interested in the excited-state dynamics of a rather high-dimensional molecular system, another simplification of the FMS equations of motion is useful. At time $t = 0$, all N_{ini} initial parent TBFs are coupled together and reproduce the molecular wavefunction – see Eq. (26) and Figure 3a. Instead of considering that all parent TBFs are coupled from time $t = 0$, we can invoke the independent first generation approximation. The initial nuclear wavepacket will usually spread rapidly in phase space at the beginning of the dynamics, implying that the initially coupled TBFs will soon become uncoupled and evolve independently. To a good approximation, we can therefore consider that they are, from time $t = 0$, uncoupled (Figure 3b). Hence, each parent TBF is sampled – positions and momenta from a Wigner distribution, amplitude set to 1 for the initial state – and run independently (compare upper and lower panels in Figure 3). In other words, we consider that the evolution of complex amplitudes is not coupled if they belong to a different parent β ($S^{JJ}_{k\beta' i\beta} \approx S^{JJ}_{ki}\delta_{\beta'\beta}$ and $H^{IJ}_{k\beta' i\beta} \approx H^{IJ}_{ki}\delta_{\beta'\beta}$, $\forall I,J$).[113,126]

In summary, when the saddle-point approximation of zeroth-order is used to approximate the Hamiltonian matrix elements, and the independent first generation uncouples the initial TBFs, FMS becomes fully compatible with on-the-fly nonadiabatic dynamics and is usually called Ab Initio Multiple Spawning (Figure 6).[112-113,133,143]

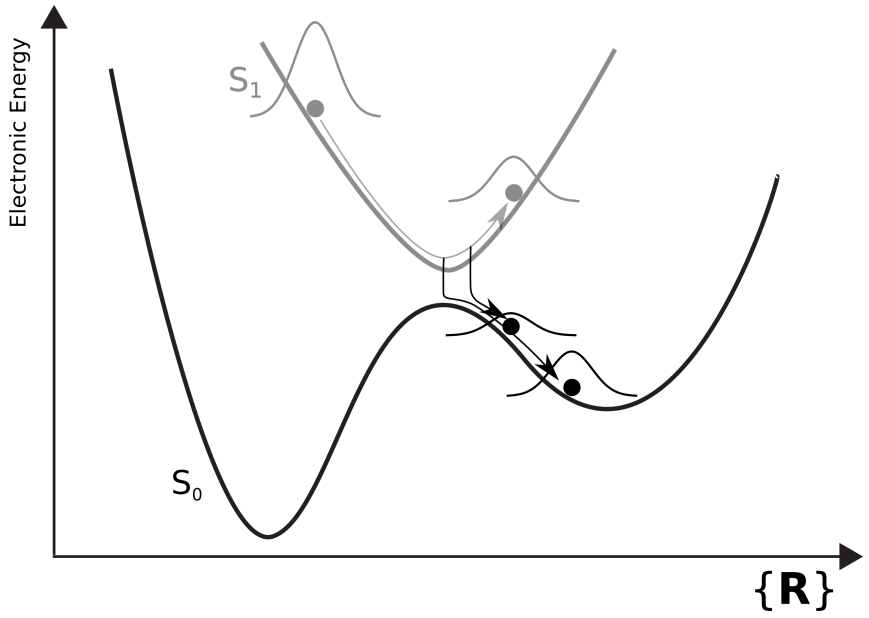

Figure 6. Schematic representation of an AIMS run, where an initial TBF on S_1 spawns two new TBFs on S_0.

4.3.1 Links between TSH and AIMS

In the previous section, we mentioned the IFG approximation, which implies that TBFs originating from different initial conditions are considered as independent during the nuclear dynamics, while those originating from the same initial condition remain fully coupled. Trajectory Surface Hopping[9,12-13] (TSH) can be seen as a method pushing the IFG a step further by invoking the so-called independent trajectory approximation (ITA). TSH uses a swarm of totally *independent* classical trajectories, each carrying a set of amplitudes, to represent the dynamics of a nuclear wavepacket. The spawning of additional trajectories is replaced by surface hops (Figure 1), meaning that the electronic state driving the classical nuclear dynamics of a given trajectory can change if a nonadiabatic region is encountered. Such hops are mediated by a stochastic algorithm, based on hopping probabilities expressed in terms of TSH complex amplitudes for each independent trajectory $[\alpha]$. Therefore, the complex amplitudes in TSH

evolve coherently along a single trajectory, whose driving electronic state can change along the dynamics.

Despite the fact that it requires the same electronic structure properties as AIMS (electronic energies, forces on the nuclei, nonadiabatic coupling vectors), the TSH algorithm is simplified by the ITA. An important difference is that TSH only needs electronic calculations at the nuclear configuration of the classical trajectory at time *t*, $\mathbf{R}^{[\alpha]}(t)$. In AIMS the couplings between the different TBFs arising from a given initial condition necessitate additional electronic energies and nonadiabatic couplings calculations at the position of centroids, as described before. To better illustrate the differences between the equations of motion for the amplitudes of the two methods, let us consider the illustrative example of a molecular system with two electronic states, *I* and *J*, at a given time *t*. The TSH equations of motion for the complex amplitudes along a trajectory [α] read

$$\begin{pmatrix} \dot{c}^{I}_{[\alpha]}(t) \\ \dot{c}^{J}_{[\alpha]}(t) \end{pmatrix} = -i \begin{pmatrix} H^{II}_{[\alpha]} & H^{IJ}_{[\alpha]} \\ H^{JI}_{[\alpha]} & H^{JJ}_{[\alpha]} \end{pmatrix} \begin{pmatrix} c^{I}_{[\alpha]}(t) \\ c^{J}_{[\alpha]}(t) \end{pmatrix} \tag{34}$$

where $H^{II}_{[\alpha]} = E_I\left(\mathbf{R}^{[\alpha]}(t)\right)$ and $H^{IJ}_{[\alpha]} = -i\mathbf{d}_{IJ}\left(\mathbf{R}^{[\alpha]}(t)\right)\cdot\dot{\mathbf{R}}^{[\alpha]}(t)$.

In AIMS, within the IFG approximation and considering a case where three TBFs evolve on state *I* and two on state *J*, we have

$$\begin{pmatrix} \mathbf{S}_{11}^{II} & \mathbf{S}_{12}^{II} & \mathbf{S}_{13}^{II} & 0 & 0 \\ \mathbf{S}_{21}^{II} & \mathbf{S}_{22}^{II} & \mathbf{S}_{23}^{II} & 0 & 0 \\ \mathbf{S}_{31}^{II} & \mathbf{S}_{32}^{II} & \mathbf{S}_{33}^{II} & 0 & 0 \\ 0 & 0 & 0 & \mathbf{S}_{11}^{JJ} & \mathbf{S}_{12}^{JJ} \\ 0 & 0 & 0 & \mathbf{S}_{21}^{JJ} & \mathbf{S}_{22}^{JJ} \end{pmatrix} \begin{pmatrix} \dot{C}_1^{(I)}(t) \\ \dot{C}_2^{(I)}(t) \\ \dot{C}_3^{(I)}(t) \\ \dot{C}_1^{(J)}(t) \\ \dot{C}_2^{(J)}(t) \end{pmatrix} =$$

$$-i\left[\left[\begin{pmatrix} H_{11}^{II} & H_{12}^{II} & H_{13}^{II} & H_{11}^{IJ} & H_{12}^{IJ} \\ H_{21}^{II} & H_{22}^{II} & H_{23}^{II} & H_{21}^{IJ} & H_{22}^{IJ} \\ H_{31}^{II} & H_{32}^{II} & H_{33}^{II} & H_{31}^{IJ} & H_{32}^{IJ} \\ H_{11}^{JI} & H_{12}^{JI} & H_{13}^{JI} & H_{11}^{JJ} & H_{12}^{JJ} \\ H_{21}^{JI} & H_{22}^{JI} & H_{23}^{JI} & H_{21}^{JJ} & H_{22}^{JJ} \end{pmatrix} - i \begin{pmatrix} \dot{S}_{11}^{II} & \dot{S}_{12}^{II} & \dot{S}_{13}^{II} & 0 & 0 \\ \dot{S}_{21}^{II} & \dot{S}_{22}^{II} & \dot{S}_{23}^{II} & 0 & 0 \\ \dot{S}_{31}^{II} & \dot{S}_{32}^{II} & \dot{S}_{33}^{II} & 0 & 0 \\ 0 & 0 & 0 & \dot{S}_{11}^{JJ} & \dot{S}_{12}^{JJ} \\ 0 & 0 & 0 & \dot{S}_{21}^{JJ} & \dot{S}_{22}^{JJ} \end{pmatrix}\right]\begin{pmatrix} C_1^{(I)}(t) \\ C_2^{(I)}(t) \\ C_3^{(I)}(t) \\ C_1^{(J)}(t) \\ C_2^{(J)}(t) \end{pmatrix}\right]. \quad (35)$$

(The system of coupled AIMS equations grows each time a new TBF is spawned.) These two equations highlight the different treatment of the amplitudes in the single-trajectory picture of TSH and in the correlated-TBFs propagation of AIMS. By virtue of the ITA, no intra- or interstate interactions between trajectories are accounted for in TSH. As a direct consequence, the interstate couplings are strictly evaluated at the molecular configuration of trajectory [α] at time *t*, as given by the term $H_{[\alpha]}^{IJ}$, neglecting any form of decoherence of the nuclear wavepackets (Figure 7b). As mentioned before, decoherence is the Achilles' heel for surface hopping[144] if no *ad hoc* corrections are added to the amplitudes propagation.[93,97,100,145-146] In AIMS, even if the IFG is applied, the TBFs resulting from a given initial conditions remain potentially coupled *via* the intra- or interstate terms, H_{kl}^{II} or H_{kl}^{IJ} (Figure 7a) The TBFs can therefore visit different regions of the molecular configuration space, resulting in an improved description of the separation of nuclear wavepackets in different electronic states.

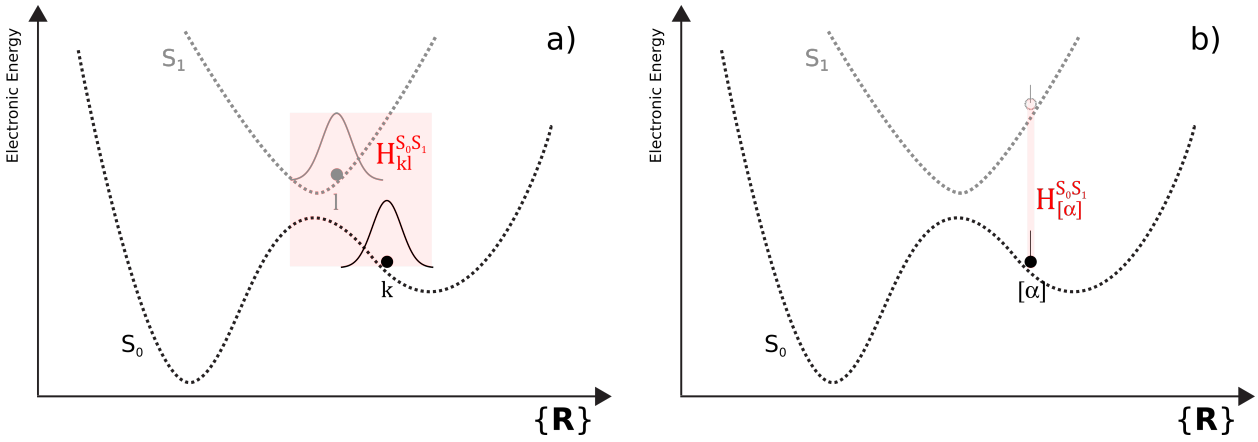

Figure 7. Snapshot of AIMS and TSH dynamics at a given time t. a) Inter- and intrastate couplings in FMS between two TBFs (l, k) evolving on different electronic states. b) Coherent propagation of the TSH amplitudes (vertical thin line) along the trajectory [α] running on state S_0 (filled black circle), implying that the amplitude on state S_1 is constrained to evolve on the support of a trajectory driven by a different electronic state (dashed empty circle).

5. Other flavors of quantum dynamics with Gaussian functions

FMS and AIMS portray the quantum dynamics of nuclear wavepackets by using an adaptive number of coupled Gaussian functions, whose centers and momenta are classically propagated. This results in a separation between the formal propagation of the grid elements (the classically-evolved Gaussian TBFs) and their associated coefficients (complex amplitudes evolved through the Schrödinger equation). The complex coefficients, as well as the time-dependent phases, do not affect the classical propagation of the TBFs, while the positions and momenta of the TBFs do determine the electronic structure quantities sampled for the integration of the Schrödinger equation.

In the following, we will discuss alternative techniques that differ from the AIMS in the way they treat the dynamics of the basis functions, and the entanglement between the basis functions and the complex coefficients. This section will mostly focus on ab initio techniques, i.e., those that are compatible with on-the-fly dynamics.

5.1 Multiconfigurational Ehrenfest method

The Multiconfigurational Ehrenfest[43,118,147] (MCE) technique proposes to represent the total molecular wavefunction as a combination of Ehrenfest wavefunctions. As discussed in Sec. 2.1, Ehrenfest dynamics emerges from a classical limit of the TDSCF equations, which represents the total molecular wavefunction as the simple product of a time-dependent electronic and nuclear wavefunction. As a result, the MCE molecular wavefunction reads

$$\begin{aligned}\Psi(\mathbf{r},\mathbf{R},t) &= \sum_{\beta}^{N_{ini}} C_{\beta}(t)\psi_{\beta}^{Ehr}(\mathbf{r},\mathbf{R},t) \\ &= \sum_{\beta}^{N_{ini}} C_{\beta}(t)\chi_{\beta}\left(\mathbf{R};\overline{\mathbf{R}}_{\beta}(t),\overline{\mathbf{P}}_{\beta}(t),\overline{\gamma}_{\beta}(t),\boldsymbol{\alpha}\right)\Phi_{\beta}^{el}(\mathbf{r};\mathbf{R},t)\end{aligned} \tag{36}$$

i.e., the total molecular wavefunction is given by a combination of Ehrenfest-like molecular wavefunctions (note that the Gaussian functions do not carry an electronic state label because each one is associated with a distinct coherent superposition of electronic states). Eq. (36) corresponds to the MCE molecular wavefunction presented in Ref. [44], which differs slightly from the one given in the original MCE paper[43] and leads to coupling between the trajectories. For the simple case of a two electronic state problem, the time-dependent electronic wavefunction becomes $\Phi_{\beta}^{el}(\mathbf{r};\mathbf{R},t) = c_{\beta}^{(1)}(t)\Phi_{\beta}^{(1)}(\mathbf{r};\mathbf{R}) + c_{\beta}^{(2)}(t)\Phi_{\beta}^{(2)}(\mathbf{r};\mathbf{R})$. Hence, a given Gaussian function β in the Ehrenfest wavefunction may (and often will) correspond to more than one electronic state. This is a major difference from FMS or AIMS, in which a TBF is assigned to a single electronic state. While a single element of the summation in Eq. (36) would suffer from the mean-field approximation inherent to Ehrenfest dynamics, the multiconfiguration representation allows one to target, in principle, an exact solution of the time-dependent Schrödinger equation.

Eq. (36) will give rise to equations of motion for the Gaussian function parameters, the N_{ini} Ehrenfest configuration amplitudes $\left\{C_\beta(t)\right\}_{\beta=1}^{N_{ini}}$, and the electronic coefficients $\left\{c_\beta^{(J)}(t)\right\}_{J=1}^{N_e}$ (one set for each Ehrenfest configuration, considering N_e electronic states). One central difference between MCE and FMS is the way the Gaussian functions evolve in time. In MCE, the dynamics follows Ehrenfest trajectories. In regions with strong nonadiabaticity, an Ehrenfest trajectory follows an average potential energy surface, given by a linear combination of the adiabatic PESs weighted by the electronic coefficients (Figure 8). In comparison, the classical propagation in FMS/AIMS is purely adiabatic (Figure 6). It is unclear which equations of motion are more accurate and this will likely depend on both the particular system and the time scale of the nonadiabatic interaction. Another technical yet practically important difference between the two techniques is that MCE does not use an adaptive basis set, i.e., all the basis functions required at time t need to be present at time $t=0$. As the basis functions in MCE evolve according to Ehrenfest dynamics, their spread is expected to be slower, and basis functions will remain coupled longer than with classical trajectories (as in FMS and AIMS). On the other hand, the mean-field potential generated in Ehrenfest dynamics might artificially trap trajectories and prevent a uniform sampling of the phase space visited by the true nuclear wavepacket. To remedy these issues, the Ab Initio Multiple Cloning[148-149] (AIMC), approach was proposed, combining features of MCE and AIMS. In AIMC, the basis functions are propagated along Ehrenfest trajectories, but a cloning process – similar to spawning – projects basis functions that are evolving on mean-field surfaces onto adiabatic electronic states, without altering the underlying nuclear wavepacket. As in spawning, the cloning procedure only alters the computational representation of the wavefunction and does not alter the wavefunction itself. The

AIMC and AIMS methods should both converge to the same result given sufficient basis functions. Indeed, this was demonstrated for the excited state population after photoexcitation of ethylene.[148] It remains an open question as to which of AIMS and AIMC converges more quickly. AIMC was also recently extended to the treatment of tunneling effects,[150] analogous to the procedure used to treat tunneling in AIMS.[151]

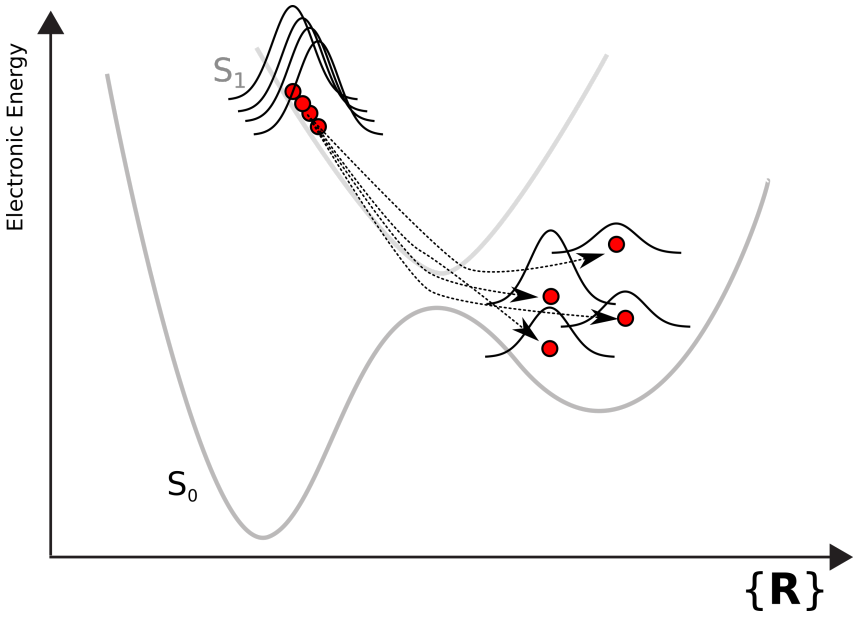

Figure 8. Schematic representation of a MCE run. A swarm of Gaussian functions follow mean-field (Ehrenfest) trajectories.

5.2 Variational Multiconfigurational Gaussians – vMCG

FMS and AIMS propagate Gaussian basis functions classically, while MCE employs Ehrenfest forces, which might better represent the short-time dynamics of nuclear wavepackets. Is there a way to define optimal trajectories for the basis functions, in the sense that would represent the optimal support for nuclear wavepackets at any time? The quantum equilibrium hypothesis[152] indicates that a ensemble of trajectories, initially represented according to

$|\Omega(\mathbf{R},t_0)|^2$, will remain $|\Omega(\mathbf{R},t)|^2$-distributed at any later time t if the ensemble follows quantum trajectories, whose driving equation for nuclei γ is given by

$$\frac{d\mathbf{R}_\gamma(t)}{dt}=\frac{1}{M_\gamma}\left[\frac{\Im\{\Omega^*(\mathbf{R},t)\nabla_\gamma\Omega(\mathbf{R},t)\}}{\Omega^*(\mathbf{R},t)\Omega(\mathbf{R},t)}\right]_{\mathbf{R}=\mathbf{R}(t)}=\left[\frac{\mathbf{J}_\gamma(\mathbf{R},t)}{|\Omega(\mathbf{R},t)|^2}\right]_{\mathbf{R}=\mathbf{R}(t)} \tag{37}$$

Eq. (37) expresses a nuclear velocity vector field from the nuclear current density (or quantum flux) $\mathbf{J}(\mathbf{R},t)$ divided by the nuclear probability density $|\Omega(\mathbf{R},t)|^2$.[152-153] An alternative way to define the optimal trajectories for a Gaussian basis set is to determine equations of motion for all the time-dependent parameters through the Dirac-Frenkel variational principle. Rooted in the MCTDH formalism, G-MCTDH proposes to replace some single-particle functions by Gaussian functions.[41] In the limit where all SPFs are replaced by Gaussian functions, the method is called variational Multi-Configurational Gaussian (vMCG), which is our focus in this section.[42,154]

5.2.1 Adiabatic dynamics within vMCG

Let us consider the general case of a nuclear wavefunction represented by N_b Gaussian functions (considering no correlation in the width matrix):

$$\begin{aligned}\Omega(\mathbf{R},t)&=\sum_i^{N_b}C_i(t)\tilde{\chi}_i(\mathbf{R},t)\\&=\sum_i^{N_b}C_i(t)\exp\left[\sum_\rho^{3N}\zeta_{i\rho}(t)R_\rho^2+\xi_{i\rho}(t)R_\rho+\eta_i(t)\right]\end{aligned} \tag{38}$$

Eq. (38) exploits the notation for Gaussian functions used in the vMCG literature. The form of Gaussian functions given in Eq. (38) corresponds to the definition given in Eq. (13) by using the following correspondences: $\zeta_{i\rho}(t)=-\alpha_{i\rho}(t)$, $\xi_{i\rho}(t)=2\alpha_{i\rho}(t)\bar{R}_{i\rho}(t)+i\bar{P}_{i\rho}(t)$, and

$\eta_i(t) = \sum_{\rho}^{3N}\left(-\alpha_{i\rho}(t)\overline{R}_{i\rho}^2(t) - i\overline{P}_{i\rho}(t)\overline{R}_{i\rho}(t)\right) + i\overline{\gamma}_i(t)$. These three parameters are grouped into a vector $\mathbf{\Lambda}_i(t) = \{\boldsymbol{\zeta}_i(t), \boldsymbol{\xi}_i(t), \eta_i(t)\}$.

If one uses Eq. (38) within the Dirac-Frenkel variational principle

$$\left\langle \delta\mathbf{\Omega} \middle| \left(\hat{H} - i\frac{\partial}{\partial t} \right) \middle| \mathbf{\Omega} \right\rangle_{\mathbf{R}} = 0 \tag{39}$$

we can extract equations for the propagation of $\{C_i(t)\}_{i=1}^{N_b}$ and $\{\mathbf{\Lambda}_i(t)\}_{i=1}^{N_b}$. The form of the equations of motion for the complex amplitudes is similar to Eq. (10). The fundamental difference between vMCG and FMS/AIMS/MCE occurs in the time-evolution equations for Gaussian parameters:

$$i\dot{\mathbf{\Lambda}} = \mathbf{A}^{-1}\mathbf{Y} \tag{40}$$

Elements of the matrix $\mathbf{A}$ and of the vector $\mathbf{Y}$ are given by

$$A_{k\sigma,i\sigma'} = C_k^*(t)C_i(t)\left(S_{ki}^{(\sigma\sigma')} - \left[\mathbf{S}^{(\sigma 0)}\mathbf{S}^{-1}\mathbf{S}^{(0\sigma')}\right]_{ki}\right) \tag{41}$$

$$Y_{k\sigma} = \sum_{i}^{N_b} C_k^*(t)C_i(t)\left(H_{ki}^{(\sigma 0)} - \left[\mathbf{S}^{(\sigma 0)}\mathbf{S}^{-1}\mathbf{H}\right]_{ki}\right) \tag{42}$$

where $S_{ki}^{(\sigma\sigma')} = \left\langle \frac{\partial\tilde{\chi}_k}{\partial\lambda_{k\sigma}} \middle| \frac{\partial\tilde{\chi}_i}{\partial\lambda_{i\sigma'}} \right\rangle_{\mathbf{R}}$, $S_{ki}^{(\sigma 0)} = \left\langle \frac{\partial\tilde{\chi}_k}{\partial\lambda_{k\sigma}} \middle| \tilde{\chi}_i \right\rangle_{\mathbf{R}}$, $H_{ki}^{(\sigma 0)} = \left\langle \frac{\partial\tilde{\chi}_k}{\partial\lambda_{k\sigma}} \middle| \hat{H} \middle| \tilde{\chi}_i \right\rangle_{\mathbf{R}}$, and $\lambda_{k\sigma}$ designates the σ-element of the $\mathbf{\Lambda}_k$ matrix. Hence, the variational character of vMCG leads to highly coupled equations for the Gaussian parameters (Figure 9), far from the simple classical or Ehrenfest propagation proposed by FMS/AIMS or MCE. Additional mathematical manipulations can be performed on Eq. (40) to reach a "CX" formalism, which presents numerical advantages and highlights the classical and non-classical parts of the equations of motion. The overall quantum propagation of Gaussian parameters leads to an improved distribution of the basis

functions, potentially covering a broader region of phase space than would be possible with the same number of classical trajectories. In addition, the non-classical propagation allows the basis functions to tunnel through barriers. We note that the width can be propagated using the time-dependent variational principle, but the dynamics can become numerically unstable and often frozen widths are used for vMCG simulations (which does not compromise the variational nature of the method).[42,103]

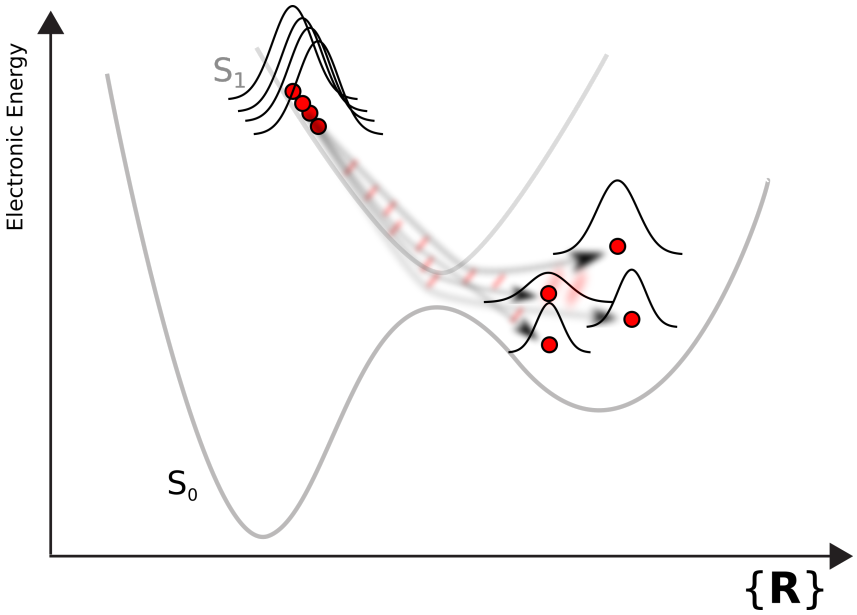

Figure 9. Schematic representation of a vMCG nonadiabatic dynamics in the single-set formalism. Blurred lines and arrows symbolize the coupling between the Gaussian functions and the resulting non-classical trajectories.

In Direct-Dynamics vMCG (DD-vMCG),[4,81,155-157] the quantum dynamics is performed on-the-fly by computing electronic structure quantities as needed at each time step. The Hamiltonian matrix elements are computed in a local harmonic approximation (LHA), which differs from the SPA discussed before by the fact that the Taylor expansion is performed around the center of the Gaussian function.[140] Using the LHA implies the expensive calculation of Hessians, in addition to energies and gradients.

5.2.2 Nonadiabatic dynamics within vMCG

Two different ways to extend vMCG to nonadiabatic dynamics have been proposed.[107] In the *multi-set* formalism, the total molecular wavefunction is expanded as in FMS, by using a linear combination of Gaussian functions to describe nuclear amplitudes on each electronic state,

$$\Psi(\mathbf{r},\mathbf{R},t)=\sum_{J}^{\infty}\sum_{i}^{N_J} C_i^{(J)}(t)\tilde{\chi}_i^{(J)}(\mathbf{R},t)\Phi_J(\mathbf{r};\mathbf{R}) \tag{43}$$

In this formalism, each (variationally-propagated) Gaussian function evolves on a given electronic state. In contrast, the *single-set* formalism employs a common set of Gaussian functions for all the electronic states, i.e., the molecular wavefunction is represented by

$$\Psi(\mathbf{r},\mathbf{R},t)=\sum_{J}^{\infty}\sum_{i}^{N_b} C_i^{(J)}(t)\tilde{\chi}_i(\mathbf{R},t)\Phi_J(\mathbf{r};\mathbf{R}) \tag{44}$$

Hence, the single-set formalism assumes that the nuclear wavefunctions for all different electronic states can be represented with a common set of N_b Gaussian functions, leading to a substantial reduction of the computational cost for direct dynamics by decreasing the number of Gaussian functions considered for a DD-vMCG run. Inserting Eq. (43) or Eq. (44) in the TDSE leads to equations of motion for the set of complex coefficients similar to those in FMS, with more complicated expressions for the overlap time-derivative matrix elements. Interestingly, it was shown that the *single-set* formalism leads to Ehrenfest dynamics upon applying a single configuration condition and a classical limit for the Gaussian basis function.[108]

6. Dissection of an Ab Initio Multiple Spawning Dynamics Simulation

The overall target of any ab initio nonadiabatic molecular dynamics is the *in silico* simulation of a complete photochemical or photophysical experiment. Before detailing how AIMS can be

used in this context, let us first start by summarizing the important steps of a typical photochemical experiment (Figure 10), highlighting the critical steps that we will need to address in an *in silico* experiment.

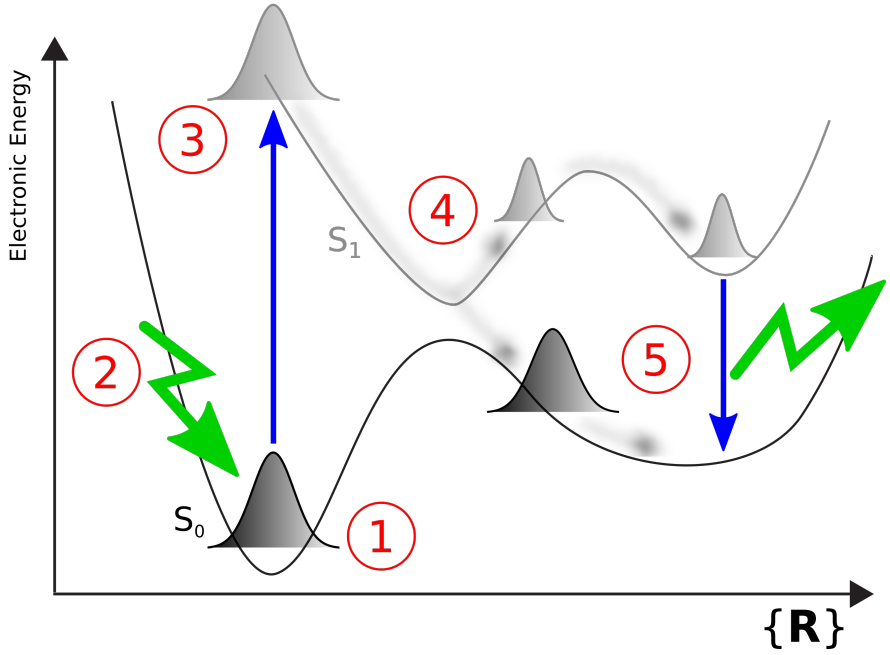

Figure 10. Different steps of an *in silico* photochemical experiment. A molecule in a given initial state (1) is photoexcited (2) and transferred to an excited electronic state (3), from which it relaxes nonadiabatically (4) until reaching either the ground electronic state or a low-lying excited state (5) from which radiative process could take place.

A molecular system is initially in its ground electronic state (step 1 in Figure 10). In a fully quantum picture at 0K, the molecule may furthermore be considered in its ground vibrational eigenstate. We can now imagine an external perturbation (step 2 in Figure 10). For the case of interest here – namely electronic photoexcitation – we consider that a UV/Vis laser pulse impinges on the molecule. The intensity and length of the laser pulse will obviously be key parameters to determine the photoexcitation process; these questions will be treated in the following. Upon light absorption, the molecule is excited into one of its electronic states based

on selection rules. In cases where an ultrashort laser pulse is used, the original ground vibrational eigenstate is projected onto a new electronic state. As the nuclear wavefunction is no longer a vibrational eigenstate of the excited electronic state – but rather a linear combination of vibrational eigenstates on this new electronic state, i.e. a nuclear wavepacket – it will evolve in time. This time-dependent relaxation of the nuclear wavepacket is precisely the point of interest for all the previously described methods. Its accurate description, beyond the Born-Oppenheimer approximation and possibly also beyond the non-relativistic limit (when spin-orbit coupling is considered), is step 4 in Figure 10. The nuclear wavepacket will likely reach regions where electronic states come close in energy, points where nuclear motion triggers coupling between electronic states and eventually leads to a splitting of the nuclear wavepacket into different components (in a Born-Huang picture, see Sec. 2.1). These nonradiative processes are fast, typically in the femto- to picosecond regime, and provide us with the timescale for *in silico* nonadiabatic simulations (step 5 in Figure 10). At later time, fluorescence or phosphorescence processes can take place, if part of the nuclear wavepacket remains on an excited electronic state.

This Section will discuss how the different steps described above can be translated into an *in silico* photochemical experiment. More specifically, we will present some additional features of the overall theory of AIMS described in the previous sections, and highlight recent developments aiming at extending AIMS dynamics to a wide variety of photochemical processes.

6.1 Initial Conditions

Often the desired initial state is either the molecule in its ground vibrational state or at a specified temperature. In AIMS, the TBFs follow classical trajectories and thus rapid convergence depends on a good choice of initial conditions (positions and momenta of the

TBFs). The essential issue is that there must be TBFs in regions of phase space that can represent the evolving nuclear wavefunction. In order to ensure that this is the case at time *t=0*, we sample the initial nuclear momenta and positions from a phase-space distribution corresponding to the desired initial quantum state. When the molecule is in its ground vibrational state, this implies sampling the positions and momenta for the initial TBFs from a Wigner distribution for the molecule in v=0, referred to as Ω_{S0}. The Wigner distribution is a phase space distribution corresponding to a desired wavefunction:[158-159]

$$W(\mathbf{R},\mathbf{P}) = \frac{1}{(2\pi)^{3N}}\int_{\infty}^{\infty} d\mathbf{s}\, \exp(i\mathbf{P}\cdot\mathbf{s})\left[\Omega_{S_0,v_0}(\mathbf{R}-\mathbf{s}/2)\Omega^{*}_{S_0,v_0}(\mathbf{R}+\mathbf{s}/2)\right] \qquad (45)$$

where Ω_{S_0,v_0} represents the ground-vibrational and -electronic nuclear wavefunction for the system with $3N$ dimensions, and $\mathbf{s}$ is a displacement vector. In short, the Wigner function is a pseudo phase-space distribution, which provides the position (momentum) distribution upon integration over momentum (position).

However, a numerically exact quantum description of the nuclear degrees of freedom is only possible for low-dimensional (or reduced-dimensional) systems. Hence, $\Omega_{S_0,v_0}(\mathbf{R})$ is in principle not available for most molecular applications, and the initial conditions need to be sampled from an approximate distribution. One way of extracting initial conditions – nuclear positions and momenta – is to sample them from a thermal distribution, for example by running a long ab initio molecular dynamics in the ground electronic state at a given temperature. While this protocol is easy to set up for molecules, one drawback is that the internal energy distribution for dynamics at 300K is too narrow with respect to the one expected at the zero-point energy (ZPE) of a molecule.[160] In other words, initial conditions sampled from an ab initio molecular dynamics are

likely to have a too narrow distribution in kinetic and potential energy. When projected onto an excited electronic state, such narrow distribution might alter the outcome of the simulation.[160]

One way to approximate a quantum distribution consists in approximating the Wigner distribution in Eq.(45) by representing $\Omega_{S_0,v_0}(\mathbf{R})$ as a product of uncoupled harmonic oscillator (UHO) eigenstates.[161] In other words, one can approximate the ground vibrational eigenstate of a molecule as the one for a combination of uncoupled oscillators, whose frequencies correspond to the molecular normal modes. In this case, an analytical solution exists for the Wigner distribution, which – in a normal mode representation – becomes[160-164]

$$W(\mathbf{R},\mathbf{P}) \approx \tilde{W}_{UHO}(\mathbf{R},\mathbf{P}) = \frac{1}{(\pi)^{3N-6}} \prod_{\rho}^{3N-6} \exp\left(-\frac{R_\rho^2}{2\sigma_{R\rho}^2}\right) \exp\left(-\frac{P_\rho^2}{2\sigma_{P\rho}^2}\right) \qquad (46)$$

where $\sigma_{R\rho}^2 = 1/2\mu_\rho\omega_\rho$ and $\sigma_{P\rho}^2 = \mu_\rho\omega_\rho/2$, i.e., nuclear positions and momenta are sampled independently. Generating Eq. (46) is therefore straightforward, as it only requires an equilibrium molecular geometry in the ground-electronic state and its corresponding normal mode analysis: frequency ω and reduced mass μ for each normal mode ρ. Initial positions and momenta can then be randomly sampled from Eq. (46), where $R_\rho = 0$ at the equilibrium geometry. This Wigner sampling can also be used to generate photoabsorption cross-sections.[165-166]

Strong approximations are nevertheless encoded in Eq. (46) when used for molecules. First, we employ a harmonic approximation for all modes, neglecting any anharmonicities – which is likely to be problematic for low-frequency modes for example.[167] Another critical problem is zero-point energy (ZPE) leakage: sampling initial conditions from Eq. (46) does generate a distribution whose average classical energy approaches the $v = 0$ energy of the quantum system,

but classical degrees of freedom can freely transfer this energy among each other, while such transfer is obviously regulated in quantum mechanics. Hence, energy from a given mode can be transferred to other modes, which leads to an imbalance considering that at least an amount equal to the ZPE should remain in any modes quantum mechanically. An extensive discussion on the sampling of initial conditions for nonadiabatic dynamics can be found in Ref. [103]. We finally note that employing the Wigner distribution obtained from classical adiabatic switching[168-169] would allow one to remove the uncoupled and harmonic approximations in the aforementioned sampling.

It is finally important to note that proper sampling of initial conditions is even more critical for methods like MCE and vMCG, which do not use an adaptive basis set and therefore keep the number of basis functions constant during the dynamics. Hence, the choice of the number of TBFs at time *t=0* as well as their initial placement is critical to ensure that the TBFs provide proper support for the nuclear wavepackets at later times. For more details, the reader is referred to Ref. [118], which discusses sampling in the context of MCE.

Having discussed the choice of initial $\bar{\mathbf{R}}$ and $\bar{\mathbf{P}}$ for the TBFs, one still needs to specify their Gaussian widths. A general protocol was recently proposed[170] to determine the frozen widths from simple frequency calculations in the ground electronic state. The protocol was tested for different molecules and the typical width obtained for a given atom is quite insensitive to the chemical environment. Furthermore, the resulting electronic population dynamics was found to be quite insensitive to the choice of widths, within the variability observed due to different bonding environments. Thus, standard values[170] for the widths depending only on atomic number can be used.

6.2 Excitation process

Once the initial conditions are selected, it remains to define how to account for the interaction with an external field triggering the electronic excitation. An obvious solution is to include the external field explicitly in the AIMS simulation (XFAIMS – eXternal Field AIMS),[171] which allows one to start the dynamics in the ground electronic state and explicitly simulate the photoexcitation process. This approach has also been explored for other trajectory-based nonadiabatic methods.[172-181] The light/matter interaction term, in the dipole approximation, can easily be included in the Hamiltonian matrix and the spawning algorithm modified accordingly. The influence of laser pulse characteristics – such as intensity, carrier-envelope phase (CEP), or duration – on the excitation process can also be studied in detail.

Nevertheless, first-order perturbation theory provides a justification for a rather simpler protocol to simulate photoexcitation.[103-104] Let us approximate a molecular system originally in its ground-electronic and vibrational state by $\Omega_{S_0,v_0}(\mathbf{R}) = \Omega^{(0)}_{S_0,v_0}(\mathbf{R})$, and apply an external time-dependent electric field $\underline{\mathbf{E}}(t)$, which will couple to the molecule through its transition dipole moment with an excited state S_1, $\underline{\boldsymbol{\mu}}_{S_1S_0}(\mathbf{R})$ (we consider the field aligned with the transition dipole moment for simplicity). The first-order correction to the nuclear wavefunction only contains a contribution for the excited state part and reads

$$\begin{aligned}\Omega^{(1)}_{S_1}(\mathbf{R},t) &= \frac{1}{i}\int_0^t dt' \exp\left(-i\hat{H}_{S_1}(t-t')\right)\left(-\mu_{S_1S_0}(\mathbf{R})E(t')\right)\exp\left(-i\hat{H}_{S_0}t'\right)\Omega_{S_0,v_0}(\mathbf{R}) \\ &= -\frac{1}{i}\int_0^t dt' E(t')\exp\left(-iE_{S_0,v_0}t'\right)\exp\left(-i\hat{H}_{S_1}(t-t')\right)\left(\mu_{S_1S_0}(\mathbf{R})\Omega_{S_0,v_0}(\mathbf{R})\right)\end{aligned} \tag{47}$$

We therefore have the physical interpretation that upon excitation an initial state is given by $\mu_{S_1S_0}(\mathbf{R})\Omega_{S_0,v_0}(\mathbf{R})$. If in addition one considers a sudden laser pulse, $E(t') = \delta(t'-t_1)$, we obtain

$$\Omega_{S_1}^{(1)}(\mathbf{R},t) = -\frac{1}{i}\exp\left(-iE_{S_0,v_0}t_1\right)\exp\left(-i\hat{H}_{S_1}(t-t_1)\right)\left(\mu_{S_1S_0}(\mathbf{R})\Omega_{S_0,v_0}(\mathbf{R})\right) \quad (48)$$

which describes the generation and evolution of the initial state, given by $\mu_{S_1S_0}(\mathbf{R})\Omega_{S_0,v_0}(\mathbf{R})$, on the excited electronic state S_1.

This description of photoexcitation by a short laser pulse implies that we can describe the initial nuclear wavepacket in the excited state as the ground-state eigenstate multiplied by the corresponding transition dipole moment. The Condon approximation proposes that the latter can be considered as a constant in the Franck-Condon region, i.e., $\mu_{IS_0}(\mathbf{R}) \approx \mu_{IS_0}$. Hence, a good approximation to this initial state would be to generate a given quantum distribution for the ground state (see previous Section) and to simply promote it to the desired excited state. This process is actually the most commonly employed in trajectory-based and trajectory-guided simulations. Alterations of this protocol are possible if the nuclear wavepacket is initially distributed among more than one excited electronic state after the pulse. We note that Heller used this sudden generation of a nuclear wavepacket onto a given electronic state as a way to compute vibrationally-resolved electronic absorption spectra, obtained from the Fourier transform of the autocorrelation function of the time-dependent nuclear wavepacket with itself at time *t=0*.[182]

6.3 Electronic structure methods for excited electronic states

We give in this section a brief discussion related to electronic structure calculations. Until now, we have indeed always considered that electronic structure quantities like electronic energies, nuclear forces, or nonadiabatic coupling vectors were provided. In AIMS, all these quantities will be computed on-the-fly for each TBF – for their classical propagation, to monitor potential new spawning events, and for the Hamitonian matrix – but also at the centroid positions

between TBFs – to couple TBFs through the Hamiltonian matrix. We here summarize the range of electronic structure methods that were interfaced with AIMS.

Key to all on-the-fly nonadiabatic methods is determining the best compromise between the accuracy of the electronic structure method and its computational efficiency.[183] The level of electronic structure theory should be sufficient to capture the different features of all involved electronic states not only in the Franck-Condon region, but also over a large range of the configuration space visited by the nuclear wavepackets. At the same time, the computational cost should be minimized as much as possible to allow for simulation of realistic molecules over timescales ranging from tens to thousands of femtoseconds.

Numerous excited-state dynamics were carried out with multiconfigurational methods like state-averaged complete active space self-consistent field (SA-CASSCF).[184] While it largely neglects dynamic correlation for practically-accessible active spaces, SA-CASSCF often provides a qualitatively correct picture of excited-states topology and their crossings and led to numerous successful simulations when combined with AIMS,[127,185] DD-vMCG,[42,186-193] or MCE.[147,194-195] Achieving accurate results with SA-CASSCF depends on judicious choice of the active space (number of orbitals and number of electrons) as well as the number of electronic states included in the averaging procedure. Previous AIMS simulations[143,196-198] invariably determined these parameters by validation with more accurate methods capable of describing dynamic correlation, and thus the results are often much more reliable than might otherwise be expected from CASSCF with standard choices of active space. Such validation would also benefit other nonadiabatic dynamics methods using SA-CASSCF or other necessarily approximate electronic structure methods.

Multi-state complete active space perturbation of second order (MS-CASPT2)[199] includes dynamic correlation effects through perturbation theory in a multistate approach. Its copmputational cost precluded its use in early nonadiabatic dynamics simulations. However, numerous applications of AIMS/MS-CASPT have now been reported,[200-206] aided by the development of schemes to obtain analytic gradients[207] and nonadiabatic coupling vectors.[203,208] Recent work shows the direct effect of dynamic correlation on AIMS dynamics for a model of retinal, trans-PSB3.[202] An alternative to MS-CASPT2 is Multi-Reference Configuration Interaction (MRCI), which also benefits from efficient implementations of analytical gradients and nonadiabatic coupling vectors.[209-210] MRCIS and MRCISD have been extensively used in combination with trajectory surface hopping[102,211-212] and with AIMS dynamics,[46,143,213-214] but its computational cost limits the size of the molecules that can be simulated. The extended multi-state complete active space second-order perturbation theory (XMS-CASPT2),[215-216] which offers a more robust description of conical intersections than MS-CASPT2,[217] has recently been used in combination with TSH.[218]

Reparametrized semiempirical methods have enabled highly efficient AIMS simulations for large molecules and condensed phases.[219-220] Linear-response time-dependent density functional theory (LR-TDDFT)[221-224] also offers an interesting compromise between efficiency and accuracy for excited-state dynamics.[11,101,225] However, its practical approximations can lead to severe deficiencies when describing charge-transfer or doubly-excited states, as well as conical intersections between the ground and first-excited electronic states.[224,226-228]

AIMS has been interfaced with different electronic structure codes like Columbus,[229] GAMESS,[230] Molpro,[127] Mopac,[231] and TeraChem.[232-235] A significant advance towards improving both accuracy and efficiency in excited-state dynamics has recently been obtained by

redesigning the algorithms behind excited state electronic structure methods as LR-TDDFT,[236] CASCI,[237] SA-CASSCF,[238-239] and FOMO-CASCI[240-241] for use with graphical processing units (GPUs).[232-235] The first GPU-accelerated AIMS dynamics were recently reported using SA-CASSCF[185] and LR-TDDFT.[242]

6.4 Nonadiabatic Dynamics

Once the initial conditions have been generated and the electronic structure method selected, Ab Initio Multiple Spawning dynamics *per se* can be initiated. Within the IFG (Sec. 4.3), each parent TBF is run independently. Hence, a typical AIMS run starts with one TBF in the selected excited electronic state, with nuclear positions and momenta sampled from the appropriate Wigner distribution on the ground state. Electronic structure quantities will be computed on-the-fly. At this early stage where only one TBF is present, electronic energies are used in the equation of motion for the complex coefficients, Eq.(18) within the saddle-point approximation described in Sec. 4.3, and for the corresponding phase, while nuclear gradients are required for the classical propagation of the TBF. Nonadiabatic coupling vectors at the TBF center are also computed to monitor the value of Λ^{eff} and to detect potential spawning regions.

Once a nonadiabatic region is detected, the spawning mode described in Sec. 4.2 is activated, potentially resulting in the generation of a new TBF in the coupled electronic state. The dynamics becomes more involved, as two TBFs have to be propagated classically, and coupled through Eq.(18), which is now composed of (2×2) matrices. Off-diagonal elements of the Hamiltonian matrix are evaluated within the saddle-point approximation (Sec. 4.3), which implies additional electronic structure calculations for the nonadiabatic coupling vectors at the centroid position (if the two TBFs are on different electronic states). Electronic phase is

monitored – through overlap of the electronic wavefunction at the previous and current time step – and propagated along each TBF and ensure a proper description of interference effects.

The spawning mode described in Sec. 4.2 is the simplest possible and prevents overly rapid growth of the number of TBFs.[127] Alternative spawning modes have been proposed,[112-113,126,132-133,243] including a version where TBFs are not only created at the maximum of the function Λ^{eff}, but also at the entry point and once the maximum of couplings is passed (this last region is defined by an additional exit threshold).[112] Three TBFs would therefore be created for a single entrance in the spawning mode, leading to an improved description of the nonadiabatic transfer of amplitudes, at a clear increase in computational cost. The spawning mode is primarily an algorithm to ensure proper generation of additional TBFs – the overall amplitude transfer is dictated by the TDSE. This is in contrast to surface hopping, where the hopping algorithm must accurately encode the physics of the nonadiabatic transitions including not only where the hops occur but also how often. Because of this, many optimizations can be envisaged to maximize the efficiency and accuracy of TBF creation in spawning, while there is less opportunity for such enhancements in surface hopping. The *optimal* spawning method was introduced as an algorithm ensuring a compromise between the best position and the best momentum for the newly created TBF.[132] In optimal spawning, the position and momentum of the new TBF are varied to maximize the overlap between the parent and child TBFs and to minimize their energy difference, hence eliminating any predefined conditions for the generation of the child TBF. We finish this paragraph on a numerical detail regarding the number of TBFs in the simulation. Let us consider an AIMS run where several TBFs are evolving on the same electronic state. As the *classical* propagation of each TBF is performed *independently* from all other TBFs, nothing prevents them from strongly overlapping. However, large overlaps between different TBFs in the

same electronic state will lead to linear dependencies in the overlap matrix $\mathbf{S}$, eventually causing numerical instabilities as the propagation of the complex coefficients in AIMS requires[244] the calculation of $\mathbf{S}^{-1}$ (see Eq. (18)).[245-246] AIMS employs a simple regularization to circumvent this issue,[109,112] but more involved techniques have been proposed in the broader context of quantum dynamics with Gaussian functions.[139,247-248]

While the coupling between TBFs as described in AIMS and FMS formally allows for the description of quantum tunneling, the practical use of classical trajectories to propagate the TBFs intrinsically limits them to exploration of classically-allowed regions of phase space. Gaussian functions propagated within the vMCG method can, on the other hand, reach non-classical regions thanks to the quantum propagation of the Gaussian parameters.[107,249] The spawning idea, nevertheless, offers ways to describe tunneling effects in FMS and AIMS by adding a same-state spawning criterion.[113,151] A similar strategy as the one described in Sec. 4.2 for nonadiabatic events can be applied (Figure 11): detection of the need for basis set expansion in case of tunneling events and generation of initial conditions for the newly spawned TBF, using a simple protocol that takes advantage of the local nature of the TBFs. The detection of tunneling events is based on the idea of labeling tunneling particles, as well as acceptor and donor sites where the tunneling particle might be attached. The same-state spawning algorithm detects potential tunneling events whenever the distance between a tunneling particle and its donor exceed a given threshold (Figure 11a). At this stage, all the potential acceptor particles are detected, and a set of structures with the tunneling particle placed close to each acceptor particle is generated and minimized. A tunneling vector – connecting the original TBF to the minimized structure – is defined for each structure whose energy is lower than the energy of the current TBF. The original TBF is then propagated classically and monitored, for each minimum. If during this

classical propagation, a geometry is encountered where the tunneling particle is closer to the new minimum than to the original one, the minimum is discarded as it implies that a classical path is possible. On the other hand, if a turning point along the tunneling vector is found, the TBF is shifted along this vector until the next classical region is found (Figure 11b). Backpropagation is then performed from this current time back to the time when the spawning mode was entered (Figure 11c). A given number of new TBFs will be spawned with zero population during this

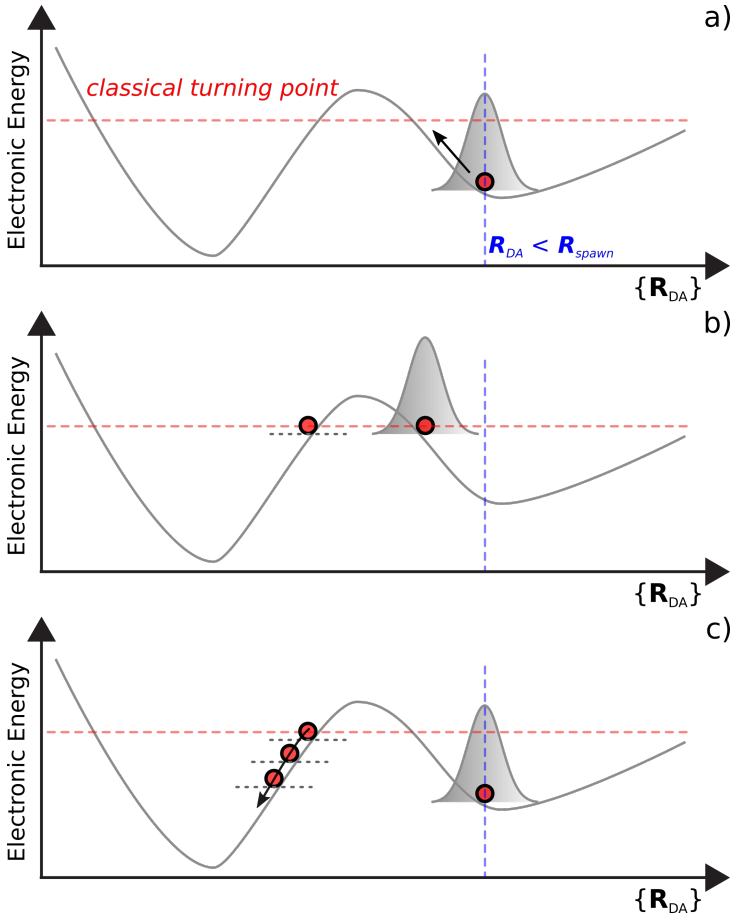

Figure 11. Schematic representation of the intrastate spawning algorithm accounting for tunneling effects. a) A TBF reaches a region where the distance between donor (D) and acceptor (A) is lower than a given threshold, triggering the spawning mode. If tunneling is detected, the TBF evolves until reaching a classical turning point along the tunneling direction. Then a new TBF with zero amplitude is spawned along the tunneling direction on the other side of the barrier. c) Backpropagation is performed for both the parent and the child TBF. A number of new children TBFs are spawned during the backpropagation step to ensure adequate support for the tunneling process. The multiple spawning dynamics can then restart, including all the newly created TBFs.

backpropagation (Figure 11c), and their initial momenta and coordinates are determined from a backpropagated trajectory originating from the point where the new classically allowed region was located. Once the backpropagation done, the FMS/AIMS run can proceed with the addition of the new TBFs.

Photogenerated electron transfer or long-range energy transfer processes have been extensively investigated due to their importance for solar-energy harvesting devices. However, the underlying photophysical mechanisms are challenging due to the potentially weak diabatic coupling between the electronic states describing the energy or electron transfer, leading to the presence of *trivially unavoided crossings* (TUCs).[250-253] TUCs can be thought of as conical intersections, for which one of the coordinates in the branching plane only very weakly lifts the degeneracy due to a (nearly or exactly) vanishing diabatic coupling between the electronic states. This implies that TUCs appear in the adiabatic representation as 3*N*-7 dimensional seams of intersection (in contrast, conical intersections form 3*N*-8 dimensional seams), exhibiting extremely large and extremely localized nonadiabatic couplings (Figure 12).

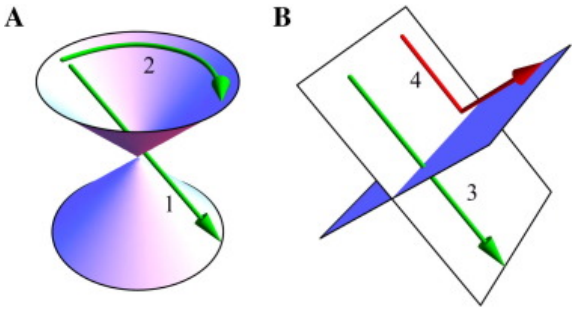

Figure 12. A. Dynamics around a conical intersection, where diabatic transfer (1) or adiabatic passage (2) of the nuclear wavepacket are both possible. B. In the case of a TUC, only the purely diabatic transfer (3) is possible because the coupling term is exactly zero or negligible. Reproduced with permission from Ref. [254]. Copyright 2015, Elsevier.

A nuclear wavepacket reaching a TUC region will be entirely transferred to the coupled adiabatic state, preserving its diabatic character. This phenomenon is especially surprising when

it leads to significant nonadiabatic transitions from a lower electronic state to an upper electronic state and has been called "upfunnelling" or "diabatic trapping" in these cases.[46,255-258] Certain nonadiabatic molecular dynamics methods can miss those localized regions for numerical reasons, and one way to monitor the presence of TUCs is by looking for abrupt changes in the electronic wavefunction of the running state – *via* wavefunction overlap at different time steps – testing for a rapid change of the corresponding electronic character.[127,259-260] Based on those considerations and the development of a norm-preserving interpolation strategy for the calculation of time-derivative couplings,[261] AIMS was adapted to efficiently detect and properly describe TUCs.[254]

Until now, we have only discussed *internal conversion* processes, which are nonradiative transitions between electronic states sharing the same spin-multiplicity. Different nonadiabatic methods like TSH[167,176-177,262-265] or MCTDH[266] were extended to include *intersystem crossing* events, i.e., transitions that involve spin changes mediated by spin-orbit coupling.[267] A recent extension of AIMS, termed *generalized* AIMS (GAIMS),[268] uses TBFs that encode, in addition to an electronic state, a given spin state and projection (depicted in Figure 13 by different line style for the TBF evolving on the triplet state T_n).

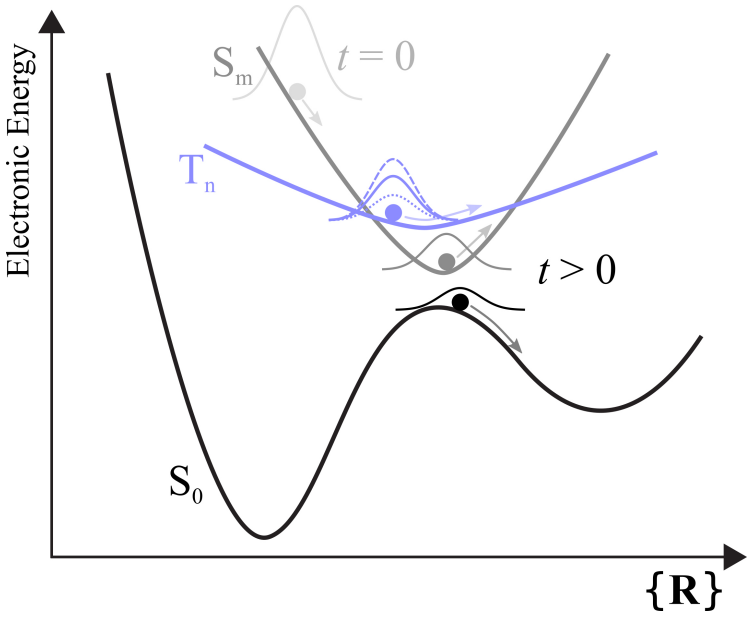

Figure 13. Schematic representation of GAIMS. An initial singlet TBF (gray) is evolving on S_m and will spawn new TBFs on S_0 (black) – internal conversion – and on the triplet state T_n (blue) as a result of spin-orbit coupling – intersystem crossing. The superimposed Gaussian shapes on the triplet TBF (blue) represents the different sublevels (m_s values) of the triplet state. Reproduced with permission from Ref. [268]. Copyright 2013, AIP Publishing.

The coupling pattern between TBFs is more complex due to the addition of spin-orbit coupling and the appearance of spin sublevels for each electronic state, but the formalism is easily extended to accommodate spin variables. The spawning algorithm is simply modified by monitoring an effective diabatic coupling between states of different spin multiplicity, containing spin-orbit coupling.

We have so far made no mention of the molecular environment, i.e. whether the chromophore was in isolation, surrounded by solvent, or embedded in a protein matrix. The challenge of describing the environment of an excited molecule has stimulated the development of various techniques, from implicit solvent models adapted to the calculation of electronically excited states[269-272] to explicit solvent methods, ranging from a purely classical description (QM/MM) to more accurate models like polarizable force fields, effective fragment potentials,[273] fragment molecular orbitals,[274] or embedding strategies.[275-277] The QM/MM technique is by far

the most common way of explicitly including the effect of neighboring molecules in the excited state of a molecule,[278-283] and has been implemented within different nonadiabatic dynamics schemes.[220,231,284-286] While a purely classical QM/MM description with the usual fixed-charge empirical force fields offers a cost-effective way of coupling the molecule of interest to its environment, it neglects the role of rapid electronic polarization of the solvent in response to changes in the electronic character of the photoexcited molecule. Techniques such as polarizable force fields[287] include a description of these effects, at a larger computational cost. AIMS dynamics can easily be combined with QM/MM to account for the role of solvent or protein environment.[127,220,231,288-290] All atoms in the simulation take part in the TBFs, and spawning results in new TBFs with a quantum mechanical description encompassing the entire solute/solvent system. In other words, despite the classical treatment of the environment from an electronic perspective, the AIMS nuclear dynamics treats all nuclei quantum mechanically. Hence, AIMS with QM/MM accounts for the effect of the environment on the coherence/decoherence of the nuclear wavepackets on different electronic states.

6.5 Convergence and analysis of results

The AIMS dynamics resulting from a given parent TBF is often denoted as an "AIMS run." Within the IFG approximation, one should average over many such runs to obtain converged results. The convergence of the results for any given observable can be determined by statistical analyses, analogous to standard ones used for classical trajectories. In low-dimensional model systems, convergence of the population dynamics with FMS has been demonstrated[112,243] after a few tens of initial conditions, i.e. "AIMS runs."

The analysis of a set of AIMS runs is somewhat more involved than methods based on classical trajectories such as surface hopping. In TSH, each trajectory has an equivalent weight in the simulation and all inter-trajectory coupling is neglected. Thus, the value of any observable is obtained by simple unweighted averaging of the observable over all trajectories. In FMS and AIMS, one needs to consider all coupled TBFs together and different TBFs will usually have different weights. For a general operator $\hat{O}$, the FMS time-dependent expectation value based on Eq. (26) reads

$$O(t)=\frac{\left\langle \Psi(t)\middle|\hat{O}\middle|\Psi(t)\right\rangle_{\mathbf{R},\mathbf{r}}}{\left\langle \Psi(t)\middle|\Psi(t)\right\rangle_{\mathbf{R},\mathbf{r}}}=\frac{\sum_{\beta\beta'}^{N_{ini}}\sum_{JI}^{N_{state}}\sum_{ij}^{N_J^\beta(t)N_I^{\beta'}(t)}\left(C_{i\beta}^{(J)}(t)\right)^* C_{j\beta'}^{(I)}(t)\left\langle \Phi_J^\beta\chi_{i\beta}^{(J)}(t)\middle|\hat{O}\middle|\chi_{j\beta'}^{(I)}(t)\Phi_I^{\beta'}\right\rangle_{\mathbf{R},\mathbf{r}}}{\sum_{\beta\beta'}^{N_{ini}}\sum_{JI}^{\infty}\sum_{ij}^{N_J^\beta(t)N_I^{\beta'}(t)}\left(C_{i\beta}^{(J)}(t)\right)^* C_{j\beta'}^{(I)}(t)S_{i\beta j\beta'}^{JI}(t)\delta_{JI}} \tag{49}$$

Within the IFG, where the different initial conditions are uncoupled, Eq. (49) becomes

$$O(t)\approx\frac{1}{N_{ini}}\sum_{\beta}^{N_{ini}}\left[\frac{\sum_{JI}^{N_{state}}\sum_{ij}^{N_J^\beta(t)N_I^\beta(t)}\left(C_{i\beta}^{(J)}(t)\right)^* C_{j\beta}^{(I)}(t)\left\langle \Phi_J^\beta\chi_{i\beta}^{(J)}(t)\middle|\hat{O}\middle|\chi_{j\beta}^{(I)}(t)\Phi_I^\beta\right\rangle_{\mathbf{R},\mathbf{r}}}{\sum_{JI}^{\infty}\sum_{ij}^{N_J^\beta(t)N_I^\beta(t)}\left(C_{i\beta}^{(J)}(t)\right)^* C_{j\beta}^{(I)}(t)S_{i\beta j\beta}^{JI}(t)\delta_{JI}}\right] \tag{50}$$

For a given AIMS run β, the population in electronic state *I*, $\hat{O}\equiv\hat{P}_I^\beta=\left|\Phi_I^\beta\right\rangle\left\langle\Phi_I^\beta\right|$, is therefore

$$\begin{aligned}P_I^\beta(t)&=\sum_{JK}^{N_{state}}\sum_{jk}^{N_J^\beta(t)N_K^\beta(t)}\left(C_{j\beta}^{(J)}(t)\right)^* C_{k\beta}^{(K)}(t)\left\langle \Phi_J^\beta\chi_{j\beta}^{(J)}(t)\middle|\hat{P}_I^\beta\middle|\chi_{k\beta}^{(K)}(t)\Phi_K^\beta\right\rangle_{\mathbf{R},\mathbf{r}}\\&=\sum_{ij}^{N_I^\beta(t)}\left(C_{i\beta}^{(I)}(t)\right)^* C_{j\beta}^{(I)}(t)\left\langle \chi_{i\beta}^{(I)}(t)\middle|\chi_{j\beta}^{(I)}(t)\right\rangle_{\mathbf{R}}\\&=\sum_{ij}^{N_I^\beta(t)}\left(C_{i\beta}^{(I)}(t)\right)^* C_{j\beta}^{(I)}(t)S_{i\beta j\beta}^{II}(t)\end{aligned} \tag{51}$$

where we neglect the denominator since the wavefunction is normalized and this normalization is preserved by FMS and AIMS. After averaging over all the initial conditions, we obtain

$$P_I(t) = \frac{1}{N_{ini}} \sum_{\beta}^{N_{ini}} \sum_{ij}^{N_I^\beta(t)} \left(C_{i\beta}^{(I)}(t)\right)^* C_{j\beta}^{(I)}(t) S_{i\beta j\beta}^{II}(t) \tag{52}$$

More care is required for operators that depend explicitly on the nuclear positions. As an example, we consider the case of the dipole moment operator $\hat{O} \equiv \hat{\mu} = \sum_{\alpha}^{N_N} Z_\alpha \hat{\mathbf{R}}_\alpha - \sum_{\lambda}^{N_{elec}} \hat{\mathbf{r}}_\lambda = \hat{\mu}_N - \hat{\mu}_e$ which (within the IFG) becomes

$$\mu(t) = \frac{1}{N_{ini}} \sum_{\beta}^{N_{ini}} \sum_{JI}^{N_{state}} \sum_{ij}^{N_J^\beta(t)} \left(C_{i\beta}^{(J)}(t)\right)^* C_{j\beta}^{(I)}(t) \left[\left\langle \chi_{i\beta}^{(J)}(t) \middle| \hat{\mu}_N \middle| \chi_{j\beta}^{(I)}(t) \right\rangle_{\mathbf{R}} \delta_{JI} - \left\langle \chi_{i\beta}^{(J)}(t) \middle| \mu_{IJ}^{e\beta} \middle| \chi_{j\beta}^{(I)}(t) \right\rangle_{\mathbf{R}} \right] \tag{53}$$

where $\mu_{IJ}^{e\beta}(\mathbf{R}) = \left\langle \Phi_J^\beta \middle| \hat{\mu}_e \middle| \Phi_I^\beta \right\rangle_{\mathbf{r}}$ is the electronic (transition) dipole moment and exhibits a nuclear dependence through the parametric $\mathbf{R}$ dependence of the electronic wavefunctions. Therefore, while the first integral in the square bracket of Eq. (53) can be evaluated analytically, the integral depending on the electronic (transition) dipole moment requires knowledge of this electronic quantity over the entire nuclear configuration space. The saddle-point approximation can be used here, resulting in the final equation

$$\mu(t) = \frac{1}{N_{ini}} \sum_{\beta}^{N_{ini}} \sum_{JI}^{\infty} \sum_{ij}^{N_J^\beta(t)} \left(C_{i\beta}^{(J)}(t)\right)^* C_{j\beta}^{(I)}(t) \left[\left\langle \chi_{i\beta}^{(J)}(t) \middle| \hat{\mu}_N \middle| \chi_{j\beta}^{(I)}(t) \right\rangle_{\mathbf{R}} \delta_{JI} - \mu_{IJ}^{e\beta}\left(\bar{\mathbf{R}}_{ij}^{(JI)}\right) S_{i\beta j\beta}^{JI}(t) \right] \tag{54}$$

which requires calculations of additional quantities (dipole moments) at the centroid positions between each pair of TBFs. Many of these will not need to be evaluated because the overlap integral is small when the TBFs are far from each other.

We denote the analysis in Eq. (49) as a *fully coherent analysis* because it includes all the phase relationships and interferences between pairs of TBFs included in the FMS or AIMS dynamics. Within the IFG, interferences between TBFs resulting from different initial parent TBFs are neglected and this should also be reflected in the subsequent analysis. This leads to

Eq. (50) which neglects off-diagonal matrix elements corresponding to TBFs that belong to different parent initial conditions. In many cases, the overlap between TBFs decays rapidly, even for TBFs originating from the same initial condition. When the overlap between TBFs is very small, a *fully incoherent analysis* can be a good approximation to Eq. (49), considering only diagonal terms, i.e.,

$$O(t) \approx \frac{1}{N_{ini}} \sum_{\beta}^{N_{ini}} \left[\frac{\sum_{I}^{N_{state}} \sum_{j}^{N_I^\beta(t)} \left| C_{j\beta}^{(I)}(t) \right|^2 \left\langle \Phi_I^\beta \chi_{j\beta}^{(I)}(t) \middle| \hat{O} \middle| \chi_{j\beta}^{(I)}(t) \Phi_I^\beta \right\rangle_{\mathbf{R},\mathbf{r}}}{\sum_{I}^{N_{state}} \sum_{j}^{N_I^\beta(t)} \left| C_{j\beta}^{(I)}(t) \right|^2} \right] \tag{55}$$

In this case, one should always include the normalization factor in the denominator because the dynamics always includes explicit calculation of the TBF overlap arising from the nonorthogonality of the Gaussians. Therefore, it is $\sum_{JI}^{N_{state}} \sum_{ij}^{N_J^\beta(t) N_I^\beta(t)} \left(C_{i\beta}^{(J)}(t) \right)^* C_{j\beta}^{(I)}(t) S_{i\beta j\beta}^{JI}(t) \delta_{JI} = 1$ which is guaranteed by the dynamics, and $\sum_{I}^{N_{state}} \sum_{j}^{N_I^\beta(t)} \left| C_{j\beta}^{(I)}(t) \right|^2$ can deviate from unity. We note that the expression $n_{j\beta}^{(I)}(t) = \sum_{i}^{N_I^\beta(t)} \mathrm{Re}\left(\left(C_{i\beta}^{(I)} \right)^* S_{i\beta j\beta}^{II} C_{j\beta}^{(I)} \right)$ is often called the "TBF population," reducing to $n_{j\beta}^{(I)}(t) = \left| C_{j\beta}^{(I)}(t) \right|^2$ when all inter-TBF overlaps are negligible.[291]

The rapid decay of the overlap between TBFs – implying that their interference is no longer important – can be exploited and used to define a "death process" for the TBFs in an AIMS run. Whenever groups of TBFs (or single TBFs) become uncoupled, their dynamics could be carried out independently with no ill effects. Therefore, we can stochastically select one of these groups to carry on the dynamics. Upon averaging many such cases, the overall dynamics will be

equivalent to a traditional AIMS run. This stochastic selection AIMS (SSAIMS) substantially limits the number of TBFs propagated during an AIMS run, while preserving an accurate description of nonadiabatic transfer (as TBFs in those regions are by definition strongly coupled).

7. Selected applications of Ab Initio Nonadiabatic Quantum Molecular Dynamics

We now turn to selected applications of AIMS, AI-MCE, and (DD-)vMCG to molecular photochemistry and photophysics. These examples aim at showcasing the descriptive – and in some cases demonstrably predictive – power of current ab initio nonadiabatic quantum molecular dynamics techniques.

7.1 Ab Initio Multiple Spawning

AIMS has been applied to the photochemistry of a large number of molecules, as testified by Table 1. Ethylene (C_2H_4) constitutes a typical example of the accuracy achieved by AIMS, not only to describe the nonadiabatic molecular quantum dynamics of this molecule, but also to reproduce and predict experimental observables. The excited-state dynamics of this prototypical molecule for double bond isomerization has been studied by a range of methods.[143,201,203,205-206,213,292-296] When combined with MS-CASPT2,[201] AIMS offers unprecedented accuracy to describe the excited-state dynamics and the lifetime of ethylene upon photoexcitation to its $\pi\pi^*$ electronic state.[206] Direct comparison with experimental observables has been achieved by predicting a femtosecond time-resolved photoelectron spectrum from AIMS dynamics, which was in excellent agreement with the measured total ion yield from a VUV/VUV pump-probe experiment. Not only did AIMS/MS-CASPT2 reproduce experimental observables, but it also

shed light on long-standing discrepancies between theory and experiment about ethylene excited-state lifetime. Indeed, excited-state dynamics simulations have predicted a lifetime ranging from 89 to 180 fs for the S_1 electronic state of ethylene, whereas experimental measurements indicate a faster relaxation of 50 fs or less. Calculations of the total ion yield based on MS-CASPT2/AIMS, however, revealed that the photoexcited ethylene visits regions of the S_1 configuration space where the experimental 7.7 eV probe pulse was insufficiently energetic to induce ionization. Therefore, experimental lifetimes based on the decay of the measured photoion yield could not be directly related to the actual population decay from S_1 but instead provided a lower bound. AIMS was also used to predict a time-dependent photoelectron kinetic energy distribution (right panel of Figure 14).[203] The corresponding experiment was performed several years later (left panel of Figure 14),[297] and largely reproduced the predicted ultrafast decrease of the photoelectron kinetic energy (PKE) spectra predicted by AIMS.

Table 1. Summary of AIMS Calculations Reported in the Literature.

Molecule	Electronic Structure Method	References
Azobenzene	SA-CASSCF	[298]
	Semiempirical method	[219]
Bridged azobenzene	SA-CASSCF	[299]
***trans-p*-coumaric acid chromophore**	SA-CASSCF	[256]
	SA-CASSCF + point charge	[300]
Malonaldehyde	SA-CASSCF	[196,301]
propanal cation	SA-CASSCF	[302-303]
uracil and thymine	SA-CASSCF	[197]
methyl salicylate	CASPT2	[200]
***o*-hydroxybenzaldehyde**	SA-CASSCF	[304]
cytosine	SA-CASSCF	[305]
butadiene	SA-CASSCF	[198]
benzene	SA-CASSCF	[306]
***trans*-azomethane**	SA-CASSCF	[230]
polyenes	Multi-state multi-reference CASPT2	[204]
hexamethylcyclopentadiene	Multi-state multi-reference CASPT2	[307]
ethylene	Multi-reference CI	[213,308]
	HF-OA-CASSCF	[143]

ethylene cation **tetramethylethylene**	SA-CASSCF QM/MM. QM= SA- CASSCF MS-CASPT2 MR-FOCI SA-CASSCF SA-CASSCF (QM/MM)	[127] [127,288] [201,203,205-206] [309] [310] [288]
cyclobutene	HF-OA-CAS	[143]
Sodium iodide	Localized-MO/GVB	[45]
Li(2p)+H_2	Multi-reference CI	[46]
***p*-hydroxybenzylidene acetone**	QM/MM. QM=SA-CASSCF	[220]
4-hydroxybenzylidene-1,2-dimethylimidazolinone	QM/MM. QM=semiempirical method (QM part comprises the chromophore, 3 amino acids and 8 water molecules.)	[220]
11-*cis* retinal protonated Schiff base	QM/MM. QM=semiempirical method	[220]
all-*trans* retinal protonated Schiff base	QM/MM. QM= semiempirical method	[289]
31-atom retinal protonated Schiff base	QM/MM. QM= semiempirical method	[290]
Retinal model PSB3	MS-CASPT2	[202]
***p*-hydroxybenzylidene-imidazolidinone**	QM/MM. QM=semiempirical method QM/MM. QM=SA-CASSCF SA-CASSCF	[231] [220] [311]
1,3-cyclohexadiene	SA-CASSCF	[312-313]
Silicon cluster models	SA-CASSCF	[314-316]
thioformaldehyde	SA-CASSCF with spin-orbit coupling	[268]
GeH_2	SA-CASSCF with spin-orbit coupling	[317]
Provitamin-D	GPU-accelerated SA-CASSCF	[185]
DMABN	GPU-accelerated LR-TDDFT	[242]
N_2CO	SA-CASSCF	[318]
Cyclobutanone	SA-CASSCF	[319]
Cyclopropenone	SA-CASSCF	[320]
2-(2′-Hydroxyphenyl)benzothiazole	GPU-accelerated FOMO-CASCI	[321]
2-(2′-Hydroxy-5′-methylphenyl)benzotriazole	GPU-accelerated FOMO-CASCI	[322]
H_2CSO sulfine	MS-CASPT2	[323]

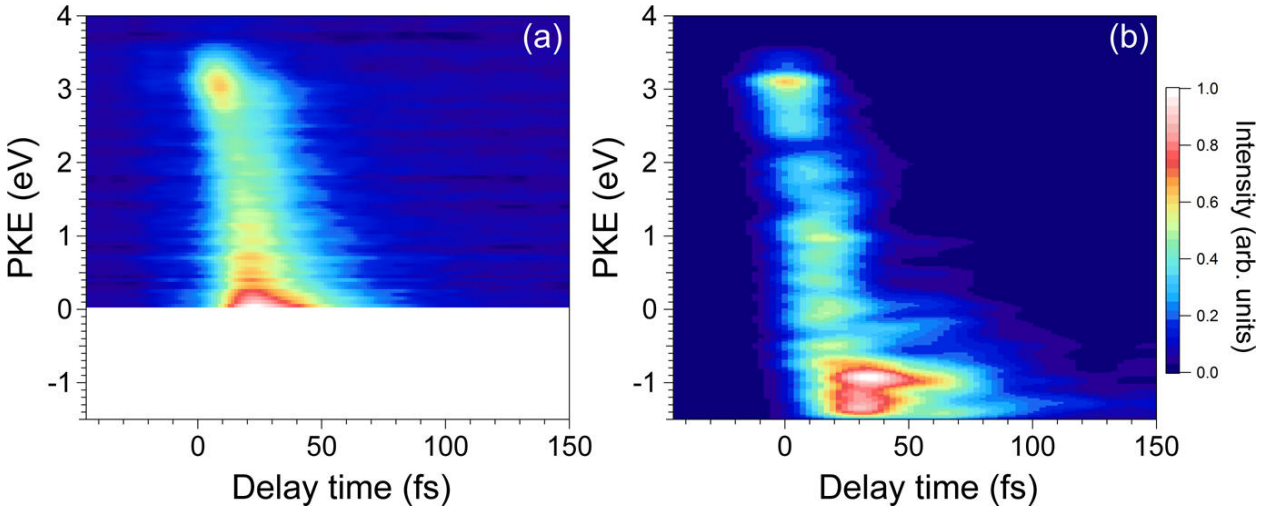

Figure 14. Experimental (a) and AIMS-predicted (b) time-resolved photoelectron kinetic energy spectra. The white area in (a) arises because the probe photon energy used in the experiment did not exactly match what was used in the prior AIMS simulations. Reproduced from Kobayashi, T.; Horio, T.; Suzuki, T. Ultrafast Deactivation of the ππ*(V) State of Ethylene Studied Using Sub-20 Fs Time-Resolved Photoelectron Imaging. *J. Phys. Chem. A* **2015**, *119*, 9518-9523. Copyright 2015, American Chemical Society.

Combining AIMS with GPU-accelerated electronic structure calculations paved the way for simulations of excited-state dynamics in large molecular systems. AIMS coupled to GPU-accelerated SA-CASSCF reproduced the experimentally observed biexponential decay of photoexcited provitamin-D_3, a molecule with 51 atoms.[185] The experimental timescales were also reproduced and the calculations indicated (in contradiction to previous[324] surface hopping simulations based on time-dependent density functional theory) that the biexponential behavior is unconnected with the nature of the photoproduct (ring-closed or ring-opened). Instead, this arises from nonequilibrium relaxation in the first excited state. The fast exponential decay is due to a first encounter of the nuclear wavepacket with the S_1/S_0 conical intersection immediately after photoexcitation, when the wavepacket is still far from equilibrium. The longer decay takes place after the remaining part of the nuclear wavepacket on S_1 has relaxed. Subsequent experiments confirmed this explanation.[325]

Applications of AIMS are not limited to organic molecules. A series of studies on nonradiative recombination in silicon nanocrystals employed AIMS to simulate the excited-state dynamics of cluster models of characteristic silicon epoxide defects containing up to nine Si atoms.[314-315] AIMS/SA-CASSCF nonadiabatic dynamics identified fast relaxation mediated by conical intersections between S_1 and S_0 (see Figure 15 for $Si_8H_{12}O$), hence proposing recombination pathways in the presence of epoxides. Importantly, reaching the conical intersection implies a photochemical ring-opening mechanism, whose mechanism slightly differs between the studied clusters. Such ultrafast decay to the ground state is also predicted for similar silicon nanocrystals with a single surface silanol group.[316] This work demonstrates that the importance of conical intersections in photochemical dynamics may extend to solid state and surface problems.

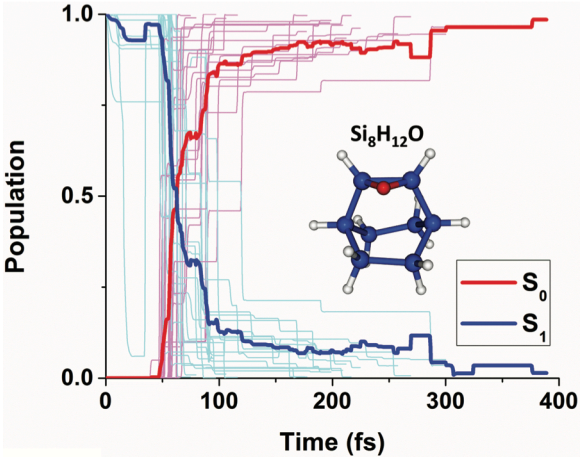

Figure 15. AIMS/SA-CASSCF excited-state dynamics of $Si_8H_{12}O$. Reproduced with permission from Ref. [314]. Copyright 2013, AIP Publishing.

What is the importance of spin-orbit coupling in deactivation processes of organic and inorganic molecules? This question has triggered the extension of a number of theoretical methodologies for excited-state dynamics, including TSH[176-177,262-265] and AIMS.[268,317] The

intersystem crossing process between the triplet state $^3B_1$ and the singlet state $^1A_1$ in GeH_2 was investigated with AIMS,[317] and the nonadiabatic dynamics results were compared to statistical nonadiabatic transition state theory. The lifetime of the $^3B_1$ state was found to be shorter with AIMS, an observation explained by the fact that transitions can take place at any point of configuration space in the neighborhood of the intersection seam, while statistical nonadiabatic transition state theory restricts transitions to occur at the minimum energy crossing point.

When combined with a QM/MM formalism, AIMS dynamics can provide information on the role of solvent or counterions in excited-state dynamics. Retinal protonated Schiff base (RPSB) is the active chromophore found in rhodopsin proteins, which convert light energy into mechanical energy through photoisomerization. The photodynamics of RPSB is highly sensitive to the environment of the molecule: while the isomerization of RPSB in methanol takes from 2 to 10 ps, it only requires hundreds of femtoseconds in proteins. Recent work compared AIMS simulations in gas and condensed (using QM/MM) phases for a large analogue of RPSB.[290] The QM/MM setup comprises the RPSB analogue as well as 85 MM methanol molecules. The electronic structure was treated at the semiempirical FOMO-CASCI level, and 30 (40) initial conditions were used for the gas phase (methanol) simulation, running for up to 10 ps. The S_1 population decay predicted by AIMS/MM is an order of magnitude slower than that obtained in gas phase (Figure 16), in agreement with experimental evidence. This tremendous slow-down of the nonradiative deactivation is largely due to electrostatic effects that generate rotational barriers in methanol (effectively a type of solvent friction[326]). The final distribution of photoproducts is, however, similar in the two sets of simulations. Interestingly, the addition of a counterion in the AIMS/MM simulation does not significantly alter the result, and can be

rationalized by the efficient Coulombic screening provided by the surrounding solvent molecules.

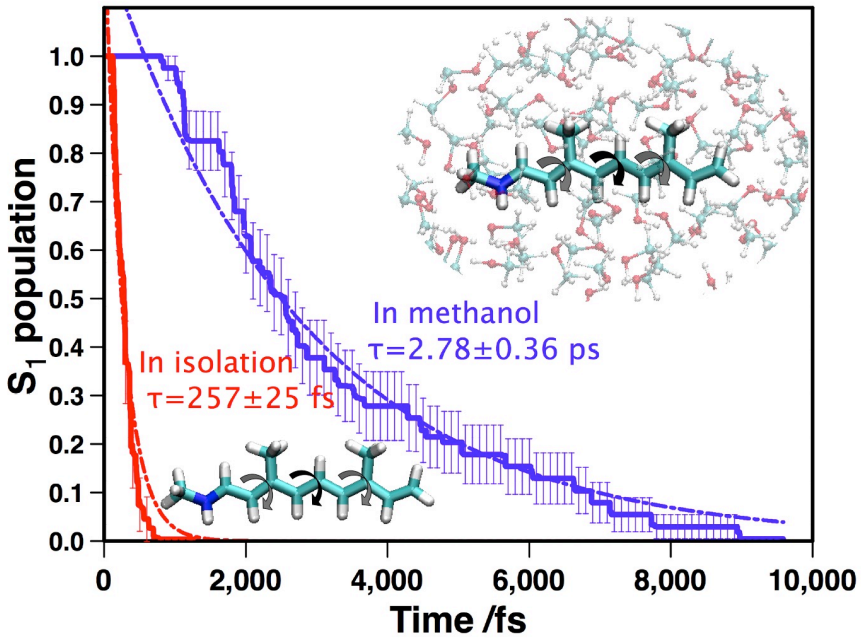

Figure 16. S_1 population decay of RPSB predicted by AIMS in gas phase (red) and in methanol (blue). Reproduced from Punwong, C.; Owens, J.; Martinez, T. J. Direct QM/MM Excited-State Dynamics of Retinal Protonated Schiff Base in Isolation and Methanol Solution. *J. Phys. Chem. B* **2015**, *119*, 704-714. Copyright 2015, American Chemical Society.

Another retinal model, PSB3, was recently used in a different context: namely to study the role of dynamical correlation effects in excited-state dynamics.[202] This study compared two sets of gas phase AIMS simulations, one employing SA3-CASSCF(6/6)/6-31G (100 initial conditions) and the other SA3-MS-CASPT2(6/6)/6-31G (46 initial conditions). Optimizations of local minima on S_1 and S_0/S_1 MECIs with the two electronic structure methods already revealed some major differences that are reflected in the dynamics simulations. While torsion around the central double bond is observed in both cases, the MS-CASPT2 nonadiabatic dynamics through the isomerization MECI proceeds more efficiently, leading to an increased population of the *cis*

ground state (78.5%). This result is in contrast with the almost 1:1 ratio between *cis* and *trans* predicted by the AIMS/SA-CASSCF dynamics.

Besides the description of a molecular environment, AIMS can also incorporate coupling between an external field and a molecule. Using a Floquet formalism (often useful for simulations in the strong-field regime), this extension of AIMS allows the study of light-induced conical intersections[327-328] that were used to alter the outcome of photoinduced ring-opening in 1,3-cyclohexadiene.[312-313] The addition of the external field generates a light-induced conical intersection that can intercept the molecule in its S_1 state before it reaches the (field-free) conical intersection between S_1 and S_0. Such early interception of the nuclear wavepacket leads to the formation of cyclohexadiene in the ground state, and therefore lowers the amount of the ring-opened hexatriene photoproduct. The AIMS simulations predict that the maximal impact of this control occurs at 50 fs after photoexcitation, in agreement with the experiment (Figure 17).

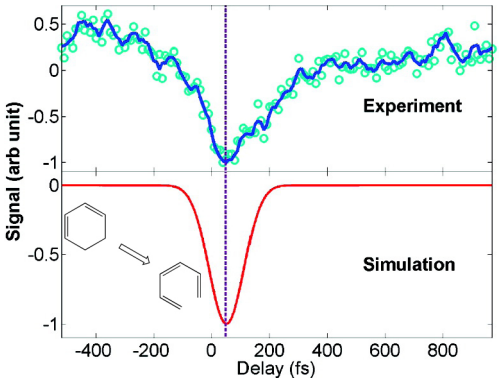

Figure 17. Comparison between AIMS predicted effect of control pulse on branching ratio (lower panel) for hexatriene (HT) with experimental result (upper panel). Adapted from Kim, J.; Tao, H. L.; White, J. L.; Petrovic, V. S.; Martínez, T. J.; Bucksbaum, P. H. Control of 1,3-Cyclohexadiene Photoisomerization Using Light-Induced Conical Intersections. *J. Phys. Chem. A* **2012**, *116*, 2758-2763. Copyright 2015, American Chemical Society.

7.2 Ab initio multiconfigurational Ehrenfest and ab initio multiple cloning

Despite their rather recent development, AI-MCE and AIMC have also been applied to a variety of different molecular systems (Table 2). A variant of AI-MCE called MCE-TDDB (multiconfigurational Ehrenfest time-dependent diabatic basis), using a diabatic basis for the matrix elements between Gaussian functions, was used to simulate the dynamics of a chromophore composed of two- and three-ring linear polyphenylene ethynylene units. This type of molecule is a building block of the larger molecular arrangement known as the "nanostar." The on-the-fly dynamics employed the collective electron oscillator method[329] for the required electronic structure quantities, based on the semiempirical method AM1[330] and on single excitation configuration interaction (CIS). The results from MCE-TDDB dynamics were compared with similar simulations performed with an equivalent of TSH called NA-ESMD[331-332] (100 trajectories) and Ehrenfest dynamics (Figure 18). While the excited state population dynamics generated by MCE-TDDB and Ehrenfest dynamics are in close agreement, the final population in S_1 given by NA-ESMD is either overestimated (classical population) or underestimated (quantum population). The discrepancy between these two variants of NA-ESMD points towards an internal inconsistency,[88,90,93,103] potentially due to a decoherence problem. Including decoherence corrections[333] in NA-ESMD led to a faster increase of the S_1 quantum population.

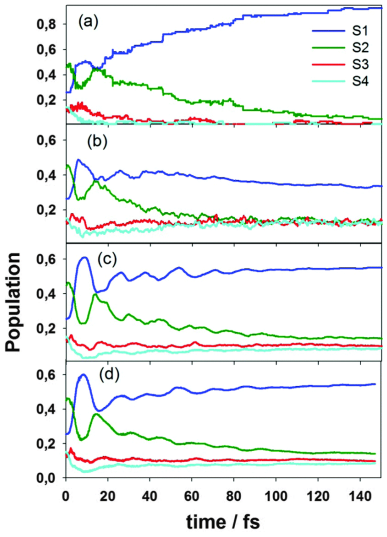

Figure 18. a) Nonadiabatic excited-state molecular dynamics (classical population), b) Nonadiabatic excited-state molecular dynamics (quantum population), c) Ehrenfest dynamics, d) multiconfigurational Ehrenfest time-dependent diabatic basis. "Classical population" refers to the proportion of trajectories running in a given electronic state, while "quantum population" refers to the quantum amplitudes attached to each trajectory, averaged for each state over the entire swarm. Reproduced with permission from Ref. [260]. Copyright 2016, published by the PCCP Owner Societies.

Table 2. Summary of AI-MCE and AIMC Calculations Reported in the Literature

Molecule	Electronic Structure Method	References
ethylene	AI-MCE/SA-CASSCF AIMC/SA-CASSCF	[147,195] [148]
phenylene ethynylene dendrimer	AI-MCE/Collective electron oscillator	[260]
pyrrole	AI-MCE/SA-CASSCF AIMC/SA-CASSCF	[194] [149]

Total kinetic energy release (TKER) spectra and velocity map imaging (VMI) of pyrrole were also simulated based on AIMC/SA-CASSCF dynamics. Due to the efficiency of AIMC/SA-CASSCF, enough statistics could be obtained to resolve fine details in both quantities. While the major features of the computed TKER spectra match the experimental ones, the use of SA-CASSCF led to a slight blue-shift in the TKER spectra. However, additional MS-CASPT2 calculations indicate that excellent agreement with experiment would be achieved by including

dynamic electron correlation. The AIMC-generated VMI exhibits an isotropic distribution in the low-energy region, and a clear anisotropy in the high-energy region, in agreement with the experimental observations.

7.3 DD-vMCG

The seminal article on the vMCG method[42] applied it to the excited-state dynamics of butatriene cation, both with reduced-dimensionality models and with a full-dimensional direct dynamics simulation. As a first validation of the vMCG method, a comparison between vMCG and full quantum dynamics was presented for a five-dimensional model Hamiltonian. Despite the small number of Gaussian functions (16 functions for each state) employed, vMCG agrees nicely at short time (< 30 fs) with the full quantum result when comparing the time-dependence of the reduced density for the lowest state in the simulation, as shown in Figure 19. Dynamics calculations were also carried out with "on the fly" computation of the potential energy surfaces at the CASSCF/3-21G* level of theory (employing a combination of CASSCF far from the coupling region with SA-CASSCF in the coupling region).[106]

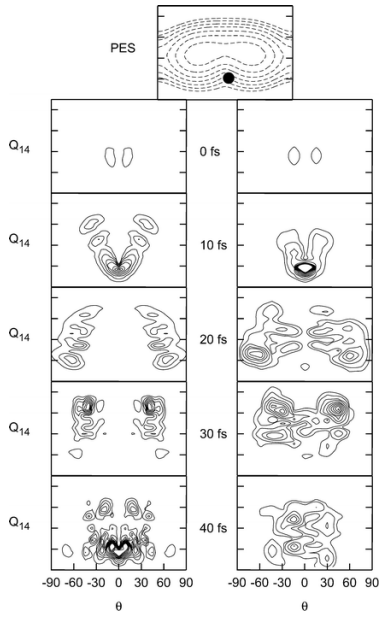

Figure 19. Comparison between full quantum dynamics (left panel) and vMCG (right) for the projection of a nuclear wavepacket on two principal coordinates in the decay of the butatriene cation. Reproduced with permission from Ref. [42]. Copyright 2004, The Royal Society of Chemistry.

DD-vMCG has been applied to a number of different molecular systems (Table 3). For example, DD-vMCG was employed to perform an *in silico* experiment of formaldehyde photodynamics. Initiating the excited-state dynamics from the top of a transition state in S_1, different photodissociation outcomes, i.e., H_2+CO *versus* H+HCO, were generated by altering the initial momentum of the nuclear wavepacket (Figure 20). The transition state on S_1 lies rather high in energy, but it allows for deactivation through a S_1/S_0 conical intersection.

Table 3. Summary of DD-vMCG Calculations Reported in the Literature

Molecule	Electronic Structure Method	References
fulvene	CASSCF	[186,189]
trimethine cyanine	CASSCF	[154,187]
formaldehyde	CASSCF	[190,193]
butatriene cation	CASSCF	[42]
benzene	CASSCF	[191]
thymine	CASSCF	[188]
NOCl	CASSCF	[157]

When the initial momentum is directed along the transition vector pointing towards the reactant (first case in Figure 20), most of the S_1 formaldehyde population is reformed, as expected. Starting at the TS with no initial momentum produces more $CO+H_2$ in the ground state. If the initial momentum is directed towards the product, a significant population of $CO+H_2$ on S_0 builds up (third case in Figure 20). Finally, adding even more energy in the mode directed towards product eventually leads to an increase of HCO+H on the ground state. The authors proposed that the ratio between $CO+H_2$ and HCO+H depends on a competition between two different momenta: that of the nuclear wavepacket when it arrives in the coupling region, and the momentum acquired by the wavepacket as a result of the nonadiabatic crossing. Hence, this *in silico* experiment shows how the momentum at the conical intersection can bias the generation of photoproducts.

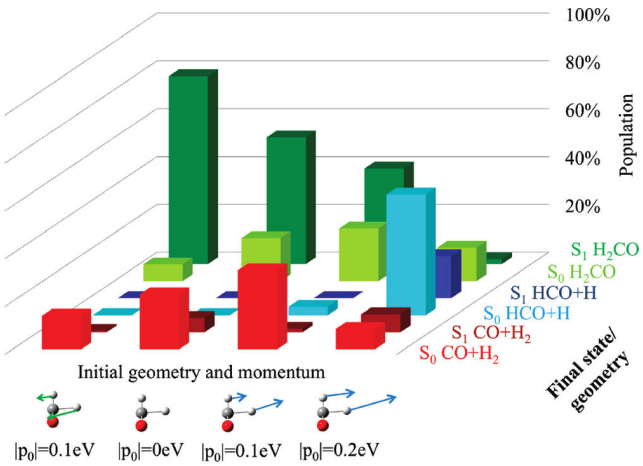

Figure 20. Different distributions of final populations can be obtained by altering the initial geometry and momentum in formaldehyde dynamics. Reproduced from Araujo, M.; Lasorne, B.; Magalhaes, A. L.; Bearpark, M.; Robb, M. A. Controlling Product Selection in the Photodissociation of Formaldehyde: Direct Quantum Dynamics from the S-1 Barrier. *J. Phys. Chem. A* **2010**, *114*, 12016-12020. Copyright 2010, American Chemical Society.

8. Summary and Outlook

Gaussian-based nonadiabatic quantum molecular dynamics offers an important alternative to more traditional trajectory-based methods for the simulation of excited-state dynamics. The different methods presented in this Review are derived from first principles and their approximations are well understood. The use of coupled traveling Gaussian functions to represent nuclear wavepackets leads to a good representation of quantum effects such as interference and decoherence, and at the same time offers the possibility to propagate the trajectory basis functions on-the-fly with out requiring *a priori* knowledge of the expected dynamics or outcomes.

Ab initio nonadiabatic quantum molecular dynamics methods are, however, always based on a compromise between the efficiency of the overall computational task to treat the photochemical or photophysical process of interest and its accuracy. On one hand, the development of more efficient electronic structure methods for excited states, the optimization of existing algorithms, or the use of new computing technologies such as GPUs will surely permit the accurate simulation of larger systems. On the other hand, the last decade has witnessed an important growth in the development of novel methods and algorithms for nondiabatic molecular dynamics. A strong stimulation has indeed been provided not only by recent new spectroscopic techniques that achieve the simultaneous time and spatial resolution needed to produce direct "molecular movies" of photochemical events, but also by the increasing need for excited-state calculations in important applications such as renewable energy, light-driven molecular machines, and atmospheric chemistry.

9. Acknowledgments

This work was supported by the AMOS program within the Chemical Sciences, Geosciences and Biosciences Division of the Office of Basic Energy Sciences, Office of Science, US Department of Energy. BFEC acknowledges funding from the European Union's Horizon 2020 research and innovation programme under grant agreement No. 701355 (NAMDIA).

10. Biographies

Basile F. E. Curchod obtained his PhD in theoretical chemistry in 2013 at EPFL (Lausanne, Switzerland), under the direction of Dr. Ivano Tavernelli and co-direction of Prof. Ursula Röthlisberger. In early 2014, he was awarded an Early.PostDoc grant from the Swiss National Science Foundation to join the group of Prof. Todd J. Martínez at Stanford University (USA). In December 2015, he initiated a short postdoctoral stay in the Theory Group directed by Prof. Eberhard K. U. Gross, at the Max Planck Institute in Halle (Germany). He has then been awarded a Marie Skłodowska-Curie Research Fellowship to join, in May 2016, the Centre for Computational Chemistry at the University of Bristol (UK). Since November 2017, he is Assistant Professor in Theoretical Chemistry at Durham University (UK).

Todd J. Martínez holds a B.A. in Chemistry from Calvin College (1989) and a Ph.D. in Chemistry from UCLA (1994). He was a Fulbright Junior Researcher and UC President's Postdoctoral Fellow at UCLA and Hebrew University before joining the faculty at the University of Illinois, Urbana–Champaign, in 1996. He has been the Ehrsam and Franklin Professor in the departments of Chemistry and Photon Sciences at Stanford University and SLAC National Accelerator Laboratory since 2009.

TOC Graphic

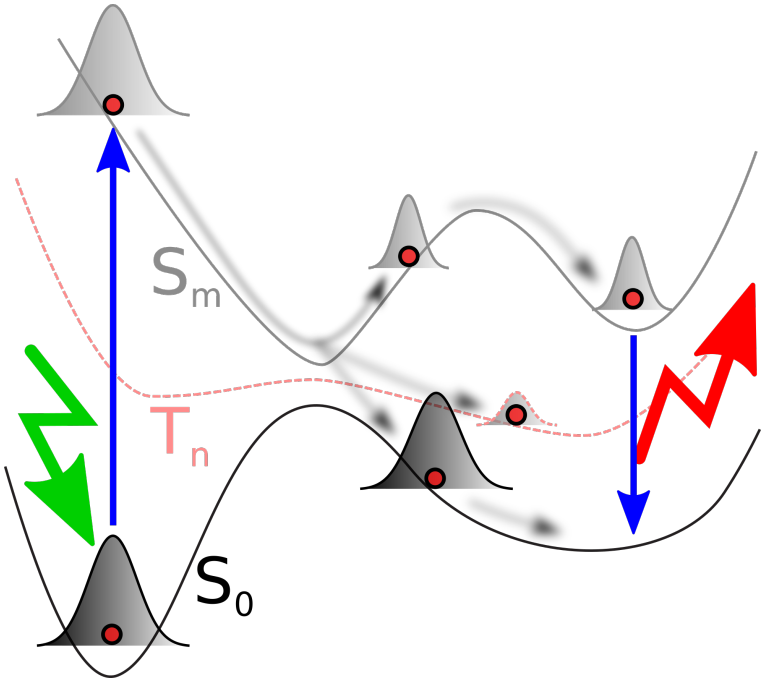

References

1. Tully, J. C. Perspective: Nonadiabatic Dynamics Theory. *J. Chem. Phys.* **2012**, *137*, 22A301.
2. Yarkony, D. R. Nonadiabatic Quantum Chemistry: Past, Present, and Future. *Chem. Rev.* **2012**, *112*, 481.
3. Tully, J. C., Nonadiabatic Dynamics. In *Modern Methods for Multidimensional Dynamics Computations in Chemistry*, Thompson, D. L., Ed. Singapore, World Scientific: 1998.
4. Worth, G. A.; Robb, M. A.; Lasorne, B. Solving the Time-Dependent Schrödinger Equation for Nuclear Motion in One Step: Direct Dynamics of Non-Adiabatic Systems. *Mol. Phys.* **2008**, *106*, 2077.
5. Beck, M. H.; Jäckle, A.; Worth, G. A.; Meyer, H. D. The Multiconfiguration Time-Dependent Hartree (Mctdh) Method: A Highly Efficient Algorithm for Propagating Wavepackets. *Phys. Rep.* **2000**, *324*, 1.
6. Worth, G. A.; Meyer, H. D.; Cederbaum, L. S. Multidimensional Dynamics Involving a Conical Intersection: Wavepacket Calculations Using the Mctdh Method. In *Conical Intersections: Electronic Structure, Dynamics & Spectroscopy*, Domcke, W.; Yarkony, D. R.; Koppel, H., Eds. 2004; Vol. 15, pp 583.
7. Wang, H. B.; Thoss, M. Multilayer Formulation of the Multiconfiguration Time-Dependent Hartree Theory. *J. Chem. Phys.* **2003**, *119*, 1289.
8. Wang, H. Multilayer Multiconfiguration Time-Dependent Hartree Theory. *J. Phys. Chem. A* **2015**, *119*, 7951.
9. Tully, J. C. Mixed Quantum Classical Dynamics. *Faraday Disc.* **1998**, *110*, 407.
10. Marx, D.; Hutter, J. *Ab Initio Molecular Dynamics: Basic Theory and Advanced Methods*. Cambridge University Press: 2009.
11. Curchod, B. F. E.; Rothlisberger, U.; Tavernelli, I. Trajectory-Based Nonadiabatic Dynamics with Time-Dependent Density Functional Theory. *ChemPhysChem* **2013**, *14*, 1314.
12. Tully, J. C.; Preston, R. K. Trajectory Surface Hopping Approach to Nonadiabatic Molecular Collisions: The Reaction of H+ with D2. *J. Chem. Phys.* **1971**, *55*, 562.
13. Tully, J. C. Molecular Dynamics with Electronic Transitions. *J. Chem. Phys.* **1990**, *93*, 1061.
14. Herman, M. F. Nonadiabatic Semiclassical Scattering. I. Analysis of Generalized Surface Hopping Procedures. *J. Chem. Phys.* **1984**, *81*, 754.
15. Sun, X.; Miller, W. H. Semiclassical Initial Value Representation for Electronically Nonadiabatic Molecular Dynamics. *J. Chem. Phys.* **1997**, *106*, 6346.
16. Kapral, R.; Ciccotti, G. Mixed Quantum-Classical Dynamics. *J. Chem. Phys.* **1999**, *110*, 8919.
17. Nielsen, S.; Kapral, R.; Ciccotti, G. Non-Adiabatic Dynamics in Mixed Quantum-Classical Systems. *J. Stat. Phys.* **2000**, *101*, 225.
18. Nielsen, S.; Kapral, R.; Ciccotti, G. Mixed Quantum-Classical Surface Hopping Dynamics. *J. Chem. Phys.* **2000**, *112*, 6543.
19. Kapral, R. Progress in the Theory of Mixed Quantum-Classical Dynamics. *Ann. Rev. Phys. Chem.* **2006**, *57*, 129.
20. Cotton, S. J.; Miller, W. H. Symmetrical Windowing for Quantum States in Quasi-Classical Trajectory Simulations: Application to Electronically Non-Adiabatic Processes. *J. Chem. Phys.* **2013**, *139*, 234112.

21. Cotton, S. J.; Miller, W. H. Symmetrical Windowing for Quantum States in Quasi-Classical Trajectory Simulations. *J. Phys. Chem. A* **2013**, *117*, 7190.
22. Cotton, S. J.; Miller, W. H. A Symmetrical Quasi-Classical Spin-Mapping Model for the Electronic Degrees of Freedom in Non-Adiabatic Processes. *J. Phys. Chem. A* **2015**, *119*, 12138.
23. Cotton, S. J.; Miller, W. H. A New Symmetrical Quasi-Classical Model for Electronically Non-Adiabatic Processes: Application to the Case of Weak Non-Adiabatic Coupling. *J. Chem. Phys.* **2016**, *145*, 144108.
24. Cotton, S. J.; Miller, W. H. The Symmetrical Quasi-Classical Model for Electronically Non-Adiabatic Processes Applied to Energy Transfer Dynamics in Site-Exciton Models of Light-Harvesting Complexes. *J. Chem. Theory Comput.* **2016**, *12*, 983.
25. Bonella, S.; Coker, D. F. Land-Map, a Linearized Approach to Nonadiabatic Dynamics Using the Mapping Formalism. *J. Chem. Phys.* **2005**, *122*, 194102.
26. Wyatt, R. E.; Lopreore, C. L.; Parlant, G. Electronic Transitions with Quantum Trajectories. *J. Chem. Phys.* **2001**, *114*, 5113.
27. Lopreore, C. L.; Wyatt, R. E. Electronic Transitions with Quantum Trajectories. Ii. *J. Chem. Phys.* **2002**, *116*, 1228.
28. Rassolov, V. A.; Garashchuk, S. Semiclassical Nonadiabatic Dynamics with Quantum Trajectories. *Phys. Rev. A* **2005**, *71*, 032511.
29. Poirier, B.; Parlant, G. Reconciling Semiclassical and Bohmian Mechanics: Iv. Multisurface Dynamics. *J. Phys. Chem. A* **2007**, *111*, 10400.
30. Curchod, B. F. E.; Tavernelli, I.; Rothlisberger, U. Trajectory-Based Solution of the Nonadiabatic Quantum Dynamics Equations: An on-the-Fly Approach for Molecular Dynamics Simulations. *Phys. Chem. Chem. Phys.* **2011**, *13*, 3231.
31. Curchod, B. F. E.; Tavernelli, I. On Trajectory-Based Nonadiabatic Dynamics: Bohmian Dynamics Versus Trajectory Surface Hopping. *J. Chem. Phys.* **2013**, *138*, 184112.
32. Agostini, F.; Abedi, A.; Suzuki, Y.; Gross, E. K. U. Mixed Quantum-Classical Dynamics on the Exact Time-Dependent Potential Energy Surface: A Fresh Look at Non-Adiabatic Processes. *Mol. Phys.* **2013**, *111*, 3625.
33. Abedi, A.; Agostini, F.; Gross, E. K. U. Mixed Quantum-Classical Dynamics from the Exact Decomposition of Electron-Nuclear Motion. *Europhys. Lett.* **2014**, *106*, 33001.
34. Min, S. K.; Agostini, F.; Gross, E. K. U. Coupled-Trajectory Quantum-Classical Approach to Electronic Decoherence in Nonadiabatic Processes. *Phys. Rev. Lett.* **2015**, *115*.
35. Agostini, F.; Min, S. K.; Abedi, A.; Gross, E. K. U. Quantum-Classical Nonadiabatic Dynamics: Coupled- Vs Independent-Trajectory Methods. *J. Chem. Theory Comput.* **2016**, *12*, 2127.
36. Min, S. K.; Agostini, F.; Tavernelli, I.; Gross, E. K. U. Ab Initio Nonadiabatic Dynamics with Coupled Trajectories: A Rigorous Approach to Quantum (De)Coherence. *J. Phys. Chem. Lett.* **2017**, *8*, 3048.
37. Heller, E. J. Time-Dependent Approach to Semiclassical Dynamics. *J. Chem. Phys.* **1975**, *62*, 1544.
38. Heller, E. J. The Semi-Classical Way to Molecular-Spectroscopy. *Acc. Chem. Res.* **1981**, *14*, 368.
39. Heller, E. J. Frozen Gaussians - a Very Simple Semi-Classical Approximation. *J. Chem. Phys.* **1981**, *75*, 2923.

40. Kulander, K. C.; Heller, E. J. Time-Dependent Formulation of Polyatomic Photofragmentation - Application to H3+. *J. Chem. Phys.* **1978**, *69*, 2439.
41. Worth, G. A.; Burghardt, I. Full Quantum Mechanical Molecular Dynamics Using Gaussian Wavepackets. *Chem. Phys. Lett.* **2003**, *368*, 502.
42. Worth, G.; Robb, M.; Burghardt, I. A Novel Algorithm for Non-Adiabatic Direct Dynamics Using Variational Gaussian Wavepackets. *Faraday Disc.* **2004**, *127*, 307.
43. Shalashilin, D. V. Quantum Mechanics with the Basis Set Guided by Ehrenfest Trajectories: Theory and Application to Spin-Boson Model. *J. Chem. Phys.* **2009**, *130*, 244101.
44. Shalashilin, D. V. Nonadiabatic Dynamics with the Help of Multiconfigurational Ehrenfest Method: Improved Theory and Fully Quantum 24d Simulation of Pyrazine. *J. Chem. Phys.* **2010**, *132*, 244111.
45. Martínez, T. J.; Levine, R. D. First-Principles Molecular Dynamics on Multiple Electronic States: A Case Study of Nai. *J. Chem. Phys.* **1996**, *105*, 6334.
46. Martínez, T. J. Ab Initio Molecular Dynamics around a Conical Intersection: Li(2p)+H-2. *Chem. Phys. Lett.* **1997**, *272*, 139.
47. Martinez, T. J.; Levine, R. D. Dynamics of the Collisional Electron Transfer and Femtosecond Photodissociation of Nai on Ab Initio Electronic Energy Curves. *Chem. Phys. Lett.* **1996**, *259*, 252.
48. Vreven, T.; Bernardi, F.; Garavelli, M.; Olivucci, M.; Robb, M. A.; Schlegel, H. B. Ab Initio Photoisomerization Dynamics of a Simple Retinal Chromophore Model. *J. Am. Chem. Soc.* **1997**, *119*, 12687.
49. Hartmann, M.; Pittner, J.; Bonacic-Koutecky, V. Ab Initio Nonadiabatic Dynamics Involving Conical Intersection Combined with Wigner Distribution Approach to Ultrafast Spectroscopy Illustrated on Na3f2 Cluster. *J. Chem. Phys.* **2001**, *114*, 2123.
50. Doltsinis, N. L.; Marx, D. Nonadiabatic Car-Parrinello Molecular Dynamics. *Phys. Rev. Lett.* **2002**, *88*, 166402.
51. Worth, G. A.; Hunt, P.; Robb, M. A. Nonadiabatic Dynamics: A Comparison of Surface Hopping Direct Dynamics with Quantum Wavepacket Calculations. *J. Phys. Chem. A* **2003**, *107*, 621.
52. Hayashi, S.; Tajkhorshid, E.; Schulten, K. Molecular Dynamics Simulation of Bacteriorhodopsin's Photoisomerization Using Ab Initio Forces for the Excited Chromophore. *Biophys. J.* **2003**, *85*, 1440.
53. Li, X. S.; Tully, J. C.; Schlegel, H. B.; Frisch, M. J. Ab Initio Ehrenfest Dynamics. *J. Chem. Phys.* **2005**, *123*, 084106.
54. Zechmann, G.; Barbatti, M.; Lischka, H.; Pittner, J.; Bonacic-Koutecky, V. Multiple Pathways in the Photodynamics of a Polar Pi-Bond: A Case Study of Silaethylene. *Chem. Phys. Lett.* **2006**, *418*, 377.
55. Born, M.; Huang, K. *Dynamical Theory of Crystal Lattices*. Clarendon, Oxford: 1954.
56. Domcke, W.; Yarkony, D.; Köppel, H., *Conical Intersections: Electronic Structure, Dynamics & Spectroscopy*. World Scientific Pub Co Inc: 2004; Vol. 15.
57. Koppel, H.; Domcke, W.; Cederbaum, L. S. Multimode Molecular Dynamics Beyond the Born-Oppenheimer Approximation. *Adv. Chem. Phys.* **1984**, *57*, 59.
58. Subotnik, J. E.; Cave, R. J.; Steele, R. P.; Shenvi, N. The Initial and Final States of Electron and Energy Transfer Processes: Diabatization as Motivated by System-Solvent Interactions. *J. Chem. Phys.* **2009**, *130*, 234102.

59. Van Voorhis, T.; Kowalczyk, T.; Kaduk, B.; Wang, L.-P.; Cheng, C.-L.; Wu, Q. The Diabatic Picture of Electron Transfer, Reaction Barriers, and Molecular Dynamics. *Ann. Rev. Phys. Chem.* **2010**, *61*, 149.
60. Worth, G. A.; Cederbaum, L. S. Beyond Born-Oppenheimer: Molecular Dynamics through a Conical Intersection. *Ann. Rev. Phys. Chem.* **2004**, *55*, 127.
61. Izmaylov, A. F.; Franco, I. Entanglement in the Born-Oppenheimer Approximation. *J. Chem. Theory Comput.* **2017**, *13*, 20.
62. McKemmish, L. K.; McKenzie, R. H.; Hush, N. S.; Reimers, J. R. Electron-Vibration Entanglement in the Born-Oppenheimer Description of Chemical Reactions and Spectroscopy. *Phys. Chem. Chem. Phys.* **2015**, *17*, 24666.
63. Micha, D. A. A Self-Consistent Eikonal Treatment of Electronic Transitions in Molecular Collisions. *J. Chem. Phys.* **1983**, *78*, 7138.
64. Gerber, R. B.; Buch, V.; Ratner, M. A. Time-Dependent Self-Consistent Field Approximation for Intramolecular Energy Transfer. I. Formulation and Application to Dissociation of Van Der Waals Molecules. *J. Chem. Phys.* **1982**, *77*, 3022.
65. Horsfield, A. P.; Bowler, D. R.; Fisher, A. J.; Todorov, T. N.; Montgomery, M. J. Power Dissipation in Nanoscale Conductors: Classical, Semi-Classical and Quantum Dynamics. *J. Phys. Cond. Mat.* **2004**, *16*, 3609.
66. Horsfield, A. P.; Bowler, D. R.; Fisher, A. J.; Todorov, T. N.; Sánchez, C. G. Beyond Ehrenfest: Correlated Non-Adiabatic Molecular Dynamics. *J. Phys. Cond. Mat.* **2004**, *16*, 8251.
67. Hunter, G. Conditional Probability Amplitudes in Wave Mechanics. *Int. J. Quantum Chem.* **1975**, *9*, 237.
68. Cederbaum, L. S. The Exact Molecular Wavefunction as a Product of an Electronic and a Nuclear Wavefunction. *J. Chem. Phys.* **2013**, *138*, 224110.
69. Abedi, A.; Maitra, N. T.; Gross, E. K. U. Exact Factorization of the Time-Dependent Electron-Nuclear Wave Function. *Phys. Rev. Lett.* **2010**, *105*, 123002.
70. Abedi, A.; Maitra, N. T.; Gross, E. K. U. Correlated Electron-Nuclear Dynamics: Exact Factorization of the Molecular Wave-Function. *J. Chem. Phys.* **2012**, *137*, 22A530.
71. Abedi, A.; Agostini, F.; Suzuki, Y.; Gross, E. K. U. Dynamical Steps That Bridge Piecewise Adiabatic Shapes in the Exact Time-Dependent Potential Energy Surface. *Phys. Rev. Lett.* **2013**, *110*, 263001.
72. Agostini, F.; Abedi, A.; Gross, E. K. U. Classical Nuclear Motion Coupled to Electronic Non-Adiabatic Transitions. *J. Chem. Phys.* **2014**, *141*, 214101.
73. Agostini, F.; Min, S. K.; Gross, E. K. U. Semiclassical Analysis of the Electron-Nuclear Coupling in Electronic Non-Adiabatic Processes. *Ann. Phys.* **2015**, *527*, 546.
74. Agostini, F.; Abedi, A.; Suzuki, Y.; Min, S. K.; Maitra, N. T.; Gross, E. K. U. The Exact Forces on Classical Nuclei in Non-Adiabatic Charge Transfer. *J. Chem. Phys.* **2015**, *142*, 084303.
75. Curchod, B. F. E.; Agostini, F.; Gross, E. K. U. An Exact Factorization Perspective on Quantum Interferences in Nonadiabatic Dynamics. *J. Chem. Phys.* **2016**, *145*, 034103.
76. Curchod, B. F. E.; Agostini, F. On the Dynamics through a Conical Intersection. *J. Phys. Chem. Lett.* **2017**, *8*, 831.
77. Smith, F. T. Diabatic and Adiabatic Representations for Atomic Collision Problems. *Phys. Rev.* **1969**, *179*, 111.

78. Mead, C. A.; Truhlar, D. G. Conditions for the Definition of a Strictly Diabatic Electronic Basis for Molecular Systems. *J. Chem. Phys.* **1982**, *77*, 6090.
79. This is because the position and momentum operators do not commute.
80. Meyer, H.-D.; Gatti, F.; Worth, G. A. *Multidimensional Quantum Dynamics: Mctdh Theory and Applications*. Wiley-VCH Verlag GmbH & Co. KGaA: 2009.
81. Gatti, F.; Lasorne, B. *Molecular Quantum Dynamics from Theory to Applications Conclusions*. 2014; p 271.
82. Kosloff, R. Time-Dependent Quantum-Mechanical Methods for Molecular Dynamics. *J. Phys. Chem.* **1988**, *92*, 2087.
83. Subotnik, J. E.; Ouyang, W.; Landry, B. R. Can We Derive Tully's Surface-Hopping Algorithm from the Semiclassical Quantum Liouville Equation? Almost, but Only with Decoherence. *J. Chem. Phys.* **2013**, *139*, 214107.
84. Barbatti, M.; Shepard, R.; Lischka, H., Computational and Methodological Elements for Nonadiabatic Trajectory Dynamics Simulations of Molecules. In *Conical Intersections: Theory, Computation and Experiment*, Domcke, W.; Yarkony, D. R.; Koeppel, H., Eds. Singapore, World Scientific: 2011; p 415.
85. Coker, D. F.; Xiao, L. Methods for Molecular Dynamics with Nonadiabatic Transitions. *J. Chem. Phys.* **1995**, *102*, 496.
86. Lu, J.; Zhou, Z. Improved Sampling and Validation of Forzen Gaussian Approximation with Surface Hopping Algorithm for Nonadiabatic Dynamics. *J. Chem. Phys.* **2016**, *145*, 124109.
87. Subotnik, J. E.; Shenvi, N. Decoherence and Surface Hopping: When Can Averaging over Initial Conditions Help Capture the Effects of Wave Packet Separation? *J. Chem. Phys.* **2011**, *134*, 244114.
88. Fang, J. Y.; Hammes-Schiffer, S. Improvement of the Internal Consistency in Trajectory Surface Hopping. *J. Phys. Chem. A* **1999**, *103*, 9399.
89. Thachuk, M.; Ivanov, M. Y.; Wardlaw, D. M. A Semiclassical Approach to Intense-Field above-Threshold Dissociation in the Long Wavelength Limit. Ii. Conservation Principles and Coherence in Surface Hopping. *J. Chem. Phys.* **1998**, *109*, 5747.
90. Granucci, G.; Persico, M. Critical Appraisal of the Fewest Switches Algorithm for Surface Hopping. *J. Chem. Phys.* **2007**, *126*, 134114.
91. Subotnik, J. E.; Jain, A.; Landry, B.; Petit, A.; Ouyang, W. J.; Bellonzi, N. Understanding the Surface Hopping View of Electronic Transitions and Decoherence. *Ann. Rev. Phys. Chem.* **2016**, *67*, 387.
92. Bittner, E. R.; Rossky, P. J. Quantum Decoherence in Mixed Quantum-Classical Systems: Nonadiabatic Processes. *J. Chem. Phys.* **1995**, *103*, 8130.
93. Granucci, G.; Persico, M.; Zoccante, A. Including Quantum Decoherence in Surface Hopping. *J. Chem. Phys.* **2010**, *133*, 134111.
94. Shenvi, N.; Subotnik, J. E.; Yang, W. Phase-Corrected Surface Hopping: Correcting the Phase Evolution of the Electronic Wavefunction. *J. Chem. Phys.* **2011**, *135*, 024101.
95. Shenvi, N.; Subotnik, J. E.; Yang, W. Simultaneous-Trajectory Surface Hopping: A Parameter-Free Algorithm for Implementing Decoherence in Nonadiabatic Dynamics. *J. Chem. Phys.* **2011**, *134*, 144102.
96. Subotnik, J. E.; Shenvi, N. A New Approach to Decoherence and Momentum Rescaling in the Surface Hopping Algorithm. *J. Chem. Phys.* **2011**, *134*, 024105.

97. Shenvi, N.; Yang, W. Achieving Partial Decoherence in Surface Hopping through Phase Correction. *J. Chem. Phys.* **2012**, *137*, 22A528.
98. Subotnik, J. E. Fewest-Switches Surface Hopping and Decoherence in Multiple Dimensions. *J. Phys. Chem. A* **2011**, *115*, 12083.
99. Jaeger, H. M.; Fischer, S.; Prezhdo, O. V. Decoherence-Induced Surface Hopping. *J. Chem. Phys.* **2012**, *137*, 22A545.
100. Zhu, C.; Nangia, S.; Jasper, A. W.; Truhlar, D. G. Coherent Switching with Decay of Mixing: An Improved Treatment of Electronic Coherence for Non-Born-Oppenheimer Trajectories. *J. Chem. Phys.* **2004**, *121*, 7658.
101. Tapavicza, E.; Bellchambers, G. D.; Vincent, J. C.; Furche, F. Ab Initio Non-Adiabatic Molecular Dynamics. *Phys. Chem. Chem. Phys.* **2013**, *15*, 18336.
102. Barbatti, M. Nonadiabatic Dynamics with Trajectory Surface Hopping Method. *WIREs Comput. Mol. Sci.* **2011**, *1*, 620.
103. Persico, M.; Granucci, G. An Overview of Nonadiabatic Dynamics Simulations Methods, with Focus on the Direct Approach Versus the Fitting of Potential Energy Surfaces. *Theor. Chem. Acc.* **2014**, *133*, 1526.
104. Tannor, D. J. *Introduction to Quantum Mechanics, a Time-Dependent Perspective*. University Science Books: Sausalito, California, 2007.
105. Meyer, H. D.; Manthe, U.; Cederbaum, L. S. The Multi-Configurational Time-Dependent Hartree Approach. *Chem. Phys. Lett.* **1990**, *165*, 73.
106. General Discussion. *Faraday Disc.* **2004**, *127*, 355.
107. Richings, G. W.; Polyak, I.; Spinlove, K. E.; Worth, G. A.; Burghardt, I.; Lasorne, B. Quantum Dynamics Simulations Using Gaussian Wavepackets: The Vmcg Method. *Int. Rev. Phys. Chem.* **2015**, *34*, 269.
108. Vacher, M.; Bearpark, M. J.; Robb, M. A. Direct Methods for Non-Adiabatic Dynamics: Connecting the Single-Set Variational Multi-Configuration Gaussian (Vmcg) and Ehrenfest Perspectives. *Theor. Chem. Acc.* **2016**, *135*.
109. Martínez, T. J.; Ben-Nun, M.; Ashkenazi, G. Classical/Quantal Method for Multistate Dynamics: A Computational Study. *J. Chem. Phys.* **1996**, *104*, 2847.
110. Martínez, T. J.; Ben-Nun, M.; Levine, R. D. Multi-Electronic-State Molecular Dynamics: A Wave Function Approach with Applications. *J. Phys. Chem.* **1996**, *100*, 7884.
111. Martínez, T. J.; Levine, R. D. Non-Adiabatic Molecular Dynamics: Split-Operator Multiple Spawning with Applications to Photodissociation. *J. Chem. Soc., Faraday Trans.* **1997**, *93*, 941.
112. Ben-Nun, M.; Martínez, T. J. Nonadiabatic Molecular Dynamics: Validation of the Multiple Spawning Method for a Multidimensional Problem. *J. Chem. Phys.* **1998**, *108*, 7244.
113. Ben-Nun, M.; Martínez, T. J. Ab Initio Quantum Molecular Dynamics. *Adv. Chem. Phys.* **2002**, *121*, 439.
114. Joubert-Doriol, L.; Sivasubramanium, J.; Ryabinkin, I. G.; Izmaylov, A. F. Topologically Correct Quantum Nonadiabatic Formalism for on-the-Fly Dynamics. *J. Phys. Chem. Lett.* **2017**, *8*, 452.
115. Meek, G. A.; Levine, B. G. The Best of Both Reps-Diabatized Gaussians on Adiabatic Surfaces. *J. Chem. Phys.* **2016**, *145*, 184103.
116. Heaps, C. W.; Mazziotti, D. A. Accurate Non-Adiabatic Quantum Dynamics from Pseudospectral Sampling of Time-Dependent Gaussian Basis Sets. *J. Chem. Phys.* **2016**, *145*, 064101.

117. Formally, one should consider that there are an infinite number of TBFs when inserting the ansatz of Eq. 17 in the TDSE. After deriving Eq. 18 for the time evolution of the complex coefficients, one can limit the number of TBFs that are included in the simulation. The reason for this formal fancy footwork is to avoid the time derivative of a discontinuous jump in the size of the Hilbert space that the wavefunction spans. In practice, this is one of the reasons for the back-propagation of child TBFs during the spawning process. One wants to ensure that when the Hilbert space expands, it is of no practical consequence. In other words, the new TBF is not needed at the time when it is introduced. At the same time, one wants to ensure that it will be needed shortly after it is introduced, to maximize efficiency.
118. Makhov, D. V.; Symonds, C.; Fernandez-Alberti, S.; Shalashilin, D. V. Ab Initio Quantum Direct Dynamics Simulations of Ultrafast Photochemistry with Multiconfigurational Ehrenfest Approach. *Chem. Phys.* **2017**, *493*, 200.
119. In AIMS, the zeroth-order saddle point approximation used for the required integrals leads to a Hermitian Hamiltonian operator without further modifications.
120. Reimers, J. R.; McKemmish, L. K.; McKenzie, R. H.; Hush, N. S. Non-Adiabatic Effects in Thermochemistry, Spectroscopy and Kinetics: The General Importance of All Three Born-Oppenheimer Breakdown Corrections. *Phys. Chem. Chem. Phys.* **2015**, *17*, 24641.
121. Meek, G. A.; Levine, B. G. Wave Function Continuity and the Diagonal Born-Oppenheimer Correction at Conical Intersections. *J. Chem. Phys.* **2016**, *144*, 184109.
122. Gherib, R.; Ryabinkin, I. G.; Izmaylov, A. F. Why Do Mixed Quantum-Classical Methods Describe Short-Time Dynamics through Conical Intersections So Well? Analysis of Geometric Phase Effects. *J. Chem. Theory Comput.* **2015**, *11*, 1375.
123. Gherib, R.; Ye, L. Y.; Ryabinkin, I. G.; Izmaylov, A. F. On the Inclusion of the Diagonal Born-Oppenheimer Correction in Surface Hopping Methods. *J. Chem. Phys.* **2016**, *144*, 154103.
124. Granucci, G.; Persico, M.; Toniolo, A. Direct Semiclassical Simulation of Photochemical Processes with Semiempirical Wave Functions. *J. Chem. Phys.* **2001**, *114*, 10608.
125. Plasser, F.; Granucci, G.; Pittner, J.; Barbatti, M.; Persico, M.; Lischka, H. Surface Hopping Dynamics Using a Locally Diabatic Formalism: Charge Transfer in the Ethylene Dimer Cation and Excited State Dynamics in the 2-Pyridone Dimer. *J. Chem. Phys.* **2012**, *137*.
126. Hack, M. D.; Wensmann, A. M.; Truhlar, D. G.; Ben-Nun, M.; Martínez, T. J. Comparison of Full Multiple Spawning, Trajectory Surface Hopping, and Converged Quantum Mechanics for Electronically Nonadiabatic Dynamics. *J. Chem. Phys.* **2001**, *115*, 1172.
127. Levine, B. G.; Coe, J. D.; Virshup, A. M.; Martínez, T. J. Implementation of Ab Initio Multiple Spawning in the Molpro Quantum Chemistry Package. *Chem. Phys.* **2008**, *347*, 3.
128. Landau, L. D. Zur Theorie Der Energieubertragung. Ii. *Phys. Z. Sowjetunion* **1932**, *2*, 46.
129. Zener, C. Non-Adiabatic Crossing of Energy Levels. *Proc. R. Soc. London, Ser. A* **1932**, *137*, 696.
130. Stueckelberg, E. C. G. Theory of Inelastic Collisions between Atoms (Theory of Inelastic Collisions between Atoms, Using Two Simultaneous Differential Equations). *Helv. Phys. Acta* **1932**, *5*, 369.
131. It is important to note that TBFs effectively never hit a conical intersection seam exactly - since the intersection seam exists in a space which is two dimensions smaller than the space of molecular coordinates, TBFs simply cannot find the seam in practice. Of course, TBFs can (and do) come close to an intersection seam. However, they rarely come close enough that the simulation experiences any numerical instability caused by the singularity of the first-order

nonadiabatic coupling or the derivative discontinuity in the potential energy surface (both required features of a conical intersection). This concept is well-illustrated by the proverbial difficulty of finding a needle (a one-dimensional object) in a haystack (a three-dimensional space).
132. Yang, S.; Coe, J. D.; Kaduk, B.; Martínez, T. J. An "Optimal" Spawning Algorithm for Adaptive Basis Set Expansion in Nonadiabatic Dynamics. *J. Chem. Phys.* **2009**, *130*, 134113.
133. Yang, S.; Martínez, T. J. Ab Initio Multiple Spawning: First Principles Dynamics around Conical Intersections. In *Conical Intersections: Theory, Computation and Experiment*, Domcke, W.; Yarkony, D. R.; Köppel, H., Eds. World Scientific Publishing Co. Pte. Ltd.: 2011; Vol. 17, pp 347.
134. Levine, B. G.; Martínez, T. J. Isomerization through Conical Intersections. *Ann. Rev. Phys. Chem.* **2007**, *58*, 613.
135. The overlap of two TBFs falls off exponentially with the difference between their positions and momenta. If the initial overlap of the child and parent TBF is very small, this implies that the Hamiltonian matrix element connecting them willl also be small and therefore the child TBF is unlikely to be populated by the TDSE.
136. Schmidt, J. R.; Parandekar, P. V.; Tully, J. C. Mixed Quantum-Classical Equilibrium: Surface Hopping. *J. Chem. Phys.* **2008**, *129*, 044104.
137. Parandekar, P. V.; Tully, J. C. Detailed Balance in Ehrenfest Mixed Quantum-Classical Dynamics. *J. Chem. Theory Comput.* **2006**, *2*, 229.
138. Parandekar, P. V.; Tully, J. C. Mixed Quantum-Classical Equilibrium. *J. Chem. Phys.* **2005**, *122*, 094102.
139. Sulc, M.; Hernandez, H.; Martínez, T. J.; Vanicek, J. Relation of Exact Gaussian Basis Methods to the Dephasing Representation: Theory and Application to Time-Resolved Electronic Spectra. *J. Chem. Phys.* **2013**, *139*, 034112.
140. Alborzpour, J. P.; Tew, D. P.; Habershon, S. Efficient and Accurate Evaluation of Potential Energy Matrix Elements for Quantum Dynamics Using Gaussian Process Regression. *J. Chem. Phys.* **2016**, *145*, 174112.
141. A subtlety here concerns the geometric phase when the adiabatic representation is used. Each TBF carries its own electronic wavefunction, with a phase that is consistent along the trajectory history. This implies that the electronic wavefunction in AIMS is path-dependent. The electronic phase should be incorporated in the saddle-point approximation for integrals. This can be done with the usual SPA formula, augmented by a phase factor which is determined by choosing the sign of the adiabatic electronic wavefunctions at the centroid to best overlap with the electronic wavefunctions carried by the bra and ket TBFs.
142. Mignolet, B.; Curchod, B. F. E. A Walk through the Approximation of Ab Initio Multiple Spawning for Excited-State Dynamics. in preparation.
143. Ben-Nun, M.; Quenneville, J.; Martínez, T. J. Ab Initio Multiple Spawning: Photochemistry from First Principles Quantum Molecular Dynamics. *J. Phys. Chem. A* **2000**, *104*, 5161.
144. Burant, J. C.; Tully, J. C. Nonadiabatic Dynamics Via the Classical Limit Schrödinger Equation. *J. Chem. Phys.* **2000**, *112*, 6097.
145. Jasper, A. W.; Stechmann, S. N.; Truhlar, D. G. Fewest-Switches with Time Uncertainty: A Modified Trajectory Surface-Hopping Algorithm with Better Accuracy for Classically Forbidden Electronic Transitions. *J. Chem. Phys.* **2002**, *116*, 5424.

146. Jasper, A. W.; Truhlar, D. G. Improved Treatment of Momentum at Classically Forbidden Electronic Transitions in Trajectory Surface Hopping Calculations. *Chem. Phys. Lett.* **2003**, *369*, 60.
147. Saita, K.; Shalashilin, D. V. On-the-Fly Ab Initio Molecular Dynamics with Multiconfigurational Ehrenfest Method. *J. Chem. Phys.* **2012**, *137*, 8.
148. Makhov, D. V.; Glover, W. J.; Martinez, T. J.; Shalashilin, D. V. Ab Initio Multiple Cloning Algorithm for Quantum Nonadiabatic Molecular Dynamics. *J. Chem. Phys.* **2014**, *141*, 11.
149. Makhov, D. V.; Saita, K.; Martinez, T. J.; Shalashilin, D. V. Ab Initio Multiple Cloning Simulations of Pyrrole Photodissociation: Tker Spectra and Velocity Map Imaging. *Phys. Chem. Chem. Phys.* **2015**, *17*, 3316.
150. Makhov, D. V.; Martínez, T. J.; Shalashilin, D. V. Toward Fully Quantum Modelling of Ultrafast Photodissociation Imaging Experiments. Treating Tunnelling in the Ab Initio Multiple Cloning Approach. *Faraday Disc.* **2016**, *194*, 81.
151. Ben-Nun, M.; Martínez, T. J. A Multiple Spawning Approach to Tunneling Dynamics. *J. Chem. Phys.* **2000**, *112*, 6113.
152. Durr, D.; Teufel, S. *Bohmian Mechanics, the Physics and Mathematics of Quantum Theory*. Springer-Verlag Berlin Heidelberg: 2009; p 145.
153. Oriols, X.; Mompart, J. Applied Bohmian Mechanics: From Nanoscale Systems to Cosmology. Oriols, X.; Mompart, J., Eds. Pan Stanford Publishing Pte. Ltd.: 2012; pp 15.
154. Lasorne, B.; Worth, G. A.; Robb, M. A. Non-Adiabatic Photochemistry: Ultrafast 7 Electronic State Transitions and Nuclear Wavepacket Coherence. In *Molecular Quantum Dynamic*, Gatti, F., Ed. Springer-Verlag: Berlin, 2014.
155. Lasorne, B.; Worth, G. A.; Robb, M. A. Excited-State Dynamics. *WIREs Comput. Mol. Sci.* **2011**, *1*, 460.
156. Lasorne, B.; Bearpark, M. J.; Robb, M. A.; Worth, G. A. Direct Quantum Dynamics Using Variational Multi-Configuration Gaussian Wavepackets. *Chem. Phys. Lett.* **2006**, *432*, 604.
157. Lasorne, B.; Robb, M. A.; Worth, G. A. Direct Quantum Dynamics Using Variational Multi-Configuration Gaussian Wavepackets. Implementation Details and Test Case. *Phys. Chem. Chem. Phys.* **2007**, *9*, 3210.
158. Wigner, E. On the Quantum Correction for Thermodynamic Equilibrium. *Phys. Rev.* **1932**, *40*, 0749.
159. Hillery, M.; O'Connell, R. F.; Scully, M. O.; Wigner, E. P. Distribution Functions in Physics: Fundamentals. *Phys. Rep.* **1984**, *106*, 121.
160. Barbatti, M.; Sen, K. Effects of Different Initial Condition Samplings on Photodynamics and Spectrum of Pyrrole. *Int. J. Quantum Chem.* **2015**, *116*, 762.
161. Sun, L. P.; Hase, W. L. Comparisons of Classical and Wigner Sampling of Transition State Energy Levels for Quasiclassical Trajectory Chemical Dynamics Simulations. *J. Chem. Phys.* **2010**, *133*, 044313.
162. Heller, E. J. Wigner Phase Space Method - Analysis for Semiclassical Applications. *J. Chem. Phys.* **1976**, *65*, 1289.
163. Goursaud, S.; Sizun, M.; Fiquetfayard, F. Energy Partitioning and Isotope Effects in Fragmentation of Triatomic Negative-Ions - Monte-Carlo Scheme for a Classical Trajectory Study. *J. Chem. Phys.* **1976**, *65*, 5453.

164. Schinke, R. Rotational State Distributions Following Direct Photodissociation of Triatomic-Molecules - Test of Classical-Models. *J. Phys. Chem.* **1988**, *92*, 3195.
165. Barbatti, M.; Granucci, G.; Persico, M.; Ruckenbauer, M.; Vazdar, M.; Eckert-Maksic, M.; Lischka, H. The on-the-Fly Surface-Hopping Program System Newton-X: Application to Ab Initio Simulation of the Nonadiabatic Photodynamics of Benchmark Systems. *J. Photochem. Photobiol. A* **2007**, *190*, 228
166. Crespo-Otero, R.; Barbatti, M. Spectrum Simulation and Decomposition with Nuclear Ensemble: Formal Derivation and Application to Benzene, Furan and 2-Phenylfuran. *Theor. Chem. Acc.* **2012**, *131*, 1237.
167. Favero, L.; Granucci, G.; Persico, M. Dynamics of Acetone Photodissociation: A Surface Hopping Study. *Phys. Chem. Chem. Phys.* **2013**, *15*, 20651.
168. Bose, A.; Makri, N. Wigner Phase Space Distribution Via Classical Adiabatic Switching. *J. Chem. Phys.* **2015**, *143*, 114114.
169. Qu, C.; Bowman, J. M. Revisiting Adiabatic Switching for Initial Conditions in Quasi-Classical Trajectory Calculations: Application to Ch4. *J. Phys. Chem. A* **2016**, *120*, 4988.
170. Thompson, A. L.; Punwong, C.; Martínez, T. J. Optimization of Width Parameters for Quantum Dynamics with Frozen Gaussian Basis Sets. *Chem. Phys.* **2010**, *370*, 70.
171. Mignolet, B.; Curchod, B. F. E.; Martinez, T. J. Communication: Xfaims-External Field Ab Initio Multiple Spawning for Electron-Nuclear Dynamics Triggered by Short Laser Pulses. *J. Chem. Phys.* **2016**, *145*, 191104.
172. Mitric, R.; Petersen, J.; Bonacic-Koutecky, V. Laser-Field-Induced Surface-Hopping Method for the Simulation and Control of Ultrafast Photodynamics. *Phys. Rev. A* **2009**, *79*, 053416.
173. Petersen, J.; Mitrić, R.; Bona\vcić-Kouteckỳ, V.; Wolf, J. P.; Roslund, J.; Rabitz, H. How Shaped Light Discriminates Nearly Identical Biochromophores. *Phys. Rev. Lett.* **2010**, *105*, 73003.
174. Mitrić, R.; Petersen, J.; Wohlgemuth, M.; Werner, U.; Bonacić-Kouteckỳ, V. Field-Induced Surface Hopping Method for Probing Transition State Nonadiabatic Dynamics of Ag3. *Phys. Chem. Chem. Phys.* **2011**, *13*, 8690.
175. Mitric, R.; Petersen, J.; Wohlgemuth, M.; Werner, U.; Bonacic-Koutecky, V.; Woeste, L.; Jortner, J. Time-Resolved Femtosecond Photoelectron Spectroscopy by Field-Induced Surface Hopping. *J. Phys. Chem. A* **2011**, *115*, 3755.
176. Marquetand, P.; Richter, M.; González-Vázquez, J.; Sola, I.; González, L. Nonadiabatic Ab Initio Molecular Dynamics Including Spin-Orbit Coupling and Laser Fields. *Faraday Disc.* **2011**, *153*, 261.
177. Richter, M.; Marquetand, P.; González-Vázquez, J.; Sola, I.; González, L. Sharc: Ab Initio Molecular Dynamics with Surface Hopping in the Adiabatic Representation Including Arbitrary Couplings. *J. Chem. Theory Comput.* **2011**, *7*, 1253.
178. Bajo, J. J.; González-Vázquez, J.; Sola, I. R.; Santamaria, J.; Richter, M.; Marquetand, P.; González, L. Mixed Quantum-Classical Dynamics in the Adiabatic Representation to Simulate Molecules Driven by Strong Laser Pulses. *J. Phys. Chem. A* **2012**, *16*, 2800.
179. Tavernelli, I.; Curchod, B. F. E.; Rothlisberger, U. Mixed Quantum-Classical Dynamics with Time-Dependent External Fields: A Time-Dependent Density-Functional-Theory Approach. *Phys. Rev. A* **2010**, *81*, 052508.

180. Curchod, B. F. E.; Penfold, T. J.; Rothlisberger, U.; Tavernelli, I. Local Control Theory in Trajectory-Based Nonadiabatic Dynamics. *Phys. Rev. A* **2011**, *84*, 042507.
181. Curchod, B. F. E.; Penfold, T. J.; Rothlisberger, U.; Tavernelli, I. Local Control Theory in Trajectory Surface Hopping Dynamics Applied to the Excited-State Proton Transfer of 4-Hydroxyacridine. *ChemPhysChem* **2015**, *16*, 2127.
182. Bergsma, J. P.; Berens, P. H.; Wilson, K. R.; Fredkin, D. R.; Heller, E. J. Electronic-Spectra from Molecular-Dynamics - a Simple Approach. *J. Phys. Chem.* **1984**, *88*, 612.
183. González, L.; Escudero, D.; Serrano-Andrés, L. Progress and Challenges in the Calculation of Electronic Excited States. *ChemPhysChem* **2012**, *13*, 28.
184. Roos, B. O.; Taylor, P. R.; Siegbahn, P. E. M. A Complete Active Space Scf Method (Casscf) Using a Density-Matrix Formulated Super-Ci Approach. *Chem. Phys.* **1980**, *48*, 157.
185. Snyder, J. W.; Curchod, B. F. E.; Martinez, T. J. Gpu-Accelerated State-Averaged Complete Active Space Self-Consistent Field Interfaced with Ab Initio Multiple Spawning Unravels the Photodynamics of Provitamin D-3. *J. Phys. Chem. Lett.* **2016**, *7*, 2444.
186. Mendive-Tapia, D.; Lasorne, B.; Worth, G. A.; Robb, M. A.; Bearpark, M. J. Towards Converging Non-Adiabatic Direct Dynamics Calculations Using Frozen-Width Variational Gaussian Product Basis Functions. *J. Chem. Phys.* **2012**, *137*, 22A548.
187. Allan, C. S. M.; Lasorne, B.; Worth, G. A.; Robb, M. A. A Straightforward Method of Analysis for Direct Quantum Dynamics: Application to the Photochemistry of a Model Cyanine. *J. Phys. Chem. A* **2010**, *114*, 8713.
188. Asturiol, D.; Lasorne, B.; Worth, G. A.; Robb, M. A.; Blancafort, L. Exploring the Sloped-to-Peaked S(2)/S(1) Seam of Intersection of Thymine with Electronic Structure and Direct Quantum Dynamics Calculations. *Phys. Chem. Chem. Phys.* **2010**, *12*, 4949.
189. Mendive-Tapia, D.; Lasorne, B.; Worth, G. A.; Bearpark, M. J.; Robb, M. A. Controlling the Mechanism of Fulvene S-1/S-0 Decay: Switching Off the Stepwise Population Transfer. *Phys. Chem. Chem. Phys.* **2010**, *12*, 15725.
190. Araujo, M.; Lasorne, B.; Magalhaes, A. L.; Worth, G. A.; Bearpark, M. J.; Robb, M. A. The Molecular Dissociation of Formaldehyde at Medium Photoexcitation Energies: A Quantum Chemistry and Direct Quantum Dynamics Study. *J. Chem. Phys.* **2009**, *131*, 144301.
191. Lasorne, B.; Bearpark, M. J.; Robb, M. A.; Worth, G. A. Controlling S-1/S-0 Decay and the Balance between Photochemistry and Photostability in Benzene: A Direct Quantum Dynamics Study. *J. Phys. Chem. A* **2008**, *112*, 13017.
192. Lasorne, B.; Sicilia, F.; Bearpark, M. J.; Robb, M. A.; Worth, G. A.; Blancafort, L. Automatic Generation of Active Coordinates for Quantum Dynamics Calculations: Application to the Dynamics of Benzene Photochemistry. *J. Chem. Phys.* **2008**, *128*, 124307.
193. Araujo, M.; Lasorne, B.; Magalhaes, A. L.; Bearpark, M.; Robb, M. A. Controlling Product Selection in the Photodissociation of Formaldehyde: Direct Quantum Dynamics from the S-1 Barrier. *J. Phys. Chem. A* **2010**, *114*, 12016.
194. Saita, K.; Nix, M. G. D.; Shalashilin, D. V. Simulation of Ultrafast Photodynamics of Pyrrole with a Multiconfigurational Ehrenfest Method. *Phys. Chem. Chem. Phys.* **2013**, *15*, 16227.
195. Kirrander, A.; Saita, K.; Shalashilin, D. V. Ultrafast X-Ray Scattering from Molecules. *J. Chem. Theory Comput.* **2016**, *12*, 957.

196. Coe, J. D.; Martínez, T. J. Ab Initio Molecular Dynamics of Excited-State Intramolecular Proton Transfer around a Three-State Conical Intersection in Malonaldehyde. *J. Phys. Chem. A* **2006**, *110*, 618.
197. Hudock, H. R.; Levine, B. G.; Thompson, A. L.; Satzger, H.; Townsend, D.; Gador, N.; Ullrich, S.; Stolow, A.; Martínez, T. J. Ab Initio Molecular Dynamics and Time-Resolved Photoelectron Spectroscopy of Electronically Excited Uracil and Thymine. *J. Phys. Chem. A* **2007**, *111*, 8500.
198. Levine, B. G.; Martínez, T. J. Ab Initio Multiple Spawning Dynamics of Excited Butadiene: Role of Charge Transfer. *J. Phys. Chem. A* **2009**, *113*, 12815.
199. Finley, J.; Malmqvist, P. A.; Roos, B. O.; Serrano-Andres, L. The Multi-State Caspt2 Method. *Chem. Phys. Lett.* **1998**, *288*, 299.
200. Coe, J. D.; Levine, B. G.; Martínez, T. J. Ab Initio Molecular Dynamics of Excited-State Intramolecular Proton Transfer Using Multireference Perturbation Theory. *J. Phys. Chem. A* **2007**, *111*, 11302.
201. Tao, H. L.; Levine, B. G.; Martínez, T. J. Ab Initio Multiple Spawning Dynamics Using Multi-State Second-Order Perturbation Theory. *J. Phys. Chem. A* **2009**, *113*, 13656.
202. Liu, L. H.; Liu, J.; Martinez, T. J. Dynamical Correlation Effects on Photoisomerization: Ab Initio Multiple Spawning Dynamics with Ms-Caspt2 for a Model Trans-Protonated Schiff Base. *J. Phys. Chem. B* **2016**, *120*, 1940.
203. Mori, T.; Glover, W. J.; Schuurman, M. S.; Martínez, T. J. Role of Rydberg States in the Photochemical Dynamics of Ethylene. *J. Phys. Chem. A* **2012**, *116*, 2808.
204. Kuhlman, T. S.; Glover, W. J.; Mori, T.; Moller, K. B.; Martínez, T. J. Between Ethylene and Polyenes - the Non-Adiabatic Dynamics of Cis-Dienes. *Faraday Disc.* **2012**, *157*, 193.
205. Allison, T. K.; Tao, H.; Glover, W. J.; Wright, T. W.; Stooke, A. M.; Khurmi, C.; van Tilborg, J.; Liu, Y.; Falcone, R. W.; Martínez, T. J.; Belkacem, A. Ultrafast Internal Conversion in Ethylene. Ii. Mechanisms and Pathways for Quenching and Hydrogen Elimination. *J. Chem. Phys.* **2012**, *136*, 124317.
206. Tao, H.; Allison, T. K.; Wright, T. W.; Stooke, A. M.; Khurmi, C.; van Tilborg, J.; Liu, Y.; Falcone, R. W.; Belkacem, A.; Martínez, T. J. Ultrafast Internal Conversion in Ethylene. I. The Excited State Lifetime. *J. Chem. Phys.* **2011**, *134*.
207. Celani, P.; Werner, H.-J. Analytical Energy Gradients for Internally Contracted Second-Order Multireference Perturbation Theory. *J. Chem. Phys.* **2003**, *119*, 5044.
208. Mori, T.; Kato, S. Dynamic Electron Correlation Effect on Conical Intersections in Photochemical Ring-Opening Reaction of Cyclohexadiene: Ms-Caspt2 Study. *Chem. Phys. Lett.* **2009**, *476*, 97.
209. Lischka, H.; Dallos, M.; Szalay, P. G.; Yarkony, D. R.; Shepard, R. Analytic Evaluation of Nonadiabatic Coupling Terms at the Mr-Ci Level. I. Formalism. *J. Chem. Phys.* **2004**, *120*, 7322.
210. Dallos, M.; Lischka, H.; Shepard, R.; Yarkony, D. R.; Szalay, P. G. Analytic Evaluation of Nonadiabatic Coupling Terms at the Mr-Ci Level. Ii. Minima on the Crossing Seam: Formaldehyde and the Photodimerization of Ethylene. *J. Chem. Phys.* **2004**, *120*, 7330.
211. Sellner, B.; Ruckenbauer, M.; Stambolić, I.; Barbatti, M.; Aquino, A. J. A.; Lischka, H. Photodynamics of Azomethane: A Nonadiabatic Surface-Hopping Study. *J. Phys. Chem. A* **2010**, *114*, 8778.
212. Barbatti, M.; Lischka, H. Nonadiabatic Deactivation of 9h-Adenine: A Comprehensive Picture Based on Mixed Quantum-Classical Dynamics. *J. Am. Chem. Soc.* **2008**, *130*, 6831.

213. Ben-Nun, M.; Martínez, T. J. Ab Initio Molecular Dynamics Study of Cis-Trans Photoisomerization in Ethylene. *Chem. Phys. Lett.* **1998**, *298*, 57.
214. Ben-Nun, M.; Martnez, T. J. Direct Observation of Disrotatory Ring-Opening in Photoexcited Cyclobutene Using Ab Initio Molecular Dynamics. *J. Am. Chem. Soc.* **2000**, *122*, 6299.
215. Shiozaki, T.; Gyorffy, W.; Celani, P.; Werner, H. J. Communication: Extended Multi-State Complete Active Space Second-Order Perturbation Theory: Energy and Nuclear Gradients. *J. Chem. Phys.* **2011**, *135*.
216. Granovsky, A. A. Extended Multi-Configuration Quasi-Degenerate Perturbation Theory: The New Approach to Multi-State Multi-Reference Perturbation Theory. *J. Chem. Phys.* **2011**, *134*, 214113.
217. Shiozaki, T.; Woywod, C.; Werner, H. J. Pyrazine Excited States Revisited Using the Extended Multi-State Complete Active Space Second-Order Perturbation Method. *Phys. Chem. Chem. Phys.* **2013**, *15*, 262.
218. Park, J. W.; Shiozaki, T. On-the-Fly Caspt2 Surface-Hopping Dynamics. *J. Chem. Theory Comput.* **2017**, *13*, 3676.
219. Toniolo, A.; Ciminelli, C.; Persico, M.; Martínez, T. J. Simulation of the Photodynamics of Azobenzene on Its First Excited State: Comparison of Full Multiple Spawning and Surface Hopping Treatments. *J. Chem. Phys.* **2005**, *123*, 234308.
220. Virshup, A. M.; Punwong, C.; Pogorelov, T. V.; Lindquist, B. A.; Ko, C.; Martinez, T. J. Photodynamics in Complex Environments: Ab Initio Multiple Spawning Quantum Mechanical/Molecular Mechanical Dynamics. *J. Phys. Chem. B* **2009**, *113*, 3280.
221. Runge, E.; Gross, E. K. U. Density-Functional Theory for Time-Dependent Systems. *Phys. Rev. Lett.* **1984**, *52*, 997.
222. Petersilka, M.; Gossmann, U. J.; Gross, E. K. U. Excitation Energies from Time-Dependent Density-Functional Theory. *Phys. Rev. Lett.* **1996**, *76*, 1212.
223. Casida, M. E., Time-Dependent Density-Functional Response Theory for Molecules. In *Recent Advances in Density Functional Methods*, Chong, D. P., Ed. Singapore, World Scientific: 1995; p 155.
224. Ullrich, C. A. *Time-Dependent Density-Functional Theory*. Oxford University Press: 2012.
225. Barbatti, M.; Crespo-Otero, R. Surface Hopping Dynamics with Dft Excited States. *Top. Curr. Chem.* **2015**, *368*, 415.
226. Levine, B. G.; Ko, C.; Quenneville, J.; Martínez, T. J. Conical Intersections and Double Excitations in Density Functional Theory. *Mol. Phys.* **2006**, *104*, 1039.
227. Dreuw, A.; Head-Gordon, M. Failure of Time-Dependent Density Functional Theory for Long-Range Charge-Transfer Excited States: The Zincbacteriochlorin-Bacteriochlorin and Bacteriochlorophyll-Spheroidene Complexes. *J. Am. Chem. Soc.* **2004**, *126*, 4007.
228. Casida, M. E. Time-Dependent Density-Functional Theory for Molecules and Molecular Solids. *J. Mol. Struc. (Theochem)* **2009**, *914*, 3.
229. Lischka, H.; Muller, T.; Szalay, P. G.; Shavitt, I.; Pitzer, R. M.; Shepard, R. Columbus - a Porgram System for Advanced Multireference Theory Calculations. *WIREs Comput. Mol. Sci.* **2011**, *1*, 191.
230. Gaenko, A.; DeFusco, A.; Varganov, S. A.; Martinez, T. J.; Gordon, M. S. Interfacing the Ab Initio Multiple Spawning Method with Electronic Structure Methods in Gamess: Photodecay of Trans-Azomethane. *J. Phys. Chem. A* **2014**, *118*, 10902.

231. Toniolo, A.; Olsen, S.; Manohar, L.; Martínez, T. J. Conical Intersection Dynamics in Solution: The Chromophore of Green Fluorescent Protein. *Faraday Disc.* **2004**, *127*, 149.
232. Ufimtsev, I. S.; Martinez, T. J. Graphical Processing Units for Quantum Chemistry. *Comp. Sci. Eng.* **2008**, *10*, 26.
233. Ufimtsev, I. S.; Martínez, T. J. Quantum Chemistry on Graphical Processing Units. 1. Strategies for Two-Electron Integral Evaluation. *J. Chem. Theory Comput.* **2008**, *4*, 222.
234. Ufimtsev, I. S.; Martínez, T. J. Quantum Chemistry on Graphical Processing Units. 2. Direct Self-Consistent-Field (Scf) Implementation. *J. Chem. Theory Comput.* **2009**, *5*, 3138.
235. Ufimtsev, I. S.; Martínez, T. J. Quantum Chemistry on Graphical Processing Units. 3. Analytical Energy Gradients, Geometry Optimization, and First Principles Molecular Dynamics. *J. Chem. Theory Comput.* **2009**, *5*, 2619.
236. Isborn, C. M.; Luehr, N.; Ufimtsev, I. S.; Martínez, T. J. Excited-State Electronic Structure with Configuration Interaction Singles and Tamm--Dancoff Time-Dependent Density Functional Theory on Graphical Processing Units. *J. Chem. Theory Comput.* **2011**, *7*, 1814.
237. Fales, B. S.; Levine, B. G. Nanoscale Multireference Quantum Chemistry: Full Configuration Interaction on Graphical Processing Units. *J. Chem. Theory Comput.* **2015**, *11*, 4708.
238. Snyder, J. W.; Hohenstein, E. G.; Luehr, N.; Martinez, T. J. An Atomic Orbital-Based Formulation of Analytical Gradients and Nonadiabatic Coupling Vector Elements for the State-Averaged Complete Active Space Self-Consistent Field Method on Graphical Processing Units. *J. Chem. Phys.* **2015**, *143*, 154107.
239. Hohenstein, E. G.; Luehr, N.; Ufimtsev, I. S.; Martinez, T. J. An Atomic Orbital-Based Formulation of the Complete Active Space Self-Consistent Field Method on Graphical Processing Units. *J. Chem. Phys.* **2015**, *142*, 224103.
240. Hohenstein, E. G.; Bouduban, M. E. F.; Song, C. C.; Luehr, N.; Ufimtsev, I. S.; Martinez, T. J. Analytic First Derivatives of Floating Occupation Molecular Orbital-Complete Active Space Configuration Interaction on Graphical Processing Units. *J. Chem. Phys.* **2015**, *143*, 014111.
241. Hohenstein, E. G. Analytic Formulation of Derivative Coupling Vectors for Complete Active Space Configuration Interaction Wavefunctions with Floating Occupation Molecular Orbitals. *J. Chem. Phys.* **2016**, *145*, 174110.
242. Curchod, B. F. E.; Sisto, A.; Martinez, T. J. Ab Initio Multiple Spawning Photochemical Dynamics of Dmabn Using Gpus. *J. Phys. Chem. A* **2017**, *121*, 265.
243. Ben-Nun, M.; Martinez, T. J. A Continuous Spawning Method for Nonadiabatic Dynamics and Validation for the Zero-Temperature Spin-Boson Problem. *Isr. J. Chem.* **2007**, *47*, 75.
244. In practice, one only needs to solve Eq. 18 for a single right hand side and thus the S matrix does not need to be inverted. Instead, one can solve a set of linear equations (Sx=b), which is much more efficient. Furthermore, these linear equations can be solved with a method like conjugate gradient, which tends to be self-regularizing and thus more stable in the presence of linear dependencies.
245. Kay, K. G. The Matrix Singularity Problem in the Time-Dependent Variational Method. *Chem. Phys.* **1989**, *137*, 165.
246. Davis, M. J.; Heller, E. J. Semi-Classical Gaussian-Basis Set Method for Molecular Vibrational Wave-Functions. *J. Chem. Phys.* **1979**, *71*, 3383.

247. Habershon, S. Linear Dependence and Energy Conservation in Gaussian Wavepacket Basis Sets. *J. Chem. Phys.* **2012**, *136*, 014109.
248. Andersson, L. M. Quantum Dynamics Using a Discretized Coherent State Representation: An Adaptive Phase Space Method. *J. Chem. Phys.* **2001**, *115*, 1158.
249. Polyak, I.; Allan, C. S. M.; Worth, G. A. A Complete Description of Tunnelling Using Direct Quantum Dynamics Simulation: Salicylaldimine Proton Transfer. *J. Chem. Phys.* **2015**, *143*, 084121.
250. Fernandez-Alberti, S.; Roitberg, A. E.; Nelson, T.; Tretiak, S. Identification of Unavoided Crossings in Nonadiabatic Photoexcited Dynamics Involving Multiple Electronic States in Polyatomic Conjugated Molecules. *J. Chem. Phys.* **2012**, *137*, 014512.
251. Nelson, T.; Fernandez-Alberti, S.; Roitberg, A. E.; Tretiak, S. Artifacts Due to Trivial Unavoided Crossings in the Modeling of Photoinduced Energy Transfer Dynamics in Extended Conjugated Molecules. *Chem. Phys. Lett.* **2013**, *590*, 208.
252. Wang, L. J.; Prezhdo, O. V. A Simple Solution to the Trivial Crossing Problem in Surface Hopping. *J. Phys. Chem. Lett.* **2014**, *5*, 713.
253. Fernandez-Alberti, S.; Kleiman, V. D.; Tretiak, S.; Roitberg, A. E. Unidirectional Energy Transfer in Conjugated Molecules: The Crucial Role of High-Frequency C C Bonds. *J. Phys. Chem. Lett.* **2010**, *1*, 2699.
254. Meek, G. A.; Levine, B. G. Accurate and Efficient Evaluation of Transition Probabilities at Unavoided Crossings in Ab Initio Multiple Spawning. *Chem. Phys.* **2015**, *460*, 117.
255. Blancafort, L.; Hunt, P.; Robb, M. A. Intramolecular Electron Transfer in Bis(Methylene) Adamantyl Radical Cation: A Case Study of Diabatic Trapping. *J. Am. Chem. Soc.* **2005**, *127*, 3391.
256. Ko, C.; Levine, B.; Toniolo, A.; Manohar, L.; Olsen, S.; Werner, H. J.; Martínez, T. J. Ab Initio Excited-State Dynamics of the Photoactive Yellow Protein Chromophore. *J. Am. Chem. Soc.* **2003**, *125*, 12710.
257. Lasorne, B.; Bacchus-Montabonel, M. C.; Vaeck, N.; Desouter-Lecomte, M. Nonadiabatic Interactions in Wave Packet Dynamics of the Bromoacetyl Chloride Photodissociation. *J. Chem. Phys.* **2004**, *120*, 1271.
258. Butler, L. J. Chemical Reaction Dynamics Beyond the Born-Oppenheimer Approximation. *Annu Rev Phys Chem* **1998**, *49*, 125.
259. Fabiano, E.; Keal, T.; Thiel, W. Implementation of Surface Hopping Molecular Dynamics Using Semiempirical Methods. *Chem. Phys.* **2008**, *349*, 334.
260. Fernandez-Alberti, S.; Makhov, D. V.; Tretiak, S.; Shalashilin, D. V. Non-Adiabatic Excited State Molecular Dynamics of Phenylene Ethynylene Dendrimer Using a Multiconfigurational Ehrenfest Approach. *Phys. Chem. Chem. Phys.* **2016**, *18*, 10028.
261. Meek, G. A.; Levine, B. G. Evaluation of the Time-Derivative Coupling for Accurate Electronic State Transition Probabilities from Numerical Simulations. *J. Phys. Chem. Lett.* **2014**, *5*, 2351.
262. Mai, S.; Marquetand, P.; Gonzalez, L. A General Method to Describe Intersystem Crossing Dynamics in Trajectory Surface Hopping. *Int. J. Quantum Chem.* **2015**, *115*, 1215.
263. Cui, G. L.; Thiel, W. Generalized Trajectory Surface-Hopping Method for Internal Conversion and Intersystem Crossing. *J. Chem. Phys.* **2014**, *141*, 124101.
264. de Carvalho, F. F.; Tavernelli, I. Nonadiabatic Dynamics with Intersystem Crossings: A Time-Dependent Density Functional Theory Implementation. *J. Chem. Phys.* **2015**, *143*, 224105.

265. Granucci, G.; Persico, M.; Spighi, G. Surface Hopping Trajectory Simulations with Spin-Orbit and Dynamical Couplings. *J. Chem. Phys.* **2012**, *137*, 22A501.
266. Parker, D. S. N.; Minns, R. S.; Penfold, T. J.; Worth, G. A.; Fielding, H. H. Ultrafast Dynamics of the S-1 Excited State of Benzene. *Chem. Phys. Lett.* **2009**, *469*, 43.
267. Marian, C. M. Spin--Orbit Coupling and Intersystem Crossing in Molecules. *WIREs Comput. Mol. Sci.* **2012**, *2*, 187.
268. Curchod, B. F. E.; Rauer, C.; Marquetand, P.; Gonzalez, L.; Martinez, T. J. Communication: Gaims-Generalized Ab Initio Multiple Spawning for Both Internal Conversion and Intersystem Crossing Processes. *J. Chem. Phys.* **2016**, *144*, 101102.
269. Karelson, M. M.; Zerner, M. C. Theoretical Treatment of Solvent Effects on Electronic Spectroscopy. *J. Phys. Chem.* **1992**, *96*, 6949.
270. Tomasi, J.; Mennucci, B.; Cammi, R. Quantum Mechanical Continuum Solvation Models. *Chem. Rev.* **2005**, *105*, 2999.
271. Cossi, M.; Barone, V. Solvent Effect on Vertical Electronic Transitions by the Polarizable Continuum Model. *J. Chem. Phys.* **2000**, *112*, 2427.
272. Mennucci, B.; Cammi, R.; Tomasi, J. Excited States and Solvatochromic Shifts within a Nonequilibrium Solvation Approach: A New Formulation of the Integral Equation Formalism Method at the Self-Consistent Field, Configuration Interaction, and Multiconfiguration Self-Consistent Field Level. *J. Chem. Phys.* **1998**, *109*, 2798.
273. DeFusco, A.; Minezawa, N.; Slipchenko, L. V.; Zahariev, F.; Gordon, M. S. Modeling Solvent Effects on Electronic Excited States. *J. Phys. Chem. Lett.* **2011**, *2*, 2184.
274. Chiba, M.; Fedorov, D. G.; Kitaura, K. Polarizable Continuum Model with the Fragment Molecular Orbital-Based Time-Dependent Density Functional Theory. *J. Comp. Chem.* **2008**, *29*, 2667.
275. Casida, M. E.; Wesolowski, T. A. Generalization of the Kohn-Sham Equations with Constrained Electron Density Formalism and Its Time-Dependent Response Theory Formulation. *Int. J. Quantum Chem.* **2004**, *96*, 577.
276. Kaminski, J. W.; Gusarov, S.; Wesolowski, T. A.; Kovalenko, A. Modeling Solvatochromic Shifts Using the Orbital-Free Embedding Potential at Statistically Mechanically Averaged Solvent Density. *J. Phys. Chem. A* **2010**, *114*, 6082.
277. Neugebauer, J.; Louwerse, M. J.; Baerends, E. J.; Wesolowski, T. A. The Merits of the Frozen-Density Embedding Scheme to Model Solvatochromic Shifts. *J. Chem. Phys.* **2005**, *122*, 094115.
278. Röhrig, U. F.; Frank, I.; Hutter, J.; Laio, A.; VandeVondele, J.; Rothlisberger, U. Qm/Mm Car-Parrinello Molecular Dynamics Study of the Solvent Effects on the Ground State and on the First Excited Singlet State of Acetone in Water. *ChemPhysChem* **2003**, *4*, 1177.
279. Kongsted, J.; Osted, A.; Mikkelsen, K. V.; Astrand, P. O.; Christiansen, O. Solvent Effects on the N ->Pi(*) Electronic Transition in Formaldehyde: A Combined Coupled Cluster/Molecular Dynamics Study. *J. Chem. Phys.* **2004**, *121*, 8435.
280. Gao, J. L.; Byun, K. Solvent Effects on the N->Pi Transition of Pyrimidine in Aqueous Solution. *Theor. Chem. Acc.* **1997**, *96*, 151.
281. Isborn, C. M.; Götz, A. W.; Clark, M. A.; Walker, R. C.; Martínez, T. J. Electronic Absorption Spectra from Mm and Ab Initio Qm/Mm Molecular Dynamics: Environmental Effects on the Absorption Spectrum of Photoactive Yellow Protein. *J. Chem. Theory Comput.* **2012**, *8*, 5092.

282. Parac, M.; Doerr, M.; Marian, C. M.; Thiel, W. Qm/Mm Calculation of Solvent Effects on Absorption Spectra of Guanine. *J. Comp. Chem.* **2010**, *31*, 90.
283. Brunk, E.; Rothlisberger, U. Mixed Quantum Mechanical/Molecular Mechanical Molecular Dynamics Simulations of Biological Systems in Ground and Electronically Excited States. *Chem. Rev.* **2015**, *115*, 6217.
284. Wohlgemuth, M.; Bonacic-Koutecky, V.; Mitric, R. Time-Dependent Density Functional Theory Excited State Nonadiabatic Dynamics Combined with Quantum Mechanical/Molecular Mechanical Approach: Photodynamics of Indole in Water. *J. Chem. Phys.* **2011**, *135*, 054105.
285. Tavernelli, I.; Curchod, B. F. E.; Rothlisberger, U. Nonadiabatic Molecular Dynamics with Solvent Effects: A Lr-Tddft Qm/Mm Study of Ruthenium (Ii) Tris (Bipyridine) in Water. *Chem. Phys.* **2011**, *391*, 101.
286. Cattaneo, P.; Persico, N. Semiclassical Simulations of Azomethane Photochemistry in the Gas Phase and in Solution. *J. Am. Chem. Soc.* **2001**, *123*, 7638.
287. Sneskov, K.; Schwabe, T.; Christiansen, O.; Kongsted, J. Scrutinizing the Effects of Polarization in Qm/Mm Excited State Calculations. *Phys. Chem. Chem. Phys.* **2011**, *13*, 18551.
288. Virshup, A. M.; Levine, B. G.; Martínez, T. J. Steric and Electrostatic Effects on Photoisomerization Dynamics Using Qm/Mm Ab Initio Multiple Spawning. *Theor. Chem. Acc.* **2014**, *133*, 1506.
289. Punwong, C.; Martínez, T. J.; Hannongbua, S. Direct Qm/Mm Simulation of Photoexcitation Dynamics in Bacteriorhodopsin and Halorhodopsin. *Chem. Phys. Lett.* **2014**, *610-611*, 213.
290. Punwong, C.; Owens, J.; Martinez, T. J. Direct Qm/Mm Excited-State Dynamics of Retinal Protonated Schiff Base in Isolation and Methanol Solution. *J. Phys. Chem. B* **2015**, *119*, 704.
291. Coe, J. D.; Ong, M. T.; Levine, B. G.; Martinez, T. J. On the Extent and Connectivity of Conical Intersection Seams and the Effect of Three-State Intersections. *J. Phys. Chem. A* **2008**, *112*, 12559.
292. Viel, A.; Krawczyk, R. P.; Manthe, U.; Domcke, W. Photoinduced Dynamics of Ethene in the N, V, and Z Valence States: A Six-Dimensional Nonadiabatic Quantum Dynamics Investigation. *J. Chem. Phys.* **2004**, *120*, 11000.
293. Brill, M. R.; Gatti, F.; Lauvergnat, D.; Meyer, H. D. Photoinduced Nonadiabatic Dynamics of Ethene: Six-Dimensional Wave Packet Propagations Using Two Different Approximations of the Kinetic Energy Operators. *Chem. Phys.* **2007**, *338*, 186.
294. Lasorne, B.; Robb, M. A.; Meyer, H. D.; Gatti, F. The Electronic Excited States of Ethylene with Large-Amplitude Deformations: A Dynamical Symmetry Group Investigation. *Chem. Phys.* **2010**, *377*, 30.
295. Jornet-Somoza, J.; Lasorne, B.; Robb, M. A.; Meyer, H. D.; Lauvergnat, D.; Gatti, F. A Generalised 17-State Vibronic-Coupling Hamiltonian Model for Ethylene. *J. Chem. Phys.* **2012**, *137*, 639.
296. Sellner, B.; Barbatti, M.; Muller, T.; Domcke, W.; Lischka, H. Ultrafast Non-Adiabatic Dynamics of Ethylene Including Rydberg States. *Mol. Phys.* **2013**, *111*, 2439.
297. Kobayashi, T.; Horio, T.; Suzuki, T. Ultrafast Deactivation of the Pi Pi*(V) State of Ethylene Studied Using Sub-20 Fs Time-Resolved Photoelectron Imaging. *J. Phys. Chem. A* **2015**, *119*, 9518.

298. Schultz, T.; Quenneville, J.; Levine, B.; Toniolo, A.; Martínez, T. J.; Lochbrunner, S.; Schmitt, M.; Shaffer, J. P.; Zgierski, M. Z.; Stolow, A. Mechanism and Dynamics of Azobenzene Photoisomerization. *J. Am. Chem. Soc.* **2003**, *125*, 8098.
299. Liu, L.; Wang, Y.; Fang, Q. New Insights into Mechanistic Photoisomerization of Ethylene-Bridged Azobenzene from Ab Initio Multiple Spawning Simulation. *J. Chem. Phys.* **2017**, *146*, 064308.
300. Ko, C.; Virshup, A. M.; Martínez, T. J. Electrostatic Control of Photoisomerization in the Photoactive Yellow Protein Chromophore: Ab Initio Multiple Spawning Dynamics. *Chem. Phys. Lett.* **2008**, *460*, 272.
301. Coe, J. D.; Martínez, T. J. Competitive Decay at Two- and Three-State Conical Intersections in Excited-State Intramolecular Proton Transfer. *J. Am. Chem. Soc.* **2005**, *127*, 4560.
302. Kim, M. H.; Shen, L.; Tao, H. L.; Martínez, T. J.; Suits, A. G. Conformationally Controlled Chemistry: Excited-State Dynamics Dictate Ground-State Reaction. *Science* **2007**, *315*, 1561.
303. Tao, H. L.; Shen, L.; Kim, M. H.; Suits, A. G.; Martínez, T. J. Conformationally Selective Photodissociation Dynamics of Propanal Cation. *J. Chem. Phys.* **2011**, *134*.
304. Coe, J. D.; Martínez, T. J. Ab Initio Multiple Spawning Dynamics of Excited State Intramolecular Proton Transfer: The Role of Spectroscopically Dark States. *Mol. Phys.* **2008**, *106*, 537.
305. Hudock, H. R.; Martínez, T. J. Excited-State Dynamics of Cytosine Reveal Multiple Intrinsic Subpicosecond Pathways. *ChemPhysChem* **2008**, *9*, 2486.
306. Thompson, A. L.; Martínez, T. J. Time-Resolved Photoelectron Spectroscopy from First Principles: Excited State Dynamics of Benzene. *Faraday Disc.* **2011**, *150*, 293.
307. Wolf, T. J. A.; Kuhlman, T. S.; Schalk, O.; Martínez, T. J.; Moller, K. B.; Stolow, A.; Unterreiner, A. N. Hexamethylcyclopentadiene: Time-Resolved Photoelectron Spectroscopy and Ab Initio Multiple Spawning Simulations. *Phys. Chem. Chem. Phys.* **2014**, *16*, 11770.
308. Ben-Nun, M.; Martínez, T. J. Electronic Absorption and Resonance Raman Spectroscopy from Ab Initio Quantum Molecular Dynamics. *J. Phys. Chem. A* **1999**, *103*, 10517.
309. Neville, S. P.; Averbukh, V.; Patchkovskii, S.; Ruberti, M.; Yun, R.; Chergui, M.; Stolow, A.; Schuurman, M. S. Beyond Structure: Ultrafast X-Ray Absorption Spectroscopy as a Probe of Non-Adiabatic Wavepacket Dynamics. *Faraday Disc.* **2016**, *194*, 117.
310. Joalland, B.; Mori, T.; Martínez, T. J.; Suits, A. G. Photochemical Dynamics of Ethylene Cation C2h4+. *J. Phys. Chem. Lett.* **2014**, *5*, 1467.
311. Olsen, S.; Lamothe, K.; Martinez, T. J. Protonic Gating of Excited-State Twisting and Charge Localization in Gfp Chromophores: A Mechanistic Hypothesis for Reversible Photoswitching. *J. Am. Chem. Soc.* **2010**, *132*, 1192.
312. Kim, J.; Tao, H. L.; White, J. L.; Petrovic, V. S.; Martínez, T. J.; Bucksbaum, P. H. Control of 1,3-Cyclohexadiene Photoisomerization Using Light-Induced Conical Intersections. *J. Phys. Chem. A* **2012**, *116*, 2758.
313. Kim, J.; Tao, H. L.; Martinez, T. J.; Bucksbaum, P. Ab Initio Multiple Spawning on Laser-Dressed States: A Study of 1,3-Cyclohexadiene Photoisomerization Via Light-Induced Conical Intersections. *J. Phys. B* **2015**, *48*, 164003.
314. Shu, Y. A.; Levine, B. G. Communication: Non-Radiative Recombination Via Conical Intersection at a Semiconductor Defect. *J. Chem. Phys.* **2013**, *139*, 081102.

315. Shu, Y. N.; Levine, B. G. Nonradiative Recombination Via Conical Intersections Arising at Defects on the Oxidized Silicon Surface. *J. Phys. Chem. C* **2015**, *119*, 1737.
316. Shu, Y.; Levine, B. G. First Principles Study of Non-Radiative Recombination in Silicon Nanocrystals: The Role of Surface Silanol. *J. Phys. Chem. C* **2016**, *120*, 23246.
317. Fedorov, D. A.; Pruitt, S. R.; Keipert, K.; Gordon, M. S.; Varganov, S. A. Ab Initio Multiple Spawning Method for Intersystem Crossing Dynamics: Spin-Forbidden Transitions between 3b(1) and (1)a(1) States of Geh2. *J. Phys. Chem. A* **2016**, *120*, 2911.
318. Xie, B. B.; Liu, L. H.; Cui, G. L.; Fang, W. H.; Cao, J.; Feng, W.; Li, X. Q. Ab Initio Implementation of Quantum Trajectory Mean-Field Approach and Dynamical Simulation of the N2co Photodissociation. *J. Chem. Phys.* **2015**, *143*, 194107.
319. Liu, L. H.; Fang, W. H. New Insights into Photodissociation Dynamics of Cyclobutanone from the Aims Dynamic Simulation. *J. Chem. Phys.* **2016**, *144*.
320. Liu, L. H.; Xia, S. H.; Fang, W. H. Photodecarbonylation Mechanism of Cyclopropenone in the Gas Phase: Electronic Structure Calculation and Aims Dynamics Simulation. *J. Phys. Chem. A* **2014**, *118*, 8977.
321. Pijeau, S.; Foster, D.; Hohenstein, E. G. Excited-State Dynamics of 2-(2 '-Hydroxyphenyl)Benzothiazole: Ultrafast Proton Transfer and Internal Conversion. *J. Phys. Chem. A* **2017**, *121*, 4595.
322. Pijeau, S.; Foster, D.; Hohenstein, E. G. Excited-State Dynamics of a Benzotriazole Photostabilizer: 2-(2'-Hydroxy-5'-Methylphenyl)Benzotriazole. *J. Phys. Chem. A* **2017**, *121*, 6377.
323. Mignolet, B.; Curchod, B. F. E.; Martinez, T. J. Rich Athermal Ground-State Chemistry Triggered by Dynamics through a Conical Intersection. *Ang. Chem. Int. Ed.* **2016**, *55*, 14993.
324. Tapavicza, E.; Meyer, A. M.; Furche, F. Unravelling the Details of Vitamin D Photosynthesis by Non-Adiabatic Molecular Dynamics Simulations. *Phys. Chem. Chem. Phys.* **2011**, *13*, 20986.
325. Smith, B. D.; Spears, K. G.; Sension, R. J. Probing the Biexponential Dynamics of Ring-Opening in 7-Dehydrocholesterol. *J. Phys. Chem. A* **2016**, *120*, 6575.
326. Burghardt, I.; Hynes, J. T. Excited-State Charge Tranfer at a Conical Intersection: Effects of an Environment. *J. Phys. Chem. A* **2006**, *110*, 11411.
327. Sindelka, M.; Moiseyev, N.; Cederbaum, L. S. Strong Impact of Light-Induced Conical Intersections on the Spectrum of Diatomic Molecules. *J. Phys. B* **2011**, *44*, 045603.
328. Demekhin, P. V.; Cederbaum, L. S. Light Induced Conical Intersections in Polyatomic Molecules: General Theory, Strategies of Exploitation, and Application. *J. Chem. Phys.* **2013**, *139*, 154314.
329. Tretiak, S.; Mukamel, S. Density Matrix Analysis and Simulation of Electronic Excitations in Conjugated and Aggregated Molecules. *Chem. Rev.* **2002**, *102*, 3171.
330. Dewar, M. J. S.; Zoebisch, E. G.; Healy, E. F.; Stewart, J. J. P. The Development and Use of Quantum-Mechanical Molecular-Models. Am1 - a New General-Purpose Quantum-Mechanical Molecular-Model. *J. Am. Chem. Soc.* **1985**, *107*, 3902.
331. Nelson, T.; Fernandez-Alberti, S.; Chernyak, V.; Roitberg, A. E.; Tretiak, S. Nonadiabatic Excited-State Molecular Dynamics Modeling of Photoinduced Dynamics in Conjugated Molecules. *J. Phys. Chem. B* **2011**, *115*, 5402.

332. Nelson, T.; Fernandez-Alberti, S.; Roitberg, A. E.; Tretiak, S. Nonadiabatic Excited-State Molecular Dynamics: Modeling Photophysics in Organic Conjugated Materials. *Acc. Chem. Res.* **2014**, *47*, 1155.
333. Nelson, T.; Fernandez-Alberti, S.; Roitberg, A. E.; Tretiak, S. Nonadiabatic Excited-State Molecular Dynamics: Treatment of Electronic Decoherence. *J. Chem. Phys.* **2013**, *138*, 224111.